ON POWER QUALITY CONTROL CENTER FOR PROVIDING UNBUNDLED POWER QUALITY SERVICES

Zhan Yanqin

School of Electrical and Electronic Engineering

A thesis submitted to the Nanyang Technological University
in fulfilment of the requirement for the degree of
Doctor of Philosophy

2006

Acknowledgments

I would like to express my deep gratitude to my supervisor, Professor Choi San Shing, for his invaluable guidance, help and encouragement throughout my research.

My special thanks go to Associate Professor D. M. Vilathgamuwa and Assistant Professor S. Rajakaruna, for their invaluable advice and help throughout my research.

The research would not be possible without the financial support provided by Nanyang Technological University in the form of a research scholarship. For this I am most grateful.

I am also deeply thankful to Ms Chew-Sim Annie, Mr.Yeoh Tiow Koon, and Mr. Lee Ting Yeng for the technical support they have given me in the course of my research.

Last but not at least, to my fiancé, Heyi, for his unfailing support, patience and cooperation that have made the completion of the research work possible. And also my parents for their invaluable support and understanding over these three years or so of my graduate program.

Summary

Re-examination of the design and operation of power distribution networks has gained much attention in recent years due to (a) the need to provide unbundled power quality supply service to customers, and (b) the technical challenges resulting from the installation of small-scale distributed generators (DG). Power Quality Control Center (PQCC) has been proposed as a possible solution to meet the challenges and the main focus of this thesis is to investigate the several technical issues pertaining to the design and applications of the PQCC.

The investigation begins with a detailed analysis of the UPS-type PQCC by developing its mathematical model. The model allows a clearer insight of the internal dynamics of the PQCC to be gained. It forms the basis for designing closed-loop control systems for the power electronic devices in the PQCC. A frequency restoration scheme based on the PQCC is then used to demonstrate the application of the derived model and the new scheme can indeed improve frequency regulation of the power system.

The potential of using the PQCC to mitigate upstream voltage sag effects on sensitive loads is also examined. The analysis shows that the load ride-through capability is dependent on the current rating of the PQCC input-side inverter. In order to reduce the fault current in the inverter during sag, a three-stage operation scheme is designed. The scheme allows the regulation of the PQCC DC-link voltage by coordinating it with the response of the DG. The design of the control system for realizing such an operation is also considered. Analysis and simulation show that the load ride-through capability has been extended considerably through the proposed scheme.

Next, by assuming the DG in the form of Solid Oxide Fuel Cell (SOFC), its functional characteristics and the role it plays within the PQCC has been studied. It shows that the ability of the SOFC to accommodate instantaneous power demand change is constrained by the limits imposed on its fuel utilization factor. Taking into consideration the DG operational constraints, a more realistic scheme of the PQCC is proposed under both steady-state and upstream voltage-sag state. The new scheme is shown to be able to

provide unbundled power quality supply much more reliably. Simulation results verify the feasibility of the proposed scheme.

Finally, analysis shows that the voltage sag ride-through capability provided by the SOFC-based PQCC could still be improved by introducing a Series Compensator (SC) into the PQCC. Two PQCC-SC structures are proposed and their ride-through capabilities are analyzed. It shows that both schemes can improve the sensitive load ride-through capability significantly. Furthermore, the preference of one scheme over the other depends on the protected load power demand and the capacity of the SC.

Table of Contents

Acknowledgements i

Summary ii

Table of Contents iv

List of Figures viii

List of Tables xi

List of Symbols xii

Chapter 1 Introduction

1.1 Motivation 1

1.2 Major Contributions of the Thesis 4

1.3 Organization of the Thesis 6

Chapter 2 A Review of Works on Power Quality, Distributed Generation and Unbundled Power Quality Supply Systems

2.1 Introduction 8

2.2 Power Quality 10

2.2.1 Power quality disturbances 11

2.2.2 CBEMA and ITIC curves 14

2.3 Distributed Generation 16

2.3.1 Types of distributed generators 18

2.3.1.1 Internal Combustion Engines 18

2.3.1.2 Micro-turbines 18

2.3.1.3 Photovoltaic 19

2.3.1.4 Fuel cells 20

2.3.2 Technical impacts of DGs on distribution system 22

2.4 Unbundled Power Quality Supply System 24

2.4.1 Custom/Premium Power Park 25

2.4.1.1 Main Custom Power devices 25

2.4.1.2 Concept of Custom Power Park 32

2.4.2 FRIENDS 34
2.5 Possible Designs of Power Quality Control Center 38
2.5.1 PQCC structures: low voltage side 39
2.5.1.1 PQCC for single-phase loads 39
2.5.1.2 DC-type PQCC 40
2.5.1.3 AC-type PQCC 41
2.5.1.4 UPQC-type PQCC 42
2.5.1.5 UPS-type PQCC 43
2.5.2 PQCC structure: high voltage side 45
2.6 Conclusions 46

Chapter 3 A General Model of Power Quality Control Center

3.1 Introduction 48
3.2 General Model of the UPS-Type PQCC 49
3.2.1 Basic state equations 50
3.2.2 Time-invariant solution 56
3.2.3 PQCC small signal model 58
3.3 PQCC System Stability Consideration 61
3.3.1 System description 62
3.3.2 Model development 64
3.3.2.1 Linear micro-turbine model 64
3.3.2.2 Main generator model 66
3.3.2.3 Combined system model 66
3.3.3 Controller design 68
3.3.4 Illustrative example 70
3.4 Conclusions 75

Chapter 4 Voltage-Sag Mitigation through Power Quality Control Center

4.1 Introduction 77
4.2 PQCC Structure and Distributed Generator Model 78
4.2.1 Previous PQCC voltage sag ride-through method 78

4.2.2 Fuel cell distributed generator 79
4.3 Proposed PQCC Voltage Sag Ride-Through Scheme 81
4.3.1 Stage 1 83
4.3.2 Stage 2 84
4.3.3 Stage 3 87
4.4 Control System Design 88
4.5 Simulation 92
4.6 Conclusions 96

Chapter 5 Fuel Cell-Based PQCC to Realize Unbundled Power Quality Supply

5.1 Additional Considerations on SOFC Characteristics 99
5.2 Proposed scheme 104
5.2.1 Steady-State operations 104
5.2.2 Operation under the loss of SOFC 107
5.2.3 Operation under upstream voltage sag 108
5.2.3.1 Scenario 1 109
5.2.3.2 Scenario 2 109
5.3 Control System Design 111
5.3.1 Control scheme under interconnected state 112
5.3.2 Control scheme under islanding mode (Scenario 2) 115
5.3.3 Current references 116
5.4 Illustrative Examples 117
5.4.1 System description 117
5.4.2 Simulation 119
5.5 Conclusions 122

Chapter 6 A New PQCC with Series Compensation Capability

6.1 PQCC-SC Scheme 1 125
6.2 PQCC-SC Scheme 2 130
6.3 Comparison of the Two Schemes under an Extremely Stiff Upstream Supply Condition 131

6.4 Numerical Example and Simulation 135
6.4.1 Numerical example 135
6.4.2 Simulation 138
6.5 Conclusions 140

Chapter 7 Conclusions and Recommendations

7.1 Conclusions 142
7.2 Recommendations 144

References 147

Appendices

Appendix A Parameters of G_{com}(s) 160
Appendix B Typical 100 kW SOFC Power Plant Experimental Data Used for Simulation Studies [99] 161

Vita 162

List of Figures

Figure 2-1	Voltage divider model	12
Figure 2-2	CBEMA curve [61]	15
Figure 2-3	ITIC curve [62]	16
Figure 2-4	Schematic fuel cell system configuration [69]	21
Figure 2-5	Basic SOFC electrode reaction [69]	22
Figure 2-6	An example distribution system	22
Figure 2-7	Schematic diagram of a SSCL [70]	26
Figure 2-8	Schematic diagram of SSTS [70]	27
Figure 2-9	Simplified single-phase diagram of D-STATCOM	28
Figure 2-10	Structure of DVR: showing the injection voltage in phase b	29
Figure 2-11	Simplified single-phase diagram of UPQC [80]	31
Figure 2-12	A Custom Power Park [70]	33
Figure 2-13	General concept of FRIENDS [37]	35
Figure 2-14	Example network structure of FRIENDS [37]	36
Figure 2-15	Configuration of PQCC for single-phase load [33]	40
Figure 2-16	Configuration of DC-type PQCC [34]	41
Figure 2-17	Configuration of AC-type PQCC [35]	42
Figure 2-18	Configuration of UPQC-type PQCC [30]	43
Figure 2-19	Configuration of UPS-type PQCC [30]	45
Figure 2-20	High Voltage side interior structure [31]	46
Figure 3-1	Main Circuit of UPS-type PQCC	50
Figure 3-2	Main circuit of Inv. 1	51
Figure 3-3	Switching function d_k^* and duty ratio d_k [91]	54
Figure 3-4	Waveforms of switching function over one switching period [91]	54
Figure 3-5	Generator supplying isolated load [47]	62
Figure 3-6	Proposed frequency control system model	63
Figure 3-7	Micro-turbine generator and rectifier model [93]	65
Figure 3-8	Linearized micro-turbine model	66
Figure 3-9	Simplified main generator model [47]	66

Figure 3-10	Combined model for system frequency regulation	67
Figure 3-11	Bode plot of the open-loop mocro-turbine model G_1(s)	72
Figure 3-12	Bode plot of closed-loop micro-turbine transfer function G(s)	72
Figure 3-13	Bode plot of closed-loop transfer function of combined system G_{com}(s)	73
Figure 3-14	Active power change of the main generator (ΔP_{m1})	73
Figure 3-15	Active power change of the micro-turbine (ΔP_{m2})	74
Figure 3-16	System frequency change ($\Delta\omega$)	74
Figure 3-17	Micro-turbine speed (ω_1)	74
Figure 4-1	Interior structure of the UPS-type PQCC proposed in [31]	79
Figure 4-2	Ideal and actual fuel cell current and voltage characteristics [13]	80
Figure 4-3	A simplified PQCC network model	82
Figure 4-4	P_{ac} vs V_{dc}	85
Figure 4-5	Proposed control scheme for Inv.1	89
Figure 4-6	Inv.1 voltage and current phasor diagram under unity power factor	91
Figure 4-7	Simplified controller block diagram	91
Figure 4-8	Ride-through for a 90% voltage sag (Stage 1)	94
Figure 4-9	Ride-through for a 60% voltage sag (Stage 2)	95
Figure 4-10	Ride-through for a 30% voltage sag (Stage 3)	96
Figure 5-1	Schematic diagram of a SOFC [99]	100
Figure 5-2	Feasible operation area of a SOFC [101]	101
Figure 5-3	A simplified PQCC model	105
Figure 5-4	PQCC feasible operating zone under Scenario 2	110
Figure 5-5	Control scheme of Inv.1under interconnected state	114
Figure 5-6	Equivalent d-q current control schemes for Inv.1	114
Figure 5-7	Control scheme for Scenario 2	116
Figure 5-8	System operation under a 90% voltage sag (scenario 1)	120
Figure 5-9	System operation under a 60% voltage sag (scenario 2)	121
Figure 5-10	System operation under sudden loss of SOFC	121
Figure 5-11	System operation under sudden loss of AC link (circuit breaker ‘B’ open)	122
Figure 6-1	PQCC-SC Scheme 1: single-phase representation	126
Figure 6-2	Phasor diagram of the proposed Scheme 1	128

Figure 6-3	PQCC-SC Scheme 2: single-phase representation	130
Figure 6-4	Variations of $V_{sag1,max}$ and $V_{sag2,max}$ with phase jump α and HQ load power factor cosθ for k = 0.52, S_{HQ} = 0.38 pu, L=0	134
Figure 6-5	Variations of $V_{sag1,max}$ and $V_{sag2,max}$ with α and k for HQ load power factor of 0.7 (lag), S_{HQ} = 0.38 pu, L=0	135
Figure 6-6	Variations of V_{sag1} with α and S_1 for S_{HQ} = 0.38 pu: Scheme 1	137
Figure 6-7	Variations of V_{sag2} with α and S_2 for S_{HQ} = 0.38 pu and cosθ = 0.8: Scheme 2	137
Figure 6-8	Variations of $V_{sag1,max}$ and $V_{sag2,max}$ with phase jump α and HQ load power factor cosθ for k = 0.52, S_{HQ} = 0.38 pu, $L\neq0$	137
Figure 6-9	Variations of $V_{sag1,max}$ and $V_{sag2,max}$ with α and k for HQ load power factor of 0.7 (lag), S_{HQ} = 0.38 pu, $L\neq0$	138
Figure 6-10	Simulation results for Scheme 1 under a 42% sag	139
Figure 6-11	Simulation results for Scheme 2 under a 51% sag	140

List of Tables

Table 3-1	System parameters	71
Table 4-1	Parametric values of the PQCC and power system	92
Table 4-2	PQCC stage selector settings	93
Table 5-1	Power quality levels of loads	111
Table 5-2	Parametric values of the PQCC and power system	118
Table 6-1	Parametric values of the PQCC and power system	136
Table B-1	100 kW SOFC power plant data [99]	161

List of Symbols

α:	Phase angle jump of the voltage sag
φ:	Phase angle of the upstream source voltage
cosθ:	Power factor of the HQ load
v_1, v_2, v_3:	Equivalent phase voltages of upstream supply system
i_1, i_2, i_3:	Phase currents of upstream supply system
i_a, i_b, i_c:	Phase currents of the SP load
d_1, d_2, d_3:	Switching functions of Inv.1
d_a, d_b, d_c:	Switching functions of Inv.2
m_1, m_2:	Modulation indexes of Inv.1 and Inv.2 respectively
φ_1, φ_2:	Phase shift of Inv.1 and Inv.2 respectively
c_f:	Capacitor in the DC link of the PQCC system
R', L':	Equivalent resistor and inductor of the SP load
R_o, L_o:	Equivalent resistor and inductor of the OQ load
R_h, L_h:	Equivalent resistor and inductor of the HQ load
R, L:	Equivalent resistor and inductor of upstream supply system
R_d:	Equivalent resistor of the DC load
V_{dc}:	DC link voltage of the PQCC system
r:	Equivalent internal resistor of the SOFC
E:	Equivalent open-circuit voltage of the SOFC
$I_{inv1,rate}$:	Current rating of Inv.1
I_{FC}:	SOFC stack current
L_f:	Link inductor between the Inv.1 and the PCC
$\vec{I}_L$:	HQ load current
$\vec{V}_L$	HQ load terminal voltage
ω:	Nominal system frequency
ω_1:	Micro-turbine electrical angular frequency
V_s:	rms value of the upstream source voltage
I_s:	rms value o the upstream source current
V_{sag}:	Upstream source voltage during voltage sag

$V_{sag,max}$:	The amplitude of the most severe sag the system can ride-through
$\vec{V}_p$:	Phase vector of the PCC voltage
V_t:	Inv.1 front-end voltage
V_{min}:	Minimum voltage level for prolonged operation of the loads
$\vec{V}_{inj}$:	Injected phase voltage of the series compensator
P_{inj}, Q_{inj}:	Injected active and reactive power of the series compensator
S_{max}:	Power rating of the series compensator
P_{DC}, P_{SP}:	Active power demand of the DC, SP respectively
P_{HQ}, P_{OQ}:	Active power demand of the HQ, OQ loads respectively
P_{dg}:	Output power of the DG
$\Delta P_{dg,max}$:	Maximum instantaneous power change of the SOFC
P_r, Q_r:	Active and reactive power transferred from the Inv.1 to the PCC
u:	Fuel utilization factor of the SOFC

Chapter 1

Introduction

1.1 Motivation

In many parts of the world, the design and operation of power systems would have to be re-examined in view of the deregulation of the utility industry [1]. Meanwhile at the load-end, power quality has becoming an increasingly important consideration due to wide-spread use of computerized and power electronic equipment, which require high quality power [2-5]. Also, these loads themselves are often the cause of poor power quality, such as the harmonics generated by power-electronic drives [6]. Hence the impacts of these loads on power quality have to be considered. Notwithstanding the above, there is still a significant portion of loads that can accept a lower-quality supply but demand it to be supplied at lower prices. Taking all these factors into consideration, an unbundled power quality supply [7-11] would certainly be a highly desirable feature in distribution systems, for it enables the utility industry to deliver different power quality levels to match customer requirements and expectation.

On the generation-side and in response to the deregulation of the industry, introducing small-scale distributed generation (DG) on the customer side of distribution systems has become one of the most significant changes observed in recent years [12-14]. DGs could be of the form of wind turbine, photovoltaic, micro-turbine, fuel cell, among others. They are introduced mainly because they are more environmentally friendly and/or are of high energy efficiency. However, introducing DG into an existing power system would pose new technical challenges [12, 15-20]. For example, DG can cause power flow along un-intended paths under certain operational conditions. This could result in undesirable system voltage profile, or cause an increase in fault level and the obstructions to fault detection, to name just a few of many other unwelcome consequences.

With these backgrounds, it is therefore not surprising to find that much of recent research attention has been directed towards exploring the design of flexible electric power distribution system for the future. The concept of "Custom Power" has been proposed in [21-24], in which the application of power electronics to control power flows in distribution systems has been considered. In the North America, studies for bringing "unbundled power quality services" to realization have been promoted by many researchers [25]. Flexible, Reliable and Intelligent Energy Delivery System, or FRIENDS for abbreviation, is yet another attempt in this development [26-29]. By using DG, power electronics technologies, demand side control, high-level communication technologies and dispersed intelligent facilities, FRIENDS is intended to have many desirable features. The most significant one is the new conceptual facility named Power Quality Control Center (PQCC) [30-36]. A PQCC plays a vital role in FRIENDS operation, such as providing unbundled power quality services. The Center is located between the high voltage distribution lines and the customers. It consists of power electronic devices for controlling power flows, static transfer switches for flexible network configuration and computers for information processing, among other functions. Distributed generators are also installed in the PQCC for efficient use of electrical energy production.

The key difference of such a flexible system from the existing distribution system is in the service differentiation [28]: in FRIENDS for example, the service is multi-menu and the range of customer's choice is much wider than that offered by existing systems. The existing system is designed to deliver a single quality power uniformly to all consumers at reasonable cost. In order to introduce such a flexible power system, the advantages of the proposed system over the existing system must be totally understood and accepted. Research work should be carried out to include the design of optimal network configurations for reliable and unbundled power quality services, developing structures of the PQCC and analyzing the impact of DGs on the proposed system. At present, much progress has been reported [30-40], where the intention is to design systems which can realize unbundled power quality supply and allow flexible changes in the configurations of distribution networks without degrading system reliability and security.

The research work to be described in this thesis is an attempt to make further contributions to achieve the above objective. The aim is to gain a better understanding of

the operation of PQCC under various power disturbance conditions, to investigate the interaction between the DG and power system while at the same time, realize unbundled power quality supply.

Before detailed examination of the PQCC functions can be carried out, a mathematical model of the PQCC is developed in Chapter 3. General analysis of the PQCC model is valuable in term of coordinating the operation of DG and the upstream supply systems and for the design of the control system for the power electronics devices in the PQCC. Using the PQCC to mitigate power system frequency variations is also considered in this Chapter. Central to the proposed technique is the intention to regulate the output power of the upstream system and the DG simultaneously in the event of load–generation imbalance. As the dynamic response of DG is considered faster than that of the main upstream generator, the proposed method is then expected to provide superior system frequency regulation than that based on conventional method.

Among the many power disturbances, voltage sags are considered the most devastating disturbances that can affect supply quality of distribution systems [41-43]. Industry surveys described in [44-46] show that in recent years some 80% to 90% of the customers' complaints pertaining to power supply quality are due to voltage sags. Therefore, it is very necessary to study the role of PQCC in mitigating upstream voltage sag effects on sensitive loads. In Chapter 4, a three-stage operation scheme of the PQCC is proposed to improve sensitive-load voltage sag ride-through capability. The main strategy is to reduce the fault current contribution from the upstream system, which in turn results in reducing the active power supplied by the faulted upstream system. This is achieved by regulating the DC-link voltage in the PQCC system and allowing the DG to adjust its output power to maintain active power balance.

In all the previous works pertaining to the design of the PQCC [30-36], the authors have strived to realize unbundled power quality service. Unfortunately, the dynamics of the DG and the interactions between the DG and the upstream system have not been studied. Based on the PQCC structure proposed in [30, 31] and by taking the DG in the form of a Solid-Oxide Fuel Cell (SOFC), Chapter 5 describes a more realistic scheme for the PQCC

to operate satisfactorily under both steady-state and system fault conditions. The intention is to exploit the flexibility offered by the converters and the DG in the PQCC.

The analysis in Chapter 5 also shows that due to certain operational constraints of the SOFC, the load ride-through capability under voltage sag condition appears to be rather restricted. In the event of severe upstream sags, the PQCC would need to be disconnected from the upstream grid and be forced to operate in an islanding mode. Such an outcome is not entirely satisfactory. Chapter 6 therefore describes an attempt to extend the work of Chapter 5. The aim is to improve the voltage sag ride-through capability of the scheme. This is achieved by introducing a Series Compensator (SC) into the PQCC structure.

1.2 Major Contributions of the Thesis

As a result of the research work, the following original contributions have been made:

A. ***Derivation of a mathematic model for the UPS-type PQCC***. As can be seen from the literature, several PQCC interior structures and the corresponding operation schemes have been proposed by several researchers [30-36]. However, no general mathematical analysis of the PQCC designs has been reported in the open literature. A mathematical model is valuable for analyzing the interaction between the DG and the upstream power systems and also for designing suitable control system for the PQCC. A detailed derivation of the analytical model of the UPS-type PQCC is described in the thesis. Based on the analysis, both the steady-state DC model and the small signal AC model have been obtained. Thus, the steady-state operating status of the PQCC can be evaluated and the various dynamic responses of power system can be simulated on a computer.

B. ***A system frequency stabilization scheme based on PQCC***. For satisfactory operation of a power system, system frequency should remain nearly constant, which ensures constancy of speed of induction and synchronous motors [47]. Excessive reduction in the frequency could result in high magnetizing currents in the motors and transformers. Conventionally, the power system can rely on the actions of generator speed-governor to minimize frequency variations. However

such restoration method can be unsatisfactory if the speed-governor is of the slow-response electromechanical type. Therefore by taking advantage of the flexibility offered by the PQCC, a new power system frequency variation mitigation scheme is proposed. It attempts to coordinate the operation of the upstream main generator and DG in the PQCC. Based on the detailed analysis of the main generator and the DG models, the proposed scheme is shown to be able to help mitigate the system frequency variation satisfactorily.

C. ***A voltage sag ride-through scheme based on PQCC***. As voltage sag is one of the most devastating power disturbances observed in power systems, many mitigation techniques have been reported [48]. In this project, using PQCC to provide similar voltage sag ride-through capability is investigated. The analysis shows that the range of voltage sags the system can ride through is determined by the current rating of the PQCC input-side inverter. Therefore a three-stage operation scheme is proposed, through incorporating a coordinated control scheme of the inverters and the DG. Stage 1 functions by maintaining the DC-link voltage at the same level as that before the sag. The PQCC input-side inverter would be protected from overloading during the sag mitigation interval. The DG remains undisturbed under this stage. Stage 2 is designed for compensating more severe sags. The purpose is to decrease the input-side inverter current through reducing the active power supplied by the upstream system. This is achieved by reducing the DC-link voltage and forcing the DG to supply the balance of the active power. For even more severe sags which cannot be compensated under Stage 2, the PQCC would reduce the DC-link voltage even further such that the DG supplies the entire protected loads. This is denoted as Stage 3. Under the proposed scheme, the system voltage sag ride-through capability has seen to be enhanced significantly.

D. ***An operational scheme of PQCC to provide unbundled power quality service***. As pointed out early, in designing the PQCC, previous works have paid little attention on the dynamics of DG [30-36], even though the DG are expected to play a central role in the PQCC operation. The unavoidable interactions between the DG and the upstream system should be carefully examined in conjunction with the aim to achieve unbundled power quality supply. In this thesis, detailed

analysis of the DG characteristic is presented by assuming the DG is in the form of a SOFC. Analysis shows that the ability of the PQCC to accommodate instantaneous power demand change is constrained [49]. This is due to limits imposed on the fuel utilization factor of the SOFC. Based on the analysis, a more practical operational scheme of the PQCC system is then proposed. It exploits fully the control of the inverters and the SOFC. Under steady-state, it is proposed that the SOFC supplies all the downstream loads. In the event of an upstream voltage sag, the PQCC is to operate in one of two scenarios in accordance to the severity of disturbances. Under Scenario 1, the PQCC operates in the same manner as that under steady-state. Scenario 2 is designed to mitigate more severe sag effects. Under this Scenario, the PQCC is disconnected from the system and the SOFC supplies all the sensitive loads. The results show that the proposed scheme can indeed provide unbundled power quality service under both steady-state and various fault conditions.

E. ***Design of PQCC-SC***. As briefly described earlier, due to the operational constraints of the SOFC, the voltage-sag ride-through capability of the PQCC system is rather restricted. The PQCC has to be disconnected from the upstream system and is to operate in islanding mode under Scenario 2. Such an outcome is unsatisfactory as it may lead to large surge current during the disconnection/reconnection of the PQCC [50]. There is also a severe constraint on the size of the load that can be supported by the PQCC under the islanding mode. Therefore in another aspect of the investigation, it is proposed that a Series Compensator (SC) be incorporated into the PQCC structure. The aim is to improve the voltage sag ride-through capability offered by the PQCC and at the same time, realize unbundled power quality services. The PQCC-SC scheme has been shown to be particularly effective in overcoming voltage-sag problems.

1.3 Organization of the Thesis

The main theme of the thesis is on the design of the PQCC. In this aspect, Chapter 1 provides a brief summary of the motivation and lists the major contributions made in this project. A review of power quality problems, DG technologies, the concept of unbundled

power quality service and the possible designs of future electric power distribution system, such as Custom Power Park and FRIENDS, are given in Chapter 2. A detailed literature review pertaining to the research area is included.

In Chapter 3, the mathematical model of the UPS-type PQCC is derived. The steady-state operating status and various dynamic responses of the PQCC can then be obtained from the model. In the latter part of Chapter 3, using the PQCC for mitigating power system frequency variations is examined. A dynamic model is developed as an example system that consists of a PQCC connected to an external generating-transmission system. A design method for the closed-loop control systems is also examined, based on frequency response technique.

A new scheme for improving the upstream system voltage sag ride-through capability is proposed in Chapter 4. Analysis is carried out first to develop a simplified DG model. This is followed by a general principal of the proposed three-stage voltage sag ride-through scheme. Based on the PQCC dynamic model derived in Chapter 3, the control system for realizing the proposed scheme is also considered and described.

In Chapter 5, the analysis and design of a realistic PQCC scheme is given. The functional characteristic of the DG, in the form of a SOFC, is examined first. Next, the proposed operational schemes of the PQCC under steady-state, upstream voltage sags or AC interconnection outage states are presented. The intention is to realize unbundled power quality supply. The control system is also designed for the proposed scheme.

Based on the results of Chapter 5, a possible improvement on the PQCC voltage sag ride-through capability is investigated in Chapter 6. The general approach of the scheme is to introduce a series compensator into the PQCC structure. Two possible configurations of the PQCC-SC schemes are examined. This is followed by a detailed analysis and comparison of their respective voltage sag ride-through capabilities.

The main findings of the research and recommendations for future works are given in Chapter 7.

Chapter 2

A Review of Works on Power Quality, Distributed Generation and Unbundled Power Quality Supply Systems

2.1 Introduction

As pointed out in Chapter 1, the design of new forms of electric power distribution system of the future has received increasing attention in recent years [7-11]. The impetus for developing a more reliable and flexible electric energy distribution system can be summarized as follows [8]:

- Unbundled power quality services

There have been considerable changes in today's power systems due to the introduction of deregulation into the electricity supply industries. Power systems that are hierarchically integrated are being separated and open to competition whenever it is shown to be practicable and profitable. The process is called "unbundling", which consists of unbundling of vertically integrated utilities, unbundling of functions within a corporation and service unbundling [1]. As a consequence, the common structure in the deregulated power network is the separation of the generation, transmission and distribution business into different entities. Customers would then be free to select their desired level of services, including power quality. This ability to provide a range of quality of power is becoming a distinct competitive advantage as utilities face increasing competition through the deregulation of the retail markets.

- Impact of distributed generation

Under the circumstance of deregulation, there is a trend for increasing amount of small-scale electrical generators, named as distributed generators (DG), to be installed on the

demand side of network. This is because DGs can be energy-efficient and provide reliable service [12-14]. At present, the cost of DG is still relatively high compared to conventional generation technology. However, the cost is decreasing and a higher awareness by the public on the need to protect the environment makes DG technology a promising one for future power system applications. With DG introduced into the system, however, unexpected power quality problems may occur as the DGs are usually operated independently from the external network [12, 15-20]. For example, there may be degradation in power quality, in the forms of harmonic distortion and transients in the voltage waveforms due to the introduction of the DGs. As the power supplied by DGs may flow reversely when a fault occurs, the demand-supply balance may collapse easily. Effects of DGs on the power system will be discussed in greater details later. The changes introduced by DG technologies suggest the possibility of designing an integrated, customer-centered electrical energy supply system which has the ability to provide extra user services, in addition to supply high-quality power.

- ❖ Change in load characteristics

On the customer side, computerized and power electronic equipment are now essential to successful manufacturing and business applications, such as those found in financial institutions, semiconductor manufacturers and assembly companies. Electrical utilities often encourage this because it reduces the aggregate rate of growth of electrical load and helps defer large investment for network expansions and generation. Accordingly, power quality becomes an increasing concern as these loads are sensitive to power disturbances. The loads can malfunction even due to minor power disturbances and the consequence would be costly to the customers [8]. For example, AC drives inevitably require a diode rectifier, a DC-bus, and an inverter. Such a system is most sensitive to AC voltage sags. These loads themselves are also the source of poor power quality. They generate harmonics, which in turn can pollute the network to a degree no longer acceptable by all customers [6]. As a consequence, this explosive growth of power-quality sensitive computer-based load will result in a growing demand by utility customers for higher quality of power than traditional supply.

On the other hand, under the circumstance of deregulation, the ability of utilities to offer a low cost electricity supply, although at a lower quality level, is an important aspect of

keeping customers satisfied and attracting new customers. In this regard, unbundling the distribution systems to meet the different needs of customers on power quality is an interesting idea. It could form the basis of the design of the future distribution systems. For example, premium quality power supply to sensitive loads would warrant higher tariffs than a thermal load, which is quiet acceptable to receive lower level of quality and reliability of supply in exchange for lower energy costs.

The above reasons clearly show that an unbundled power quality supply system is highly desirable. However there are also concerns on some of the accompanied technical challenges. While this thesis focuses on exploring the development of unbundled power quality supply system, attention is also given to issues associated with power quality and DG technology. Therefore in this Chapter, a general review on power quality and DG technology would be provided before the unbundled power quality supply systems are described.

2.2 Power Quality

As introduced before, power quality problems have attracted increasing attention in recent years. The reasons include [51, 52]: (a) load equipment is more sensitive to power quality variations; (b) some load equipment can also cause voltage disturbances; (c) customers are better informed about power quality disturbances and are challenging the utilities to improve the quality of power delivered; and (d) for a highly integrated network, the failure of any component will have much more impacts on the security of the network.

Power quality is a combination of voltage quality and current quality [51, 52]. It is concerned with deviations of voltage and/or current from the ideal. In an AC system, the ideal voltage and/or current should be a single-frequency sinusoidal wave of constant frequency and constant magnitude. A widely used definition of power quality is:

- The ability of a power system to operate loads without disturbing or damaging them, a property mainly concerned with voltage quality at points of common coupling.

- ❖ The ability of loads to operate without disturbing or reducing the efficiency of the power system, a property mainly, but not exclusively, concerned with the quality of the current waveform.

In most cases, power quality is actually the quality of the voltage, as the power supply system can only control the quality of the voltage. It has little control over the current particular loads might draw.

2.2.1 Power Quality Disturbances

Technical terms and definitions of some main power quality phenomena can be described as follows [51, 52]. Discussion is also given to those disturbances which gain much attention in the present investigation.

Voltage sags: A sag is a decrease to between 0.1 and 0.9 pu in *rms* voltage or current at the power frequency for duration from 0.5 cycles to 1 min. Besides the voltage magnitude reduction during a sag, there is also a phase shift associated with it. Voltage sags are usually associated with system faults but can also be caused by energization of heavy loads or starting of large motors.

Generally speaking, voltage sags could be divided into three-phase balanced sags and unbalanced sags. Balanced voltage sags mainly originate from three-phase faults. A voltage divider model shown in Figure 2-1 can be used to explain the origin of a sag due to a three-phase fault [42]. The figure shows the upstream supply system is represented by a Thevenin equivalent voltage source E with the source impedance Z_s. Z_f is the feeder impedance between the point of common coupling (PCC) bus and the fault location F. The waveforms (single phase) of the source voltage and the PCC voltage, which is also the load voltage, are shown in the figure for a three-phase fault at F. It clearly shows the PCC voltage (V_{sag}) decreases during the fault although the source voltage (E) is constant. V_{sag} would recover to its pre-sag level once the fault is cleared. Unbalanced voltage sags are caused by either single-phase to ground fault or two-phase fault or combination of these. The three phases of unbalanced sags normally show different magnitudes and phase shifts. Furthermore, the three phase quantities of unbalanced sags change according to the winding connection of system transformers and load connections [42]. Symmetrical

components theory is the basic tool for analyzing unbalanced sags [42], which can not only help one to visualize system unbalances, but also facilitates detailed analysis.

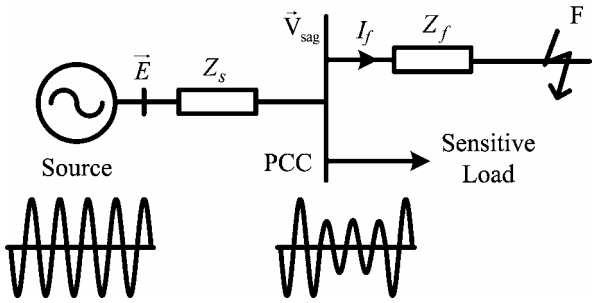

Figure 2-1 Voltage divider model

Voltage sags are the most widespread disturbances affecting distribution systems. These events are random in character. Even a modest reduction in voltage, for example a reduction to 70% on one phase, may trip the supply to an entire production plant. Such sensitive loads includes adjustable-speed drives, process-control equipment and computers, whereby the consequences of equipment dropout are extremely expensive. In general, it is reasonable to consider voltage sags as the cause of 70 – 90% of power quality problems [44-46].

Based on the mechanism leading to the voltage sag problems, measures taken to deal with voltage sags can be generally categorized as follows [48]:

- Reducing the fault-clearing time: This means reducing the sag durations. For example, by installing current-limiting fuses [53] or modern static circuit breakers [50], it is possible to clear fault within half a cycle of the power frequency.
- Changing system design such that a fault leads to less severe sag at the equipment terminals: a common practice is to supply sensitive load with a dedicated feeder or to install current-limiting reactors or fuses in all the other feeders originating from the same bus as the sensitive load. For example in Figure 2-1, a current-limiting fuse should be installed to limit I_f and protect the sensitive load.
- Installing power conditioning devices either at the equipment terminals or at the customer-utility interface: This kind of devices should be able to react within about one-half cycle and provide near-normal power for a few seconds until the supply voltage is fully restored. Various power conditioning devices are available,

including Ferroresonant transformers [54], UPS systems [55], dynamic voltage restorer [56-58], solid-state transfer switch [59] and static var compensator [60] and so on.

- ❖ Improving equipment immunity (voltage tolerance): As most customers rarely have influence on load equipment specifications, the improvement of the equipment immunity solely lies in the hands of manufacturers. Before the equipment is installed, information on its immunity to the voltage quality should be obtained.

Voltage swells: As the opposite of voltage sag, a voltage swell is defined as an increase in *rms* voltage at the power frequency for durations from 0.5 cycle to 1 min. Typical range is between 1.1 and 1.8 pu. Similar to sags, swells are usually associated with unbalanced system fault conditions. Swells can also be caused by switching off a large load or energizing a large capacitor bank. Excessive voltage rise could cause insulation failures and damage equipment.

Voltage interruptions: Voltage interruptions mean the complete loss of voltage of below 0.1 pu on one or more phase. Momentary interruptions are defined as those incidents lasting between 0.5 cycles and 3 s, temporary interruptions have a time span of between 3s and 60 s, and sustained interruptions are those that last for a period longer than 60 s.

Transients: Transients is a sudden, non-power frequency change in the steady-state condition of voltage, current, or both. Broadly speaking, transients can in turn be classified into two categories, *impulsive*, which is unidirectional in polarity (primarily either positive or negative), and *oscillatory*, which includes both positive and negative polarity values. Although most transients are usually generated near the user due to the operation of other equipment, switching operations on the utility network can pose a more serious problem. For example, capacitor switching can lead to transients with a magnitude of 2~3 pu and the high energy levels can considerably shorten the life of surge protection devices.

Harmonics: Harmonics are common power quality issue in the utility industry. It is defined as sinusoidal voltages or currents having frequencies that are multiples of the

fundamental power frequency. Generally harmonics are caused by nonlinear characteristics of power system devices and loads. For example, the switches of power electronics devices in the adjustable-speed drives could inject high order harmonics components into the power system and leads to the distorted waveforms in the current. In recent years, in particular with the growth of non-linear loads such as personal computers and power electronic devices, the combined effects of many such devices can result in harmonic distortion of voltage/current greater than 5~10% levels and exceed the normal industry regulation standards.

Notches: Notching is a periodic voltage disturbance lasting less than 0.5 cycles. Mainly power electronics devices cause notching when the current is commutated from one phase to another during the momentary short-circuit between the two participating phases.

Voltage fluctuations/flickers: Voltage fluctuations are systematic variations in the envelope or a series of random voltage changes with magnitudes that do not normally exceed the range of 0.9 to 1.1 pu. Typical cause of flickers includes the operations of power converters on electrical devices.

Power frequency variations: Power frequency variations are defined as the deviation of the power system fundamental frequency from its specified nominal value. It is directly related to the rotational speed of the generators supplying the system. Under normal conditions, there are slight variations in frequency as the dynamic balance between load demand and generation changes [47]. The size of the frequency shift and its duration depends on the load characteristics and the response of the generators' speed-governor control systems to load changes. On modern interconnected bulk power systems, significant frequency variations are rare. Frequency variations are much more likely to occur for loads in isolated systems that are supplied by generators of relatively low capacity.

2.2.2 CBEMA and ITIC Curves

The well-known Computer Business Equipment Manufacturer Association (CBEMA) curve [61], shown in Figure 2-2, can be used to evaluate the voltage quality of a power

system with respect to voltage interruptions, sags and swells. This curve was originally produced as a guideline to help CBEMA members in the design of the power supply for their computers. Figure 2-2 shows that the curve describing the magnitude of voltage sags/swells against the duration of voltage variations which can be withstood by equipment. The smaller (larger) the magnitude of the sag (swell) is, the less the equipment withstand time is. The region between the two boundaries is the tolerance envelope, within which electronic equipment is expected to operate reliably. The region below the envelope is presumed to cause the load to drop out due to lack of energy. Conversely, the region above the envelope can cause other malfunctions such as insulation failure, over-voltage trip and over-excitation.

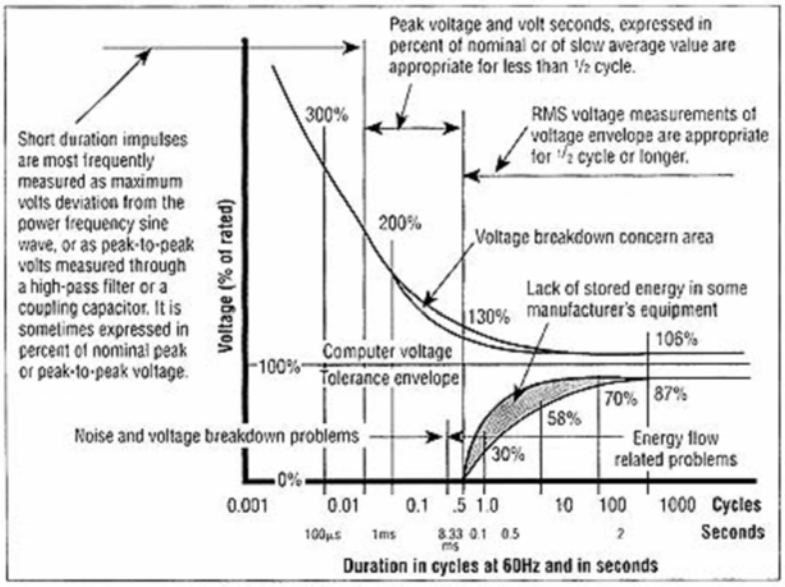

Figure 2-2 CBEMA curve [61]

Due to the prominence of the CBEMA curve among the computer and electronic industries, a revised version of CBEMA curve is developed by the Information Technology Industry Council (ITIC) [62]. See Figure 2-3. The withstand limits at different durations of the ITIC curve are very similar to that of the original CBEMA curve. Under a voltage sag (swell) condition, the withstand time decreases when the voltage magnitude reduces (increases). The main difference is that the ITIC version is piecewise and hence is easier to digitize than the continuous CBEMA curve. In the following Chapters of this thesis where appropriate, the ITI curve would be used to describe the load voltage-sag tolerance characteristic.

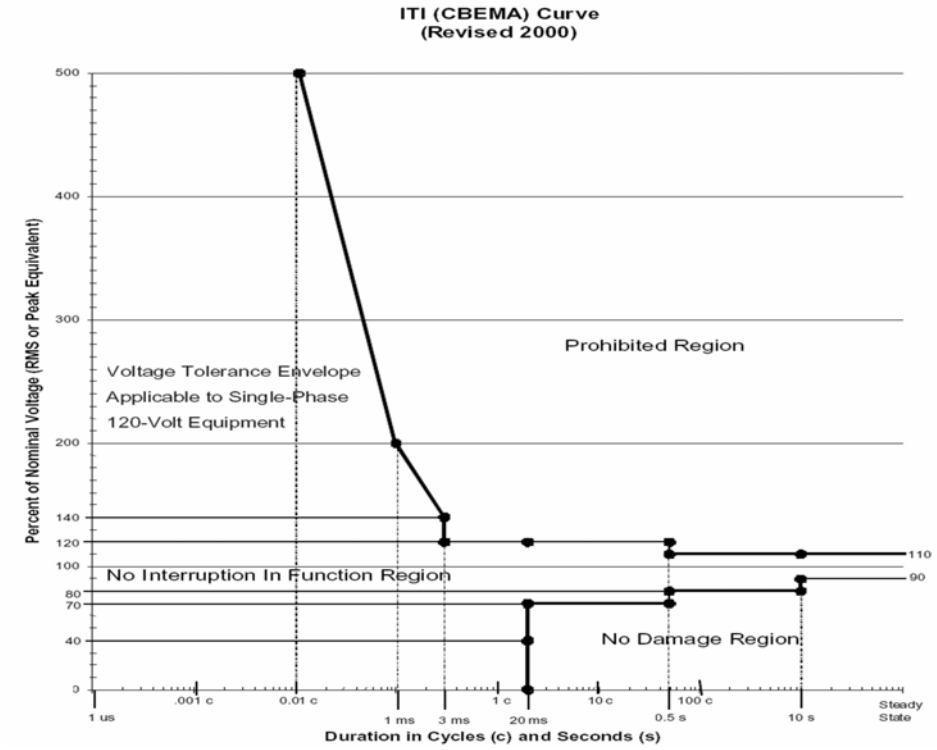

Figure 2-3 ITI curve [62]

2.3 Distributed Generation

In Section 2.2, various power quality problems have been briefly described. As mentioned in Section 2.1, the introduction of DG into the network could bring with it many technical concerns when developing unbundled power quality systems. In this Section, some main types of DGs and their effects on the existing power system will be described.

At present, there is no universally agreed definition of what constitutes DG and how it differs from conventional or central generation. Some common attributes of DG may however be listed [12-14]: (a) DGs are not centrally planned (by the utility); (b) DGs are not centrally dispatched; (c) DGs are normally smaller than 50-100 MW; (d) they are usually connected to distribution system.

Modern electrical power systems have been developed mainly following the arrangement of large central generators feeding electrical power, through generator transformers to a high voltage interconnected transmission network. The transmission system is used to transport bulk power, sometimes over considerable distances. The power is then extracted

from the transmission network and passed down through a series of distribution transformers to final circuits for delivery to customers [12]. The conventional arrangement of a modern large power system offers a numbers of advantages. For example, the interconnection high-voltage transmission network allows generator reserve requirements to be minimized and the most efficient generation schedule to be dispatched at any time. Bulk power can be transported over large distances with limited electrical losses.

However, over the last few years, a number of developments have combined to lead to the increased interest in DG schemes. The main reasons for the greater incentive of introducing DGs include [12-14]:

- The call to reduce gaseous emissions (mainly CO_2): Environmental impact is a major consideration when developing any electrical power scheme. There is a generally accepted concern over gaseous emissions from fossil-fuelled plant. Most governments have programs to support the exploitation of the so-called new renewable energy resources;
- Improve energy efficiency and rational use of energy: Cogeneration or Combined Heat and Power (CHP) schemes can make use of the waste heat from DGs for either industrial processes or space heating. Such schemes effectively increase the overall energy efficiency;
- Deregulation or competition policy: The move to open competitive markets in electricity has increased the uncertainties of power supply. In response to this, there has been a massive increase in demand for backup generation. When conditions are proven to be attractive, the power generated by DGs can also be fed back into the grid;
- Diversification of energy sources: In some countries, fuel diversity offered by DGs is considered to be valuable. In these countries, the shortage of power is so acute that any generation is to be welcomed;
- Additional commercial considerations: These include the availability of modular generating plant, ease of finding sites for smaller generators, short construction times and DG may be sited closer to load, which reduces transmission costs.

2.3.1 Types of Distributed Generators

A brief description of several types of more important DGs will now be included [13].

2.3.1.1 Internal Combustion Engines

For an Internal Combustion Engine (ICE), its fuel is burnt inside the engine and produces expanding gases, which are used directly to provide mechanical power and drive a generator [63]. The main components of a ICE include: (a) Cylinder block, which contains fuel combustion; (b) Pistons, which fit in the cylinder and ride up and down; (c) Valve, through which the air enters the combustion chamber and the products of combustion leave the combustion chamber; (d) Cooling system for heat rejection; (e) Turbocharger or rotary compressors which is used to increase the power density of the engine. Commonly used fuel for ICE includes gasoline, diesel, hydrogen, methane and natural gas. The size of ICE ranges from 10 to 200 kW, with relatively high efficiency of 32 - 36%.

An ICE is a traditional technology for emergency power generation used all over the world. Over 600,000 of such units are installed in the US with combined power capacity of over 100,000 MW [18]. Operating experience of ICE is therefore extensive. The cost of ICE unit is also the least of any DG technology. However, the problems with ICE are the high NO_x emissions and the high noise level [13]. The low frequency noise can be attenuated at low costs with noise abatement material and enclosure. Natural gas ICE generators can offer a solution to the emissions problem but do not solve it entirely.

2.3.1.2 Micro-turbines

Micro-turbine (MT) is a Brayton cycle gas combustion turbine, which produces shaft power using atmospheric air and natural gas fuel [64, 65]. The unit size ranges from 25 to 500 kW. The essential components of a MT power plant include: (a) the turbine engines running on gas fuel; (b) a single or dual shaft permanent magnet (PM) generator to produce electrical power [65], which rotates at a speed range from 50,000 to 120,000 RPM; (c) recuperators (heat exchangers) to achieve high engine efficiency; (d) power conditioners to convert the high frequency AC power provided by the PM generator to

meet the customer needs; and (e) gas boost compressors to provide natural gas fuel at appropriate pressure.

Unlike the traditional backup generators, a MT is designed to operate for extended periods of time and requires little maintenance. It can be used for standby, peak-shaving and co-generation applications. In addition, the fuel-to-electricity conversion efficiency of MT can reach 25 – 30%. The efficiency is even higher if CHP could be applied. MT also generates low air pollution emissions (NO_x emission lower than 7 PPM).

However, MT also shows some undesirable features [13], such as high maintenance cost compared to other technologies which use few moving parts, questionable part load efficiency, limited field experience and it emits high frequency noise which can be relatively easy to control.

2.3.1.3 Photovoltaic

Photovoltaic (PV) systems can directly convert energetic photons in sunlight into DC electricity through the P-N junctions on the surface of the PV cell [66]. Under no-load condition, the typical PV cell open-circuit voltage is 0.5 – 0.6 V. The output power of a PV cell essentially depends on its efficiency, the size of surface area and the intensity of sunlight.

The DC output power of PV systems can be converted into AC using a DC/AC converter which is then used to supply local loads or fed back to the grid. Its power capacity can range from 100 W to 1MW with 6 - 19% efficiency [13]. As sunlight is a diffuse resource, large array areas are needed to produce significant amount of power. However, offsetting this is the zero cost of the fuel itself. Other advantages also include the excellent modularity of the unit and PV is emission-free. As a PV system strongly depends on the weather condition and can only generate power during the day, energy storage devices such as batteries have to be equipped in the PV system to meet the load demand continuously [13]. The batteries need maintenance. The installation cost of a PV system is also high.

2.3.1.4 Fuel cells

A fuel cell (FC) is a device in which hydrogen and oxygen combine without combustion to produce electricity [67-69]. It consists of a pair of electrodes (anode and cathode) and an electrolyte. Typical capacity of a FC at present technological development ranges from 50 kW to 2 MW [13]. The FC generates the truly clean power as its only byproduct is water. Its efficiency is very high (50 - 60%) and modularity is also excellent. However, the cost of a FC is still high and as its fuel is hydrogen, a new fuel distribution infrastructure will be required for widespread installation of FC power plant [13]. As FC would be considered in latter Chapters as a suitable form to be included in the PQCC, a more detailed description of the FC will be given herewith.

The basic features of a fuel cell system are illustrated in Figure 2-4 [69]. As shown in the figure, a fuel cell system is composed of six subsystems: (a) The Fuel Cell Stack, where the anode and cathode chemical reactions occur and electrical power is generated; (b) The Fuel Processor, which converts the hydrocarbon-rich fuel into a hydrogen-rich fuel stream; (c) Air Management, which decides whether the oxygen (typically air) is provided to the FC cathode at low pressure or high pressure. High pressure air leads to higher power density and higher stack efficiency. However, the power required to compress the air to high pressure reduces the net available power from the FC system; (d) Water Management, which manages the water in the FC for a variety of purposes. For example, water should be available from the FC reaction, but it must be removed from the exhaust gas; (e) Thermal Management, which controls the thermal energy released by the FC stack. This thermal energy can be used by the FC itself or transferred externally; and (f) Power Conditioning System, which converts the electricity generated by a FC to current and voltage that is suitable for interconnection to the external electrical system.

Generally, FC is characterized by the type of electrolyte used [67-69]. There are four major types of FC: phosphoric acid, proton exchange membrane, molten carbonate and solid oxide. They have similar structures and chemical reactions. As the Solid Oxide Fuel Cell (SOFC) will be the type considered in this research, it is the focus of the following paragraph.

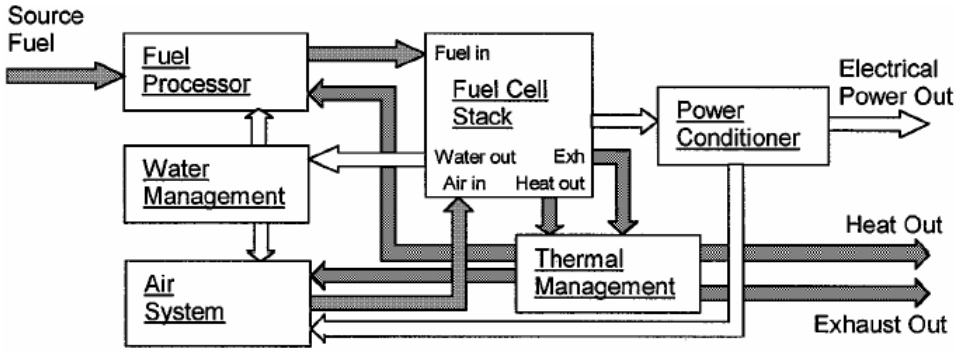

Figure 2-4 Schematic fuel-cell system configuration [69]

SOFC is primarily designed for medium or large-scale stationary power generation applications. A solid ceramic material is used as the electrolyte at operating temperature of 800 – 1000 °C. The basic components of a SOFC fuel stack can be illustrated using the schematic diagram of Figure 2-5 [69]. Hydrogen fuel is supplied to the anode, where the fuel is oxidized, generating electrons (e^-), which travel through the external circuit. At the cathode, the oxygen, which is normally air, is reduced, consuming the electrons from the external circuit. Oxygen ions (O^{2-}) travel through the electrolyte to balance the flow of electrons. DC current (I_{FC}) in the external circuit connected across the two electrodes is generated due to the releasing of the electrons (e^-) at the anode. The anode and cathode reactions of are [67-69],

$$\begin{aligned} &\text{Anode:} \quad H_2 + O^{2-} \rightarrow H_2O + 2e^- \\ &\text{Cathode:} \quad \frac{1}{2}O_2 + 2e^- \rightarrow O^{2-} \end{aligned} \tag{2.3.1}$$

The ideal performance of a fuel cell is determined by the cell open-circuit voltage level that it can theoretically produce under given temperature and pressure. This voltage is defined by the well-known Nernst equation [67, 68]. The Nernst equation for SOFC is

$$E = N_0 E_0 + \frac{N_0 RT}{2F} \ln\left(\frac{p_{H_2} p_{O_2}^{0.5}}{p_{H_2O}}\right) \tag{2.3.2}$$

where E_0 is the EMF associated with the reaction-free energy of a cell at standard pressure, N_0 is the number of stack cells in series. The parameter R is the gas constant (8.31 J/mol°K), T is the SOFC operating temperature typically in the range of 800 to 1000°C, F is the Faraday constant (96487 C/mol), p_{H_2}, p_{O_2} and p_{H_2O} are the reactant partial pressures of hydrogen, oxygen and water respectively. Interested readers can refer to [67, 68] for the detailed derivation of the Nernst equation. Note that (2.3.2) shows that

the theoretical voltage *E* generated by the SOFC can be improved by operation at higher pressures for a given temperature.

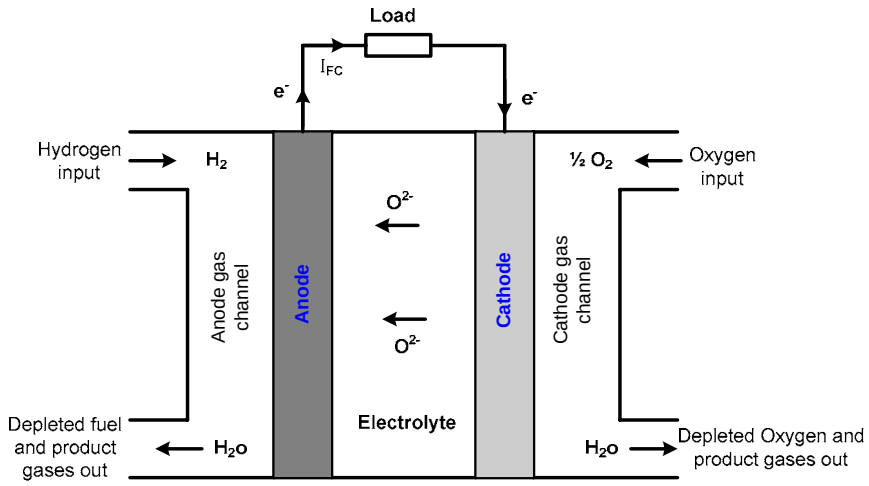

Figure 2-5 Basic SOFC electrode reaction [69]

2.3.2 Technical Impacts of DGs on Distribution Systems

Modern distribution systems have been designed to accept bulk power at the bulk supply transformers and then re-distribute it to customers. Thus the flow of both real and reactive power is from the higher to the lower voltage levels. However, with significant penetration of DGs into the network, power flows may be reversed. The distribution network is no longer a passive circuit, but an active one in which the power flows and voltages are determined by DGs as well as the loads. The change in real and reactive power flows caused by DGs has important technical and economic implications. In this Section the main technical impacts of DGs [12, 15-20] on the distribution system are described using an example distribution system shown in Figure 2-6. It consists of a radial upstream system where the DG is connected to the distribution network.

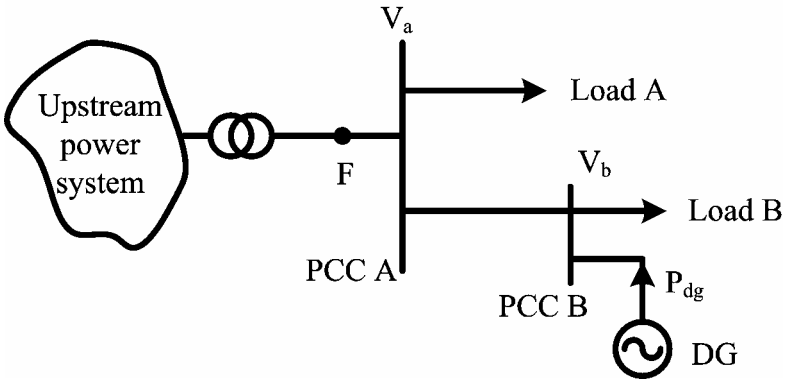

Figure 2-6 An example distribution system

❖ Network voltage profile changes

Normally, the voltage profile of a radial distribution system gradually drops along the distribution lines. For example in Figure 2-6 and without the DG, $V_a > V_b$. When a DG is installed at the bus PCC B, it can have positive impacts on the control of V_b by enabling reactive power compensation if the DG output is allocated appropriately [17]. Conversely, if the output power of the DG (P_{dg}) flows reversely, it can cause under/over-voltage in the network.

❖ Increase in network fault levels

The DG reduces the equivalent Thevenin impedance of the network and increases its fault level. Returning to Figure 2-6, suppose a fault occurs at F. The fault current at F would increase due to the introduction of the DG, which in turn increases the network fault level. In urban areas, often the existing fault level approaches the rating of the switchgear. Therefore the increase in fault level would require the upgrade of the distribution network switchgear. This can be an extremely expensive exercise. Therefore the increase in fault level can be a serious impediment to the introduction of the DG into the network.

❖ Power quality

The main potential impacts of DGs on network power quality are voltage flicker and harmonic voltage distortion. The DG can cause voltage flicker on the network caused by current changes during the connection and disconnection of the generators. Variations in its output power due to fluctuations of energy resource can also cause voltage flicker, such as the case of wind turbines and photovoltaic. Similarly, incorrectly designed or specified DG with power electronic interfaces may inject harmonics which can lead to unacceptable network voltage distortion. Furthermore, if large numbers of single-phase generators are connected in the future network, then voltage unbalance may become significant. Generally, DGs may improve network power quality by effectively increasing the short-circuit level of the distribution network or deteriorate the power quality by introducing distorted current.

❖ Protection

A number of different aspects of DG protection can be identified: (a) protection of the generator equipment from internal faults: it is quiet straightforward and techniques used to protect any large motors are usually quite adequate; (b) protection of the faulted distribution network from fault currents supplied by the DG. It relies on the distribution network protection to clear the fault and isolate the DG. Sequentially the DG will be

tripped by its own protection; (c) anti-islanding or loss-of-mains protection: a relay is required to trip the DG when it becomes islanded. DGs may also affect the operation of existing protection systems of distribution network if they contribute towards the flows of fault current which were not expected when the protection was originally designed.

- ❖ Stability

For DGs which only generate relatively small amount of power from renewable energy sources, considerations of generator transient stability tend not to be of great significant. However, if a DG is viewed as providing support for the power system, its transient stability becomes of considerable importance. For example in Figure 2-6, if the DG can supply relatively large amount of power in comparison with the upstream central generator, then the tripping of the DG may cause significant system frequency deviation, quite apart from the significant impact this will have on the voltage level.

- ❖ Network operation

DG also has important impacts on the operation of the distribution network as circuits can now be energized from a number of points. Therefore more sophisticated protective schemes for isolation and earthing must be designed and implemented. They are needed to protect not only the personnel doing maintenance working on the line, but also the loads connected to them. For example in Figure 2-6, if there is maintenance work on the line between the PCC A and B, it must ensure that both the upstream system and the DG are safely isolated. Also when a DG is connected to a network, it may become more difficult to arrange for outages for planned maintenance.

2.4 Unbundled Power Quality Supply Systems

As introduced in Section 2.1, recent trend toward the deregulation of the electricity utility industry will certainly change the structure of electric power systems in the future. Much related to the deregulation, Section 2.2 shows that power quality has also become an increasingly important issue. Utilities are being challenged to allow customers to choose the level of power quality according to their individual needs. Installation of DGs on the customer side is yet another significant change as a result of the deregulation. However, DGs bring on board a much larger number of technical challenges for the successful operation of the distribution systems, as described in Section 2.3. With such

developments, the design of new forms of distribution system has gained much attention as a fruitful area for further work by many researchers. The focus of their work is to realize unbundled power quality services and at the same time, attempt to overcome the technical problems caused by DGs. In this Section, some conceptual designs of future electric distribution system would be described.

2.4.1 Custom/Premium Power Park

The concept of Custom Power was introduced by N. G. Hingorani [21-24]. Similar to the Flexible AC Transmission Systems (FACTS) for transmission systems, the term Custom Power pertains to the use of power electronic controllers for distribution systems. Whereas FACTS improves the reliability and quality of power transmission by simultaneously enhancing both power transfer volume and stability, Custom Power improves the quality and reliability of power delivered to customers. Custom Power devices, or controllers, are devices that include static switches, inverters, injection transformers, and/or energy storage modules that have the ability to perform current interruption and voltage regulation functions in a distribution system. Under this scheme, a customer receives a prespecified quality power. This prespecified quality may contain a combination of specifications of the following [70]: (a) Frequency of rare power interruptions; (b) Magnitude and duration of over- and under-voltage within specified limits; (c) Low harmonic distortions in the supply voltage; (d) Low phase unbalance; (e) Low flicker in the supply voltage; and (f) Frequency of the supply voltage within specified limits.

2.4.1.1 Main Custom Power devices

The power electronic controllers that are used in the Custom Power solution can be network reconfiguring type or compensating type [70-74]. The network reconfiguration devices are essentially switchgear, including current limiting, current breaking and current transferring devices. The solid state or static versions of the devices include Solid State Current Limiter (SSCL), Solid State Breaker (SSB) and Solid State Transfer Switch (SSTS). The compensating devices either compensate a load, i.e., correct its power factor, unbalance or improve the quality of the supplied voltage. These devices are either

connected in shunt, in series, or a combination of both. The devices include Distribution-STATCOM (DSTATCOM), Dynamic Voltage Restorer (DVR) and Unified Power Quality Conditioner (UPQC).

Solid State Current Limiter (SSCL) [70, 75]: The schematic diagram of a SSCL is shown in Figure 2-7 [70]. It consists of a pair of opposite-poled switches in parallel with the current limiting inductor L_m. The bidirectional switch is usually made of GTOs or IGBTs which have fast current interruption capability. In addition, a series *RC* combination (resistance R_m and capacitance C_s) is connected in parallel with the opposite poled switch. This *RC* combination constitutes the unpolarized snubber network. The current limiter is connected in series with a feeder such that it can restrict the current in case of a downstream fault. Under normal state the opposite poled switch remains closed. These switches are opened when a fault is detected such that the fault current flows through the current limiting inductor.

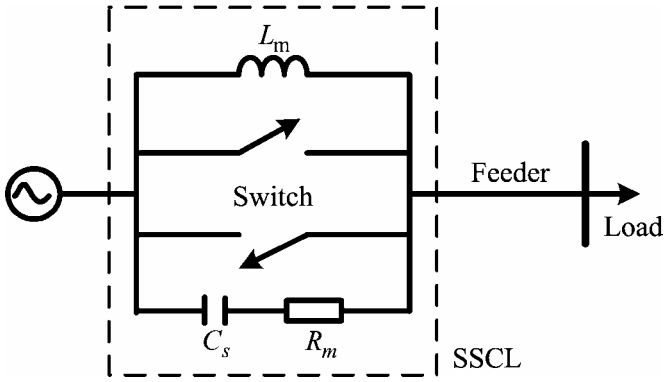

Figure 2-7 Schematic diagram of a SSCL [70]

Solid State Circuit Breaker (SSCB) [70]**:** a SSCB has almost the same topology as that of an SSCL except that the limiting inductor is connected in series with an opposite poled thyristor pair. The thyristor pair is switched on simultaneously as the bidirectional switch is switched off once a fault is detected. This will force the fault current to flow through the limiting inductor. The thyristor pair is blocked after a few cycles if the fault persists. The current through the thyristor pair will cease to flow at the next available zero crossing of the current. There still may be a small amount of current flowing to the fault through the snubber circuit. However, the magnitude of this current is small and can be easily interrupted by a mechanical switch which is always placed in series with the SSCB.

Solid State Transfer Switch (SSTS) [59, 70]**:** The schematic diagram of a SSTS is shown in Figure 2-8 [70]. This device is used to transfer power from the primary feeder to the alternate feeder in case of a voltage sag/swell or fault in the primary feeder. An SSTS contains two pairs of opposite poled switch S_{w1} and S_{w2}. Suppose the primary feeder supplies power to the load. This is done through switch S_{w1} while S_{w2} remains open. If a sudden voltage sag occurs in the primary feeder, S_{w2} is switched on and S_{w1} is switched off such that the load is supplied through the alternate feeder.

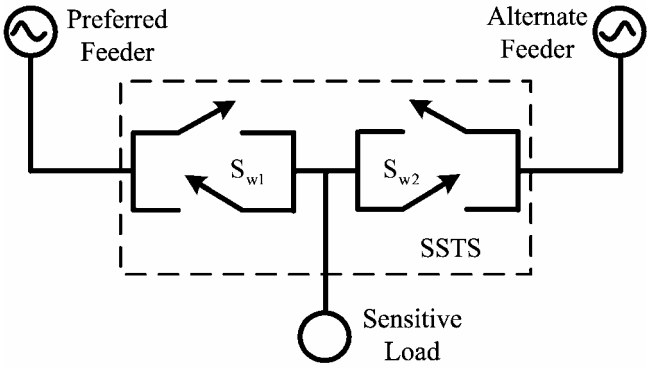

Figure 2-8 Schematic diagram of SSTS [70]

Distributed-STATCOM (D-STATCOM) [70, 76]**:** A basic configuration of D-STATCOM is shown in Figure 2-9. The main component of D-STATCOM is a PWM-based three-phase voltage source converter, which can be controlled to synthesize the injection voltage/current to mitigate current disturbances. The filter is also necessary since it filters out the high-order harmonics produced by the converter. The main functions of the shunt injection transformer are current boosting and electrical isolation. The energy storage device is necessary to provide the required energy for the compensation. It would be made up of either ultra-high energy density capacitors (e.g. capacitors using double layer technology), or advanced batteries, or flywheel energy storage or superconducting magnetic energy storage. The primary aims of D-STATCOM in a distribution system are to mitigate [70]:

- The effect of poor load power factor such that the current drawn from the source has a near unity power factor;
- The effect of harmonic contents in loads such that current drawn from the source is nearly sinusoidal;
- The DC-offset in loads such that the current drawn from the source has no offset;

- The effect of unbalanced loads such that the current drawn from the source is balanced.

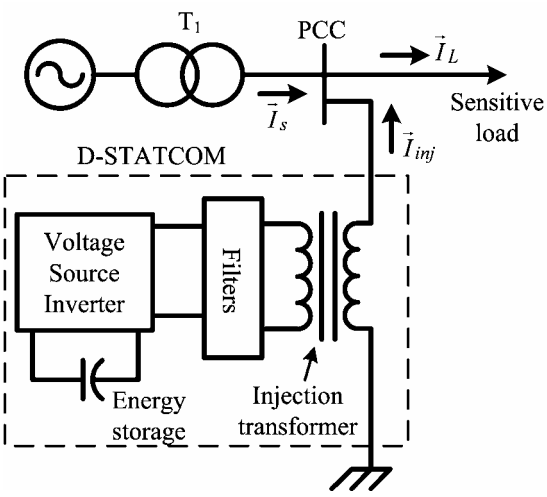

Figure 2-9 Simplified single-phase diagram of D-STATCOM

D-STATCOM is also used to eliminate unbalance, harmonics and flicker in the voltage. Generally a D-STATCOM operates in current control mode [70]. Its ideal behavior can be represented by a current source. As shown in Figure 2-9, if the sensitive load current $\vec{I}_L$ is nonlinear and unbalanced, the current $\vec{I}_s$ flowing through the feeder will also be unbalanced and distorted. To alleviate the problem, the compensator must inject a current such that $\vec{I}_s$ contains only the fundamental frequency component and has only positive sequence. That is $\vec{I}_L = \vec{I}_s + \vec{I}_{inj}$. $\vec{I}_{inj}$ will contains all the harmonics in $\vec{I}_L$ and the unwanted components.

Dynamic Voltage Restorer (DVR) [56-58, 70]: A DVR is used to protect sensitive loads from a sag/swell or disturbance in the supply voltage. By inserting a voltage of required magnitude and frequency, the DVR can restore the load voltage to the desired amplitude and waveform even when the source voltage is unbalanced or distorted. The DVR has been proven to be very effective in overcoming voltage sag problems [56-58]. As it is the device which would be considered in Chapter 6, its operations will be explained in greater detail as follows.

A possible configuration of a three-phase DVR is shown in Figure 2-10. The main functional components of a DVR include [70]:

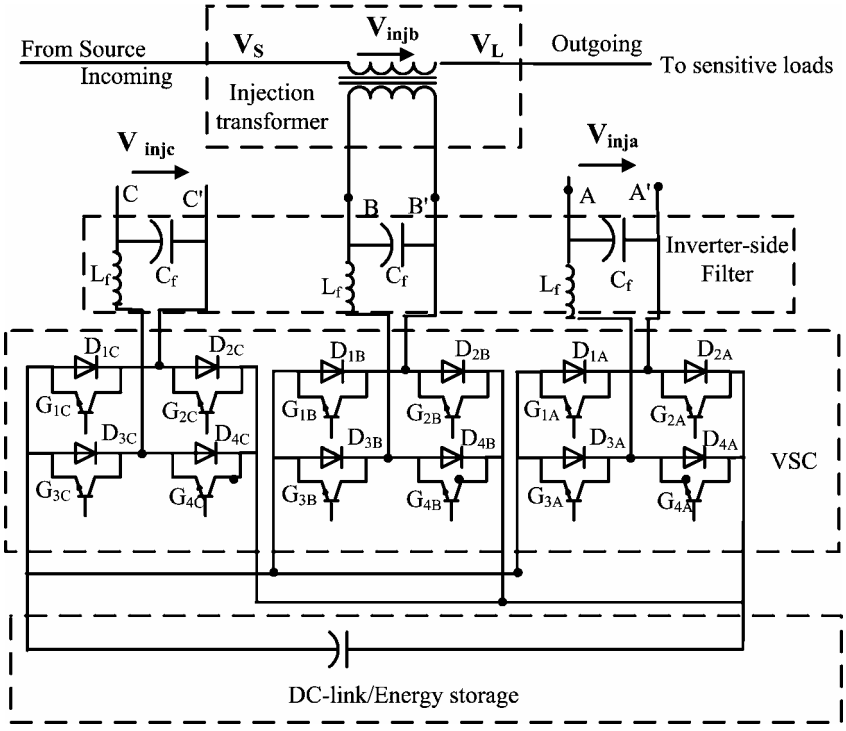

Figure 2-10 A possible structure of DVR: showing the injection voltage in phase b

❖ Voltage Source Converter (VSC)

In a DVR, a three single-phase full-leg PWM controlled VSC is used. It consists of four pairs of IGBT and diode as shown in Figure 2-10. It is capable of injecting a set of three-phase AC output voltages (V_{inja}, V_{injb}, V_{injc}) which is in series and synchronized with the upstream distribution feeder voltages V_s. The amplitude and phase angle of the injected voltage are variable, thereby allowing control of the real and reactive power exchange between the DVR and the distribution system.

❖ Harmonic Filter

The switching of the VSC will generate a large amount of high-order harmonics. Therefore a filtering system is necessary to offer a clean injected voltage on the primary-side of the injection transformer. Generally, the filter system will consist of a *LC* section. The values of the filter components will be dependent of the switching frequency of the VSC. The filtering system can be placed either on the primary side (line-side filter system) or on the secondary side (inverter-side filtering system).

❖ Energy Storage Device

The energy storage device would act as a buffer by supplying energy to, or absorbing energy from the external system. The load ride-through capability afforded by the DVR is

to a large extent determined by the energy storage capacity provided for. For most DVR applications, the energy storage device can be an electrolytic capacitor bank.

- Injection Transformer

The injection transformer is used to boost and couple the injection voltage generated by the VSC to the incoming supply voltage. The winding ratio of the transformer has to be selected to enable the VSC to compensate for the deepest voltage dips at the minimum DC-link voltage.

Although not shown in Figure 2-10, a control and protection system is needed for the proper operation of a DVR. Once a voltage disturbance is detected, the control system of the DVR will decide the magnitude and phase of the injection voltage. It requires the DVR to possess quick response characteristic and guarantee a high quality waveform.

At present, there are three known voltage restoration strategies to compensate for voltage disturbance [77-79]. They are called pre-sag compensation, in-phase injection and energy-saving injection.

The pre-sag compensation strategy [77, 78] is to compensate for the difference between the sag/swell and pre-sag/swell voltages by injecting AC voltage in phase with the incoming pre-disturbance three-phase network voltages. This strategy applies to both balanced and unbalanced voltage disturbances. The restored voltage will be theoretically the same as the pre-disturbance voltage and thus is superior to other methods from the perspective of voltage restoration. However, this method is based on the assumption that the capacity of energy storage device and the voltage injection capability of a DVR are sufficiently large. Furthermore, if there is a phase angle jump when the sag/swell happens, the pre-sag compensation may cause a second phase angle jump.

The second strategy is the in-phase injection [77]. The generated DVR voltage is always in phase with the measured supply voltage, regardless of the load current and the pre-disturbance voltage. This is the most simple restoration scheme. It is especially suitable for single-phase DVR, since it would ignore the phase shift of the supply voltage. For three-phase system, the situation is quite different because three-phase disturbances could be unbalanced, particularly when the disturbances have different phase shift on each

phase. If the in-phase compensation is adopted, the three-phase compensated voltages are likely to remain unbalanced unless the phase shift has been taken into account.

Notice that the first two restoration schemes are only suitable if the capacity of the energy storage device of the DVR is sufficiently large and no limit is placed on the injection voltage magnitude. Energy-saving compensation strategy [79] therefore tries to fully utilize the capability of the energy storage. It uses information about the load current to minimize the depletion of the stored energy while maintaining the load voltage magnitude constant. The method is very attractive since it increases the ride-through ability of the DVR. However this will cause a voltage phase shift at the load terminals.

Unified Power Quality Conditioner (UPQC) [70, 80]: A UPQC is a device that is similar in construction to a Unified Power Flow Conditioner (UPFC). A UPFC is used in a power transmission system to perform shunt and series compensation at the same time [81]. Similarly a UPQC can also perform both the tasks in a distribution system. One schematic diagram of UPQC is shown in Figure 2-11 [80]. It uses two voltage source inverters (VSI) that are connected to a common DC energy storage capacitor. One of the VSI is connected in series with the AC line while the other is connected in shunt with the same line. A UPQC combines the operations of a D-STATCOM and a DVR together. The series component of a UPQC can insert voltage (V_{inj}) to ensure that the load terminal voltage is balanced and free of distortion. Simultaneously, the shunt component of the UPQC can compensate for the distorted load current (I_L) such that the upstream source current (I_s) is balanced sinusoids. Both these objectives must be met irrespective of unbalance or distortion in either source or load side.

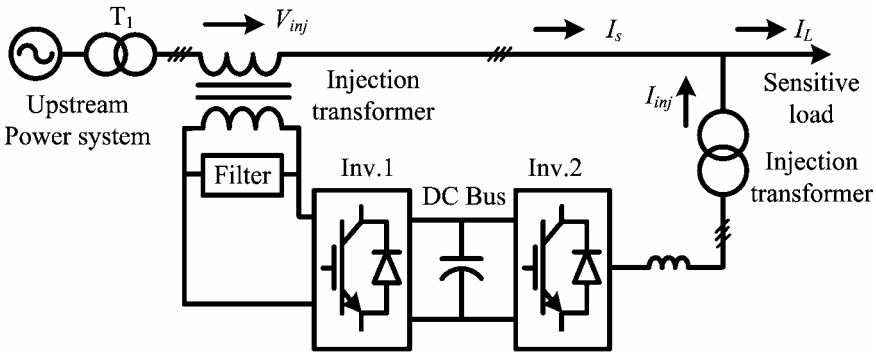

Figure 2-11 Simplified single-phase diagram of UPQC [80]

2.4.1.2 Concept of Custom Power Park [22, 70, 82]

The so-called "Custom Power Park" is proposed to be installed on the demand side of the network. Power quality can be improved through the application of Custom Power devices described earlier, according to customer needs. By integrating multiple power quality technologies and utilizing a communications network between the devices, this concept is distinguished from previous technologies which rely only on stand-alone pieces of equipment.

One of the conceptual system structures of "Custom Power Park" is shown in Figure 2-12 [70]. The Park is extended for such customers in IT industry, semi-conductor manufacturing, where highly reliable, premium power is necessary. As shown in the figure, electrical power to the park is supplied through two feeders from two independent substations. The Park is equipped with a DVR, DSTATCOM, as well as standby generator (DG). As shown in Figure 2-12, unbundled power quality services are available. Three levels of power quality supplies have been provided in the example system, denoted as Grades A, AA and AAA [22, 70].

Grade A: This is the basic value-added power at the Park. Since the transfer switches (SSTS) protect the incoming feeders, the reliability of the power supply is usually superior to normal utility supply. In addition, this grade has the benefit of low harmonic due to the compensations of the D-STATCOM.

Grade AA: This includes all the features of Grade A. In addition, it receives the benefit of the standby generator. The generator can be brought into service in about 10-20 seconds in case of a serious emergency such as power failure in both feeders.

Grade AAA: over and above Grade AA, Grade AAA receives the benefit of DVR, which injects the right amount of voltage (including harmonics) to the AAA feeder voltage to ensure virtually sag-free, interruption-free and harmonic-free voltage to the customer.

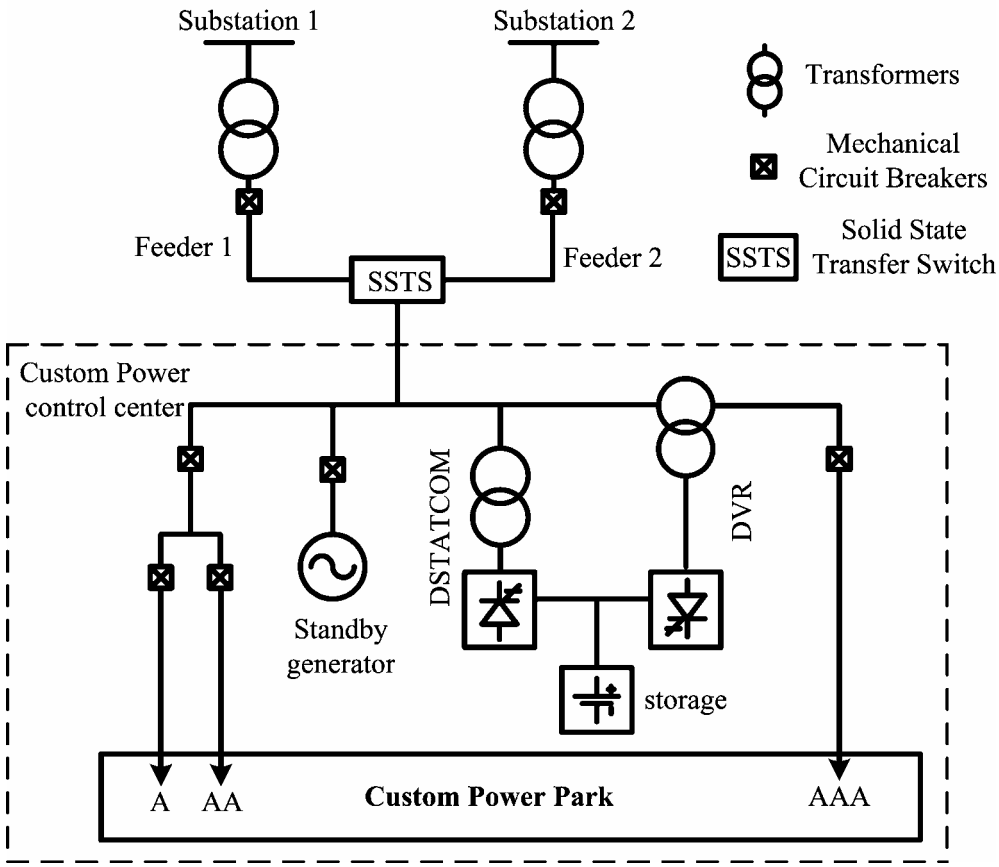

Figure 2-12 A Custom Power Park [70]

Under normal operating conditions, the standby generator stays off and is disconnected from the bus. Customers of both Grades A and AA receive the same service. When both feeders are lost, the loads of Grade A would be removed through the opening of the appropriate circuit breakers. However, the loads of Grade AA are supplied by the standby generator though it will lose power over the interval when the generator switches on. The Grade AAA customers are not affected by the lost of feeders as their voltage is maintained by the combination of DVR, D-STATCOM and the energy storage device until the standby generator comes into service. Since the standby generator has to be started instantaneously, brought to speed and synchronized within less than 20 seconds, it must be driven by a diesel or a gas turbine.

Due to the increased demand for high quality electrical power, Custom Power technologies have been rapidly developed to meet this demand. Various Custom Power devices have been proposed and installed to provide protection against power disturbances. For example, in Ohio, the Delaware Premium Power Park, which is the

world's first distributed Power Quality Park, is being developed since 1999 by American Electric Power (AEP), S&C in conjunction with EPRI. The researchers spent more than two years to monitor power and identify the range of the power the customers need. Recently some of the simulation results pertaining to the proposed Power Park have been reported [82, 83]. Future work would include implementation of the scheme and monitoring its performance. More investigations and applications of Custom Power technologies have also been reported in [70, 84]. However, it is to be realized that the use of Custom Power device is still in its infancy: there is limited experience from Custom Power equipment installations and operations.

2.4.2 FRIENDS

Flexible, Reliable and Intelligent Electric Energy Delivery System or FRIENDS is also one possible form of electric power delivery system for the future [26-29]. It was proposed by Nara and Hasegawa in 1994. By using DG, demand side control, power electronics technologies, high level communication technologies and dispersed intelligent facilities, FRIENDS is intended to achieve the following functions [28]: (a) Flexibility in reconfiguration of the system in normal and fault states; (b) High Reliability in power supply; (c) Multi-menu services or customized power quality services to allow consumers to select the quality of electric power and supplier; (d) Load leveling and energy conservation; (e) Enhancement of information services to customers; and (f) Efficient demand side management.

The general concept of FRIENDS is shown in Figure 2-13 [37]. Compared with the Custom Power Park concept, FRIENDS is of a more global concept. Whereas Custom Power Park is designed toward a local system, such as industrial and commercial application, it is seen from Figure 2-13 that FRIENDS is developed to integrate the whole network operation. In FRINEDS, through the so-called "Power Quality Control Centers" (PQCCs), each consumer can select the quality of electrical power independently. Similar as the Custom Power Park concept, PQCC is essentially a power quality enhancement facility installed between the high voltage distribution lines and the customers. It is equipped with static switches, active filters and other power electronics devices. The

distributed small scale generation resources and energy storage systems are also allocated on the PQCC for high reliability and energy conservation.

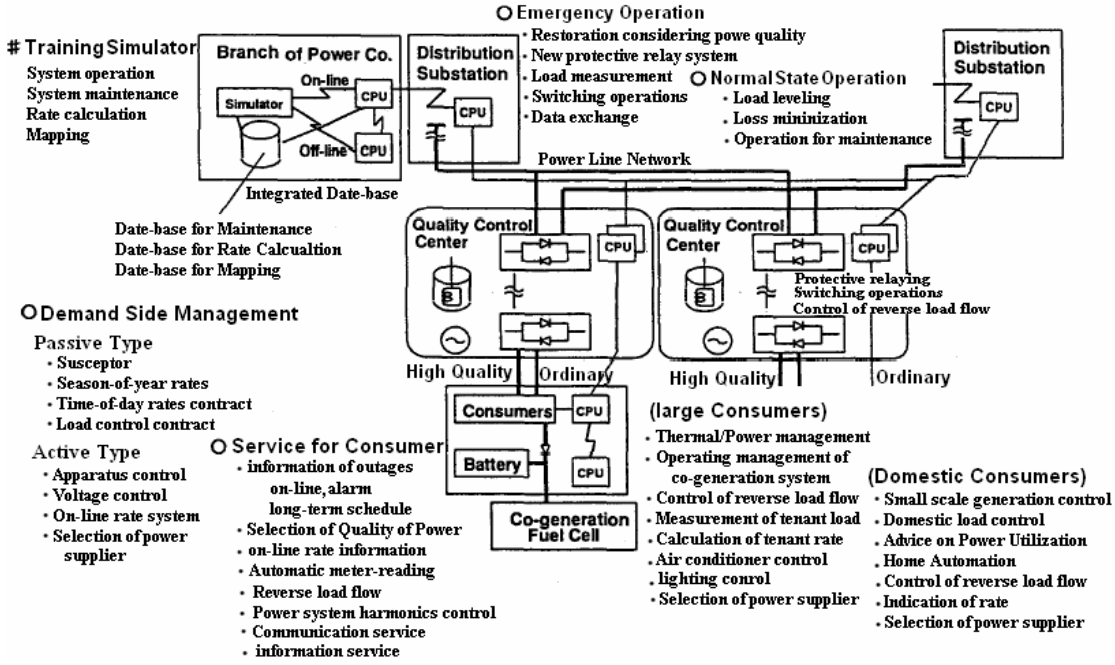

Figure 2-13 General concept of FRIENDS [37]

To operate the FRIENDS efficiently, the following technologies play important roles [37]: (a) static protection and control apparatus, which manage the operation of the power electronic devices and the DG in the network; (b) micro-computers and/or engineering work stations which are allocated in the system. Their principle functions are summarized in Figure 2-13. It is seen that many new functions and information services are included, which cannot be provided by the existing distribution system; (c) data communication lines, which connect among the computers and supply various types of information services to consumers. Therefore the PQCC is not only a highly sophisticated control center which controls and protects the equipment in the Center, but also an information processing and exchange center between the suppliers and the customers.

An overall conceptual power delivery network structure of FRIENDS is given in Figure 2-14 [37], where a PQCC is represented as a circle. In the figure, one PQCC is supplied from several high voltage distribution substations to enforce supply reliability. This is in the same way as that indicated in Figure 2-13. The system therefore can operate either as a meshed network or as an open loop radial network according to the operating strategy. A

number of static open and closed switches [85, 86] are equipped within the PQCC to establish such flexibility.

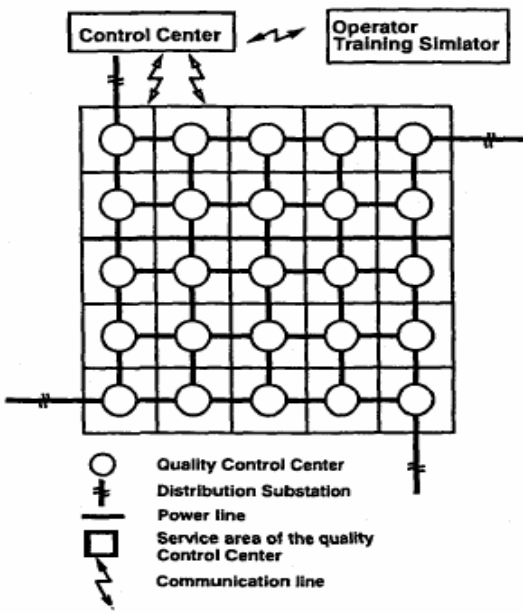

Figure 2-14 Example network structure of FRIENDS [37]

FRIENDS is a good example in realizing an intelligent and flexible distribution system. The PQCC is to be installed at a distribution substation level, and emanating from the station would be feeders, each providing the specific level of power quality. Such system would certainly be feasible if one were to consider the case of an industrial park where the various electrical loads served from this substation would demand different levels of supply quality. For example, for those manufacturing processes where any disruption would incur huge financial losses, the customers would be prepared to pay for the highest quality of power supply for their critical loads, if the utility company can build (or re-build) the network to provide such a service. By the same token, those electrical loads which can accept lower quality supply can be connected to the respective feeders.

Current research topics to realize FRIENDS system include [28]:

- Design of the PQCC. As described above, most of the functions of FRIENDS are to be realized in the PQCC. Therefore the interior structures of PQCC should be carefully designed. Such design work can be divided into three major parts [28]: (a) configurations on both the high-voltage and low-voltage sides; (b) equipment to be installed in the PQCC; (c) the means of delivering unbundled power quality

power. Some basic plans for each of these parts have been proposed [30-36] and the details would be described later.

- Design of the algorithm for the optimization of network planning and operation [37, 38]. As mentioned before, one of the major characteristics of FRIENDS is the ability of varying its network structure by connecting or disconnecting the switches in the PQCC. This function ensures that FRIENDS system can meet the various operating strategies. For example, under normal state, an optimal network configuration can be designed to minimize the distribution losses. Under a contingency, an optimal restoration scheme can be designed such that no line is overloaded and the loads outside the faulted section are supplied without interruption. These issues can be easily formulated as mathematical programming problems and solved by developing computationally efficient control algorithms.
- Demand side prospects of FRIENDS. Under the circumstances of FRIENDS, while the PQCC is of great benefit to customers, the customer behavior also has influence on the overall power system. For example, the customer behavior model is necessary for designing a rate/tariff scheme for FRIENDS. Therefore the behavior of customers and their impact on the overall system must be analyzed. Some possible designs of the customer behavior models for the competitive demand side market have been reported in [39].
- Estimation of power demand by quality level. In order to determine the equipment to be installed in PQCC, it is desirable to estimate the load demand curve under the unbundled power quality environment. A possible way to estimate the load demand curve is to assort the electrical loads into different quality levels and determine what type of apparatuses should be installed in each quality level supply. The authors of [40] have developed a so called bottom-up model to simulate the activities of the household appliances. The accuracy of the model is verified by comparing the simulation results with the actual measured data. Such analysis is useful for designing a highly intelligent control scheme of FRIENDS.

As a potential candidate of the fundamental system technologies needed for the future power distribution system, much research work has to be carried out to realize FRINEDS. The overall advantages of FRIENDS over the existing system, including environmental and economic factors, must be quantified. The major apparatuses to be installed in PQCC

are being developed due to the development of Custom Power and FACTS. Therefore in some regions where the basic of power supply is insufficient, PQCC may be installed for the gradual development towards the form of FRIENDS. The early stage of PQCC would be similar to the idea of Custom Power Park.

2.5 Possible Designs of Power Quality Control Center

The most significant feature of FRIENDS is the new conceptual facility called PQCC. As pointed out previously, the PQCC is installed between loads and distribution substations. In the context of FRIENDS, it permits switching between the multiple distribution network lines fed to the PQCC so as to reduce power losses in the distribution network and ensures continuity of supply during network faulted state. PQCC is also to provide unbundled power quality services for customers connected to it.

The main components of PQCC include [33]:

- Thyristor switch: it is used for achieving optimal network operation by reducing losses in distribution lines. Using seamless switching control method for the switch, it can avoid interruptions of power supply during upstream disturbances.
- Voltage regulator (DVR, D-STATCOM): DVR can maintain the load voltage by inserting a voltage of required magnitude and frequency during upstream disturbances. D-STATCOM compensates the lines voltage fluctuations or flickers.
- Uninterrupted Power Supply (UPS): UPS is for short term outages, typically for duration of less than 5 minutes.
- Distributed Generator (DG): DG can be used as a co-generator or for emergency situation. As a co-generator, it is online at all time. For emergency generation, it starts to operate only after the UPS is no longer able to support the loads.
- Active Filter (AF) [87]: it compensates for unbalance loads and harmonics produced by loads.

There are many ways in combining the above devices to form a PQCC. The optimal combination should be selected by considering its location, costs and functions. Hitherto, several possible structures of PQCC have been proposed [30-36]. In conjunction with the

PQCC structures, the authors of [30-36] have also used the following terms to describe power quality levels: normal or ordinary quality, high quality power and super premium power. These are defined as follows:

- Ordinary Quality (OQ): the PQCC does not improve quality. The quality supplied to loads is the same as that in the upstream system. The advantage of this is lower tariff for customers.
- High Quality (HQ): Voltage disturbances are corrected in the PQCC using some voltage regulating devices. For example, voltage sags of larger than 70% nominal magnitude, and for up to one second are compensated, whereas sags of higher severity are not compensated.
- Super Premium Quality (SP): Not only all sags but also outages are compensated for by the PQCC using energy storage devices and local generators.

2.5.1 PQCC Structures: Low Voltage Side

2.5.1.1 PQCC for single-phase loads

The simplest circuit, which enables the PQCC to deliver different power quality levels to single-phase loads, is shown in Figure 2-15 [30, 33]. The system can provide three levels of power quality to single-phase loads using the three-phase four-wire AC system. As shown in the figure, a single-phase UPS is used on the SP load line, which can provide continuous power supply even when there is total power loss in the primary feeder. A single-phase voltage regulator, such as a DVR, is used on the HQ load line. It can compensate part of upstream voltage sags. OQ load line has the same quality as the primary feeder. Although it is not shown in the figure, DG can also be installed in the PQCC. It can be connected to the UPS and the voltage regulator to supply part of the energy needs.

It is also seen a three-phase inverter is used in the PQCC. Its main function is the same as an active filter: to compensate for load unbalance between the three phases and to mitigate the harmonics generated by the non-linear loads. The current in the primary side of the upstream transformer is therefore balanced and sinusoidal. An energy storage device is connected to the DC-link of the inverter, which is in the form of a capacitor or a

battery. This energy storage device is able to absorb the reverse power flow from the DG under system faulted state.

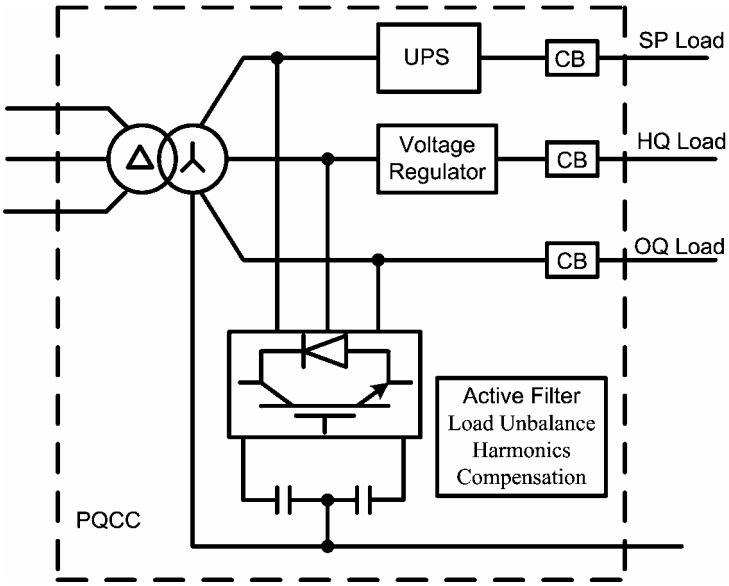

Figure 2-15 Configuration of a PQCC for single-phase load [33]

2.5.1.2 DC-type PQCC

The PQCC configuration for DC loads is shown in Figure 2-16 [30, 34]. The system has three DC-loop lines: the high quality loop, the normal quality loop and the ground loop.

On the high quality line, the loop is connected to the upstream system using the bi-directional rectifiers, which can compensate voltage fluctuations in the DC loop and improve the power factor of the upstream AC system by controlling the upstream current. DGs, such as fuel cells and micro-turbines, are installed on the high quality line. Their output powers are to stay constant. Voltage interruptions and sags which occur on the high quality loop therefore can be compensated by these DGs. However, on the normal quality loop, in order to reduce costs, the line is connected to the upstream system using the diode rectifiers with the Power-Factor-Corrector (PFC). The PFC consists of a GTO and a diode. By switching the GTO at constant duty ratio, power factor of the AC source can be improved and the DC voltage can also be kept constant. DGs installed on the normal quality loop are wind turbines and PV cells, whose output power vary due to the energy source fluctuations.

Characteristics of this system are [34],

- DGs can be installed easily using a DC/DC converter which utilizes less switching devices than ac/dc converters.
- Two kinds of voltage levels can be selected. For example there are 2 kV and 4 kV in Figure 2-16.
- This system is composed of only three lines to deliver two qualities of power.

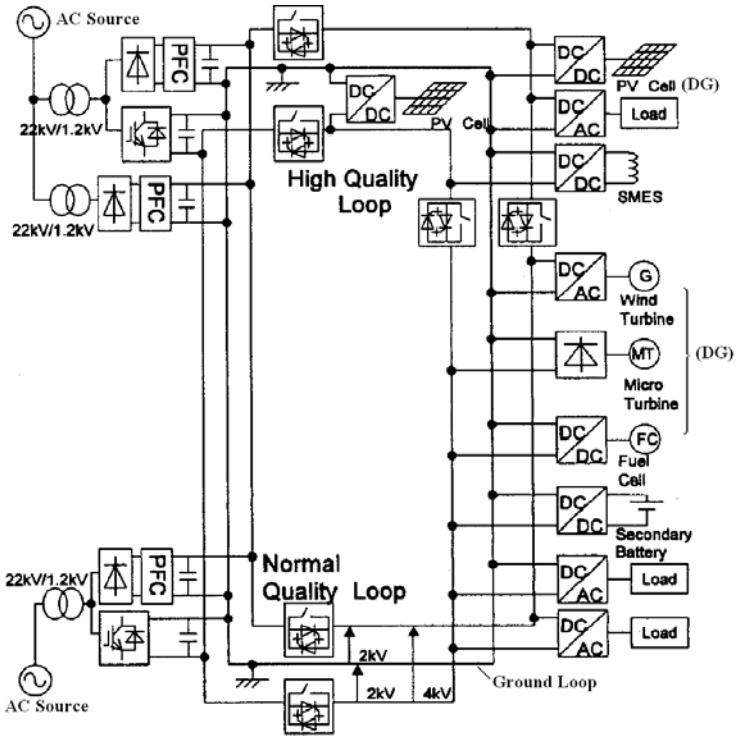

Figure 2-16 Configuration of DC-type PQCC [34]

2.5.1.3 AC-type PQCC

One configuration of the AC-type PQCC is shown in Figure 2-17 [30, 35]. The system is composed of three AC/DC converters, a hybrid transfer switch, an unbundled power quality supply system using three-phase four-wire AC system and DGs.

It is seen from the figure the normal quality line has the same quality as the upstream system. For the high quality line, voltage sags and fluctuations are compensated by the Inverter 2. The injected energy is supplied by DGs, such as micro-gas turbine and fuel cell, which are connected to the DC-link of Inverter 2.

The supply reliability of the premium quality load is greatly improved as it is supplied through two feeders. Hybrid Transfer Switches (HTS) are used to transfer the power supply from the primary feeder to the standby feeder should there be a fault on the primary feeder. The detailed configuration and operation of HTS would be described later. On the premium quality line, bi-directional rectifier (Inverter 1) is used to compensate for upstream disturbances.

The AC-type PQCC can also provide unbundled power quality supply to the single-phase loads using three-phase four-wire AC system, as can be seen in the figure. Its configuration is similar to that shown in Figure 2-15. Its operation is therefore not described here.

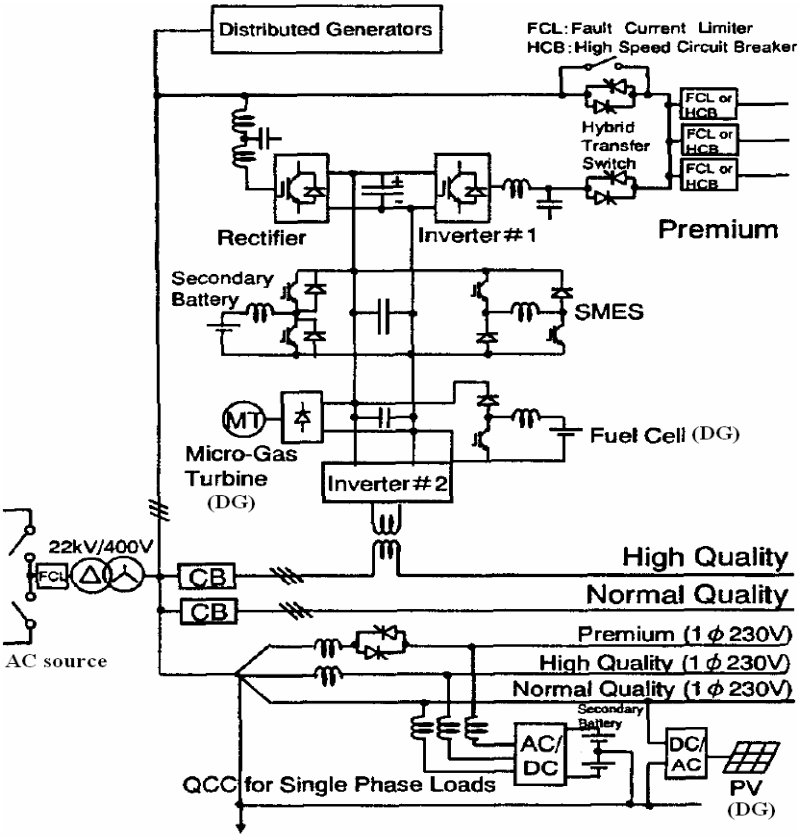

Figure 2-17 Configuration of AC-type PQCC [35]

2.5.1.4 UPQC-type PQCC

The configuration of the UPQC-type PQCC is given in Figure 2-18 [30, 31]. It uses the basic circuit of the UPQC and consists of two PWM controlled invertors (Inv.1 and Inv.2)

with interconnection transformers, DC-bus and DG. Four solid-state relays are installed for realizing the unbundled power quality supply. The operation of the UPQC-type PQCC under normal state and upstream supply outage state are as follows.

- Normal state operation: S_1, S_3 and S_4 in Figure 2-18 normally switch on, whereas S_2 switches off. The OQ load and the HQ load are connected to the upstream network only through a transformer. Therefore they have the same level of waveform quality as the upstream line. Inv.1 will attempt to absorb current harmonics appearing on the SP load side and also compensate for its power factor. By this arrangement, high quality sinusoidal waveform voltages can be achieved at the SP load terminal. However, for the SP load, voltage disturbances such as voltage sag, swell, momentary interruption and under/over voltage that originate in the upstream network can be compensated for by injecting a series voltage component from Inv.2. It will ensure the SP load terminal voltage remain unchanged.
- Upstream supply outage state: if the distribution network experiences a fault and no power can be transmitted from the network to the PQCC, the OQ load will be disconnected from the network. The remaining loads are supplied by the DG connected to the DC-bus. This operation can be realized by switching off S_1, S_3, S_4 and switching on S_2. The power supplied by the DG will be transferred to the HQ and SP loads through Inv.1 and S_2.

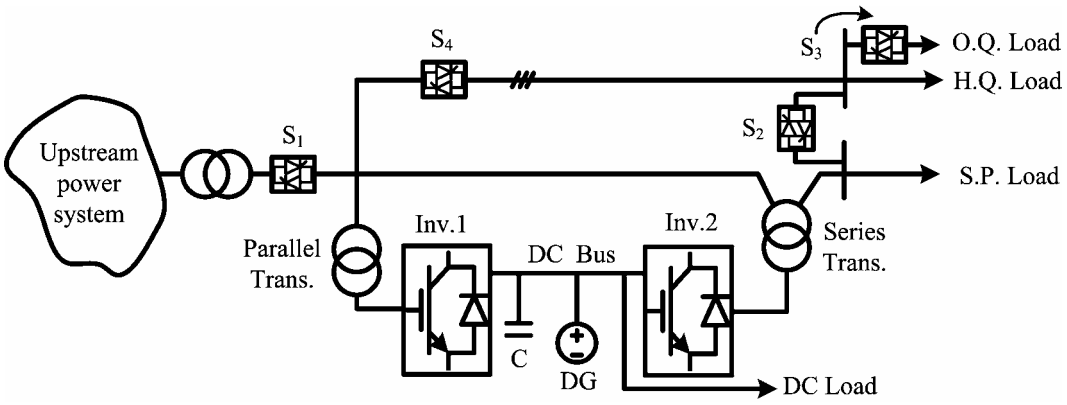

Figure 2-18 Configuration of UPQC-type PQCC [30]

2.5.1.5 UPS-type PQCC

The structure of the UPS-type PQCC is shown in Figure 2-19 [30, 31]. As this type of

PQCC will be chosen as the target system for further research in the follow Chapters, its operation and functions would be described in greater detail.

Similar to the conventional UPS system, it consists of two PWM-controlled inverters (Inv.1 and Inv.2) and a DC-bus. The PQCC is also equipped with a DG on the DC-bus. A step-down transformer is envisaged between the upstream power system and the PQCC. Under such an arrangement, three different quality levels for AC loads and one quality level for DC loads have been realized. The operation of the UPS-type PQCC is given as follows [30, 31]:

- Normal state operation: the OQ and HQ loads are supplied by the upstream network directly through a transformer and therefore they have the same waveform quality levels. However the SP load has very high level of waveform quality which is improved by the two PWM-controlled converters. Under normal state, although the SP and DC load are supplied by the upstream system, it is also expected that the DG meets part of these load demands. Therefore, Inv.1 is operated in rectifier mode.
- Faulted state operation: if the PQCC cannot be supplied by the upstream network due to an upstream fault for example, the OQ load will be disconnected from the network by the solid-state switch. The remaining loads are supplied by the DG. With this operation, the supply reliability of HQ, DC and SP loads can be improved. In the process, Circuit Breaker (CB) is tripped. Inv.1 enters the inversion mode and transfers power from the DG to meet the HQ load requirement. Inv.2 is still operated in inversion mode to supply the SP load

The UPS-type PQCC also has the function of power conditioning [31]:

- Power factor correction

Often industry loads tend to have low power factor. Conventionally shunt capacitors and synchronous condenser have been installed in order to overcome this problem. However, the UPS-type PQCC can inject reactive power through the actions of Inv.1 and the power factor of the upstream network can be regulated to the desired level.

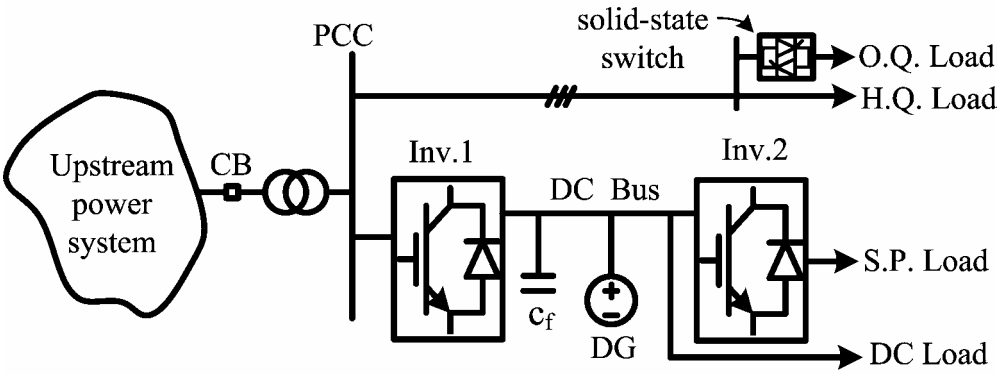

Figure 2-19 Configuration of UPS-type PQCC [30]

- Compensation of unbalance and harmonics of load current

Unbalance and harmonic components of the load current can be absorbed by Inv.1 and the PQCC can be treated as a balanced three-phase load. The principle of this compensation is similar to that of parallel-type active filter.

- DC-bus voltage regulation

A DC capacitor is connected to the DC-bus of the UPS-type PQCC. Charging and discharging the capacitor (c_f) can cause DC-bus voltage deviation. It is possible to regulate the DC-bus voltage by adjusting the DC-bus active power balance. On the DC side, the active power demand of the DC and SP loads are uncontrollable. Thus the active power supplied by the DG (P_{DG}) and the power transferred between the upstream AC side and Inv.1 (P_{Inv1}) must play a role as a "buffer" to regulate the DC-bus voltage. Under normal state, P_{Inv1} can play the role of the buffer in order to allow the DG to operate freely. However, P_{DG} should play the energy buffer role under the upstream system faulted state because P_{Inv1} must be regulated to meet the demand of HQ load.

2.5.2 PQCC Structure: High Voltage Side

Most important functions of the PQCC, as far as the high voltage side is concerned, is to minimize the distribution network loss, avoid the overloading of distribution lines and help clear fault quickly, through changing the configuration of the distribution network flexibly. One configuration of the high voltage supply has been proposed, as shown in Figure 2-20 [31, 85, 86].

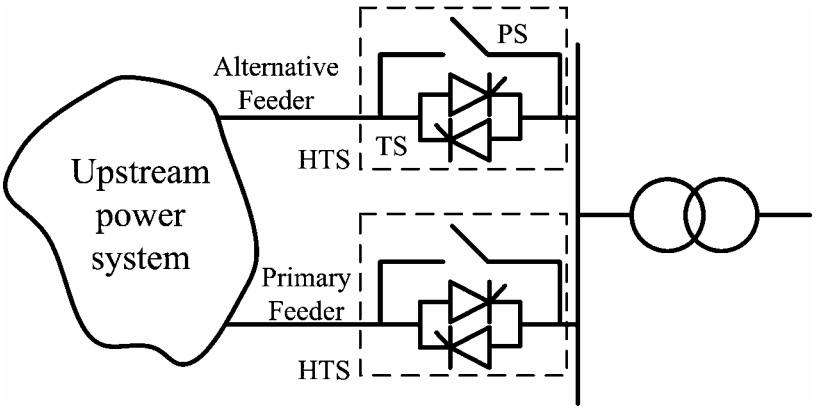

Figure 2-20 High Voltage side interior structure [31]

It is seen in the figure that the upstream power system is interconnected to the PQCC through two feeders: primary and alternative. Each feeder is equipped with hybrid transfer switches (HTS) at the feeder terminals. The main function of the HTS is to transfer power from the primary to the alternative feeder should the primary feeder develops a fault. The switches are realized through the use of a pair of anti-paralleled thyristors (referred to as TS) and a mechanical switch (referred to as PS). The process for switching off a HTS is as follows [31]: first the "open" command signal is provided. PS is then opened and TS is turned on simultaneously. The arc voltage across the terminal of PS initiates current commutation from the PS to the TS. When the commutation is completed, TS conducts the entire load current and blocks the current at the first zero crossing, thus completing the "switch off" process. The process for switching on a HTS is the reverse of the above process. The conduction losses across the HTS can be reduced because normally, the load current is through the PS and the resistance in the PS is less than that in the TS. Several control methods of the HTS switching have been proposed [85, 86].

2.6 Conclusions

The Chapter begins with a brief description of the common forms of power quality disturbances encountered in electrical networks. Various types of distributed generation technologies and the technical problems they can introduce into existing power system are also described. On the concept of Unbundled Power Quality service, a historical perspective has been given focusing on the research and development works pertaining to the realization of such service in the future power distribution systems. The systems

described include the Custom Power Park and FRIENDS. A description of Power Quality Control Center structure and functions is also included.

The research on the PQCC is still in an active stage because a variety of technical issues remain to be solved. These include system designs, PQCC operation and applications. The following Chapters will attempt to address some of the issues concerning the application of the PQCC to realize unbundled power quality services.

Chapter 3

A General Model of Power Quality Control Center

3.1 Introduction

As pointed out in Chapter 2, unbundled power quality supply has been recognized to be one of the most important features of the future power distribution system. To meet such a requirement, several new forms of electrical power distribution system have been proposed in recent years. FRIENDS is one of the most promising designs. The most important and original idea of FRIENDS is to install a new conceptual facility called Power Quality Control Center (PQCC) between the distribution substations and customers to achieve various functions of FRIENDS.

PQCC plays a vital role in FRIENDS operation. In term of hardware, they are equipped with static switches, active filter and other power electronics devices for controlling power flows or improving power quality. PQCC can also provide unbundled power quality services to customers by using information exchange through data communication lines. In addition, DG will be installed in the PQCC to act as backup power source.

As introduced in Chapter 2, the research work on designing the interior structures of PQCC has gained much attention. Several types of PQCC have been proposed [30-36]. Although the PQCC configurations and the corresponding operational schemes of these designs have been suggested in [30-36], no general mathematical analysis has been reported in the open literature on these designs. This is in spite of the fact that modeling of inverter linking upstream AC system with DC link has been reported widely in the literature. Mathematical PQCC models would be valuable in term of coordinating the operation of DG and the upstream systems and also for the designing of the control systems of the power electronics devices in the PQCC.

Based on the interior structure of the UPS-type PQCC proposed in [30, 31], this Chapter therefore strives to develop a general mathematical model of the UPS-type PQCC. UPS-type PQCC, as introduced in Chapter 2, is chosen as the study object in this project due to its very simple yet flexible configuration. In the following parts of this thesis, the UPS-type PQCC would be referred to as the PQCC for abbreviation. Based on the basic electric circuit theory and sinusoidal Pulse-Width-Modulation (PWM) [88] technique, the steady-state and dynamic response of the UPS-type PQCC would be examined separately in this Chapter. Small signal linearization technique is used to analyze the PQCC small perturbation response.

The developed model of the PQCC is then incorporated into a power system that consists of the PQCC connected to a main generator-transmission system. The purpose is to demonstrate the usefulness of the model for dynamic stability study. The DG in the PQCC is assumed to be in the form of a micro-turbine. In order to mitigate the system frequency variations due to the generation-load imbalance, a new system stability control scheme is designed through regulating the operation of the DG and the system main generator simultaneously. The DG and the main power system can also be controlled to share their real output power changes equitably. Simulation results are then given to confirm the validity of the proposed control scheme. Some of the materials contained in this Chapter have been reported in [89, 90].

3.2 General Model of the UPS-type PQCC

The configuration of the UPS-type PQCC has been shown in Figure 2-19. It consists of two PWM converters (Inv.1 and Inv.2) and a DC-bus. Unlike conventional UPS, however, the PQCC also entails a DG connected to the DC-bus. With this arrangement, unbundled power quality services are realized: three levels of power quality in the AC supply, named as Ordinary Quality (OQ), High Quality (HQ), and Super Premium Quality (SP), plus one quality level in DC.

In developing a general model for the UPS-type PQCC, the initial focus is on the behavior of the inverter-DC link system. With this respect, the HQ and OQ loads are therefore ignored as they are not directly supplied by the PQCC. The external upstream

supply system could be represented quite simply by three ideal voltage sources v_1, v_2, v_3, in series with the respective Thevenin source impedances. Such impedance is represented by a series R, L combination. Inv. 1 and Inv. 2 are three-phase SPWM converters. They are represented by six on-off switches with a finite resistance. The switches are composed of an IGBT with a freewheeling diode. On the DC-link, although the exact form of the DG has not been considered at this stage, in order to obtain a preliminary assessment of the impact of the DG on the system dynamic, the DG is approximated by a constant voltage source E in series with a resistor r in this analysis. The capacitor c_f shown connected to the DC-bus is only used for filtering purposes and is not sufficiently large to be an effective energy storage device. The DC and SP loads are assumed as constant impedance type. The DC load is represented by an equivalent resistor R_d and the SP load is shown as equivalent Thevenin impedance $R'+j\omega L'$. Figure 3-1 therefore shows the equivalent main circuit of the PQCC.

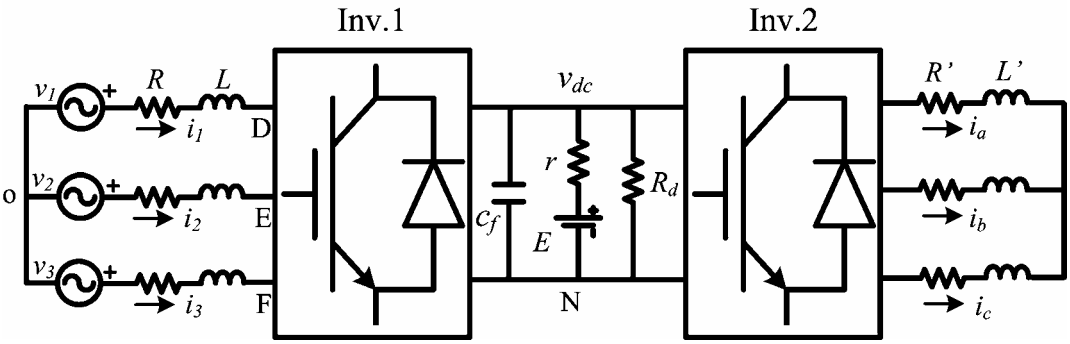

Figure 3-1 Main Circuit of UPS-type PQCC

3.2.1 Basic State Equations

The system shown in Figure 3-1 is assumed to be a balanced three-phase system. It is therefore only necessary to analyze one phase of the power system. The approach used here to analyze the PWM scheme is similar to that proposed in [91, 92]. Based on the electric circuit theory, phase 1 of the upstream source side in Figure 3-1 can be represented by the following circuit equation,

$$L(di_1/dt) + Ri_1 = v_1 - (v_{DN} + v_{NO}) \tag{3.2.1}$$

Figure 3-2 shows the detailed circuit configuration of Inv.1. As discussed before, Inv.1 consists of six switching devices ($S_1 - S_3$, $S_1' - S_3'$) with equivalent resistance (R_s) [91]. Each switching device consists of an IGBT with a diode. Inv.2 has the similar

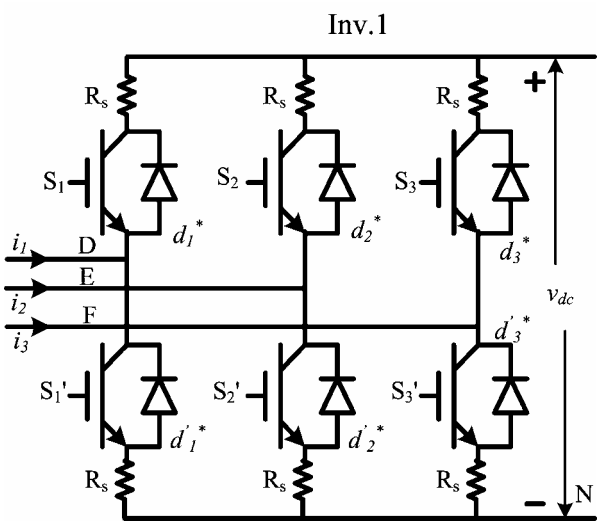

Figure 3-2 Main circuit of Inv. 1

configuration and hence would not be described here. According to the basic PWM theory [88], the switching devices of the inverter should be operated as follows: for phase 1, when the switch S_1 is on, switch S_1' should be off. The switching function under this condition is

$$d_1^* = 1;\ d_1'^* = 0$$

$$v_{DN} = i_1 R_S + v_{dc}$$

where d_1^* and $d_1'^*$ are the switching functions of S_1 and S_1' respectively. v_{dc} is the DC-link voltage. In the interval when S_1 is off, S_1' should be on, the corresponding switching function is

$$d_1^* = 0;\ d_1'^* = 1$$

$$v_{DN} = i_1 R_S$$

Combining the above switching functions with (3.2.1), it becomes,

$$L(di_1/dt) + Ri_1 = v_1 - [(i_1 R_S + v_{dc})d_1^* + (i_1 R_S)d_1'^* + v_{NO})] \qquad (3.2.2)$$

Since only either S_1 or S_1' is allowed to conduct at any one moment, i.e.,

$$d_1^* + d_1'^* = 1,$$

Substituting the above equation into (3.2.2), it yields,

$$L(di_1/dt) = -(R + R_S)i_1 - (v_{dc}d_1^* + v_{NO}) + v_1 \qquad (3.2.3)$$

For practical systems, it is reasonable to assume the source resistance is much larger than Inv.1 resistance, i.e., $R >> R_s$, therefore (3.2.3) becomes

$$L(di_1/dt) = -Ri_1 - (v_{dc}d_1^* + v_{NO}) + v_1 \tag{3.2.4}$$

Similarly, for phases 2 and 3,

$$L(di_2/dt) = -Ri_2 - (v_{dc}d_2^* + v_{NO}) + v_2 \tag{3.2.5}$$

$$L(di_3/dt) = -Ri_3 - (v_{dc}d_3^* + v_{NO}) + v_3 \tag{3.2.6}$$

For a three-phase system without a neutral line,

$$i_1 + i_2 + i_3 = 0 \tag{3.2.7}$$

Since the upstream power system is assumed a balanced source,

$$v_1 + v_2 + v_3 = 0 \tag{3.2.8}$$

The voltage v_{NO} can be obtained by combining (3.2.4) – (3.2.8), that is

$$v_{NO} = \frac{-v_{dc}}{3}\sum_{k=1}^{3} d_k^* \tag{3.2.9}$$

Substituting (3.2.9) into (3.2.4), (3.2.5) and (3.2.6), the differential equations for the upstream side can be obtained

$$L(di_1/dt) = v_1 - v_{dc}(d_1^* - \frac{1}{3}\sum_{k=1}^{3} d_k^*) - Ri_1 \tag{3.2.10}$$

$$L(di_2/dt) = v_2 - v_{dc}(d_2^* - \frac{1}{3}\sum_{k=1}^{3} d_k^*) - Ri_2 \tag{3.2.11}$$

$$L(di_3/dt) = v_3 - v_{dc}(d_3^* - \frac{1}{3}\sum_{k=1}^{3} d_k^*) - Ri_3 \tag{3.2.12}$$

Similarly, the differential equations on the SP load side can also be derived:

$$L'(di_a/dt) = v_{dc}(d_a^* - \frac{1}{3}\sum_{n=a}^{c} d_n^*) - i_aR' \tag{3.2.13}$$

$$L'(di_b/dt) = v_{dc}(d_b^* - \frac{1}{3}\sum_{n=a}^{c} d_n^*) - i_bR' \tag{3.2.14}$$

$$L'(di_c/dt) = v_{dc}(d_c^* - \frac{1}{3}\sum_{n=a}^{c} d_n^*) - i_cR' \tag{3.2.15}$$

where d_a^*, d_b^* and d_c^* are the switching functions of Inv. 2. i_a, i_b, i_c represents the phase currents of the SP loads. The differential equation describing the DC side dynamics is also given as

$$c_f(dv_{dc}/dt) = i_1d_1^* + i_2d_2^* + i_3d_3^* + \frac{E - v_{dc}}{r} - \frac{v_{dc}}{R_d} - (i_ad_a^* + i_bd_b^* + i_cd_c^*) \tag{3.2.16}$$

Equations (3.2.10) - (3.2.16) therefore form a complete differential equation set to describe the PQCC dynamics.

As pointed out before, Inv.1 and Inv.2 in the PQCC are assumed to be based on PWM control scheme. The basic principle of PWM control can be characterized by the waveforms shown in Figure 3-3 and Figure 3-4 [91, 92]. In order to obtain a sinusoidal output voltage waveform at a desired frequency, a sinusoidal control signal $V_{control}$ at the desired frequency is compared with a triangular waveform V_{tri}, as shown in Figure 3-3 (a). Take phase 1 in Figure 3-2 as example. When $V_{control} > V_{tri}$, S_1 is switched on and $v_{DN} = v_{dc}$. However, when $V_{control} < V_{tri}$, S_1' is switched on and $v_{DN} = 0$. The control signal $V_{control}$ is regulated through two variables. One is the modulation index m, defined as $m = \hat{V}_{control} / \hat{V}_{tri}$. $\hat{V}_{control}$ is the peak value of the sinusoidal control signal, $\hat{V}_{tri}$ is the amplitude of the triangular carrier signal which is always kept constant. In Figure 3-3 (a), it is assumed to be 1 pu. Another control variable is the phase shift φ with respect to the reference voltage V_{ref}. V_{ref} is obtained from the grid where the converter is connected. By varying φ, the crossover points of $V_{control}$ and V_{tri} will change, which in turn change the output voltage.

As seen from Figure 3-3, the frequency of $V_{control}$ is the desired power supply frequency. It is much lower than the inverter switching frequency (the frequency of V_{tri}). Therefore over one switching period, $V_{control}$ can be seen to be approximately as constant and the switching function d_k^* can therefore be replaced by its average value (or duty ratio) d_k in that switching period, as shown in Figure 3-4. Therefore from Figure 3-4, the relationship between d_k and $V_{control}$ can be expressed as:

$$d_k = t_{on}/T = (V_{control} + \hat{V}_{tri}) / (2\hat{V}_{tri}) = 0.5 + 0.5(V_{control} / \hat{V}_{tri}) \qquad (3.2.17)$$

Since it is assumed that for the triangular waveform,

$$\hat{V}_{tri} = 1$$

From Figure 3-3, it is also seen the waveform of control single can be represented as (phase k, $k = 1, 2, 3$):

$$V_{control} = m \cos[\omega t - \varphi - 2\pi(k-1)/3]$$

Substituting the above two equations into (3.2.17), d_k can be derived for phase k as:

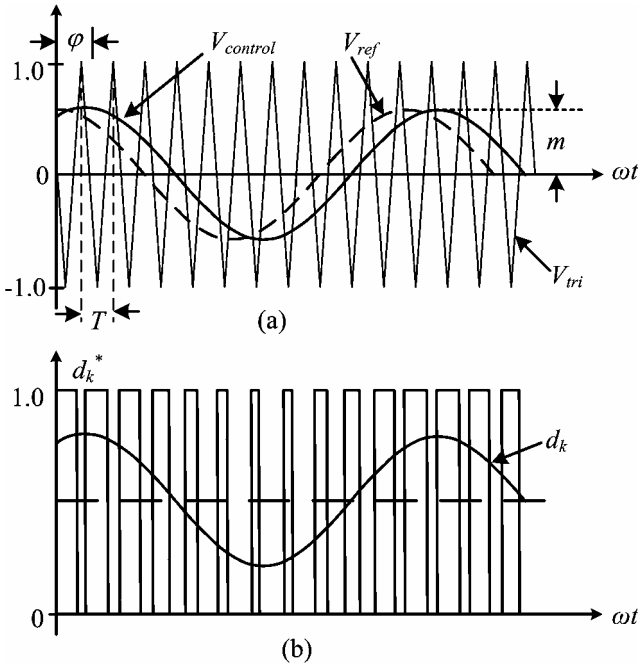

Figure 3-3 Switching function d_k^* and duty ratio d_k [91]

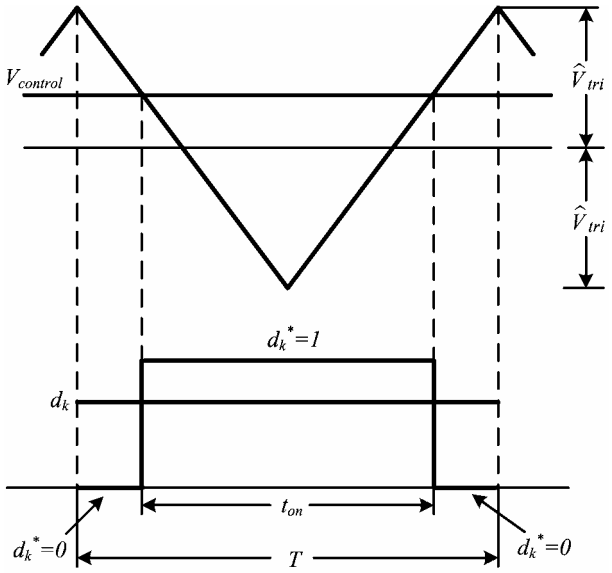

Figure 3-4 Waveforms of switching function over one switching period [91]

$$d_k = 0.5m \cos [\omega t - \varphi - 2\pi(k-1)/3] + 0.5 \quad (3.2.18)$$

Whence, the duty ratio for Inv.1 is expressed as

$$d_1 = 0.5m_1 \cos (\omega t - \varphi_1) + 0.5 \quad (3.2.19)$$

$$d_2 = 0.5m_1 \cos (\omega t - \varphi_1 - 2\pi/3) + 0.5 \quad (3.2.20)$$

$$d_3 = 0.5m_1 \cos (\omega t - \varphi_1 - 4\pi/3) + 0.5 \quad (3.2.21)$$

where, m_1, φ_1 are the control variables of Inv.1. Similarly the duty ratios for Inv. 2 are,

$$d_a = 0.5m_2 \cos(\omega t - \varphi_2) + 0.5 \tag{3.2.22}$$

$$d_b = 0.5m_2 \cos(\omega t - \varphi_2 - 2\pi/3) + 0.5 \tag{3.2.23}$$

$$d_c = 0.5m_2 \cos(\omega t - \varphi_2 - 4\pi/3) + 0.5 \tag{3.2.24}$$

m_2, φ_2 are the control variables of Inv.2.

According to the above derivations, it is therefore reasonable to replace the switching functions d_k^* (k = 1, 2, 3) and d_n^* (n = a, b, c) in (3.2.10) – (3.2.16) by their average values given in (3.2.19) – (3.2.24). Accordingly, the PQCC can then be described by a matrix differential equation:

$$Z\dot{\boldsymbol{x}} = A\boldsymbol{x} + B\boldsymbol{v} \tag{3.2.25}$$

where the state variable vector $\boldsymbol{x}$, the input vector $\boldsymbol{v}$ and the coefficient matrices are:

$$\boldsymbol{x} = \begin{bmatrix} i_1 & i_2 & i_3 & v_{dc} & i_a & i_b & i_c \end{bmatrix}^{\mathrm{T}} \tag{3.2.26}$$

$$\boldsymbol{v} = \begin{bmatrix} v_1 & v_2 & v_3 & E & 0 & 0 & 0 \end{bmatrix}^{\mathrm{T}} \tag{3.2.27}$$

$$Z = \begin{bmatrix} L & 0 & 0 & 0 & 0 & 0 & 0 \\ 0 & L & 0 & 0 & 0 & 0 & 0 \\ 0 & 0 & L & 0 & 0 & 0 & 0 \\ 0 & 0 & 0 & c_f & 0 & 0 & 0 \\ 0 & 0 & 0 & 0 & L' & 0 & 0 \\ 0 & 0 & 0 & 0 & 0 & L' & 0 \\ 0 & 0 & 0 & 0 & 0 & 0 & L' \end{bmatrix} \tag{3.2.28}$$

$$A = \begin{bmatrix} -R & 0 & 0 & -(d_1 - \frac{1}{3}\sum_{k=1}^{3} d_k) & 0 & 0 & 0 \\ 0 & -R & 0 & -(d_2 - \frac{1}{3}\sum_{k=1}^{3} d_k) & 0 & 0 & 0 \\ 0 & 0 & -R & -(d_3 - \frac{1}{3}\sum_{k=1}^{3} d_k) & 0 & 0 & 0 \\ d_1 & d_2 & d_3 & -(\frac{1}{r} + \frac{1}{R}) & -d_a & -d_b & -d_c \\ 0 & 0 & 0 & d_a - \frac{1}{3}\sum_{n=a}^{c} d_n & -R' & 0 & 0 \\ 0 & 0 & 0 & d_b - \frac{1}{3}\sum_{n=a}^{c} d_n & 0 & -R' & 0 \\ 0 & 0 & 0 & d_c - \frac{1}{3}\sum_{n=a}^{c} d_n & 0 & 0 & -R' \end{bmatrix} \tag{3.2.29}$$

$$B = \begin{bmatrix} 1 & 0 & 0 & 0 & 0 & 0 & 0 \\ 0 & 1 & 0 & 0 & 0 & 0 & 0 \\ 0 & 0 & 1 & 0 & 0 & 0 & 0 \\ 0 & 0 & 0 & \frac{1}{r} & 0 & 0 & 0 \\ 0 & 0 & 0 & 0 & 0 & 0 & 0 \\ 0 & 0 & 0 & 0 & 0 & 0 & 0 \\ 0 & 0 & 0 & 0 & 0 & 0 & 0 \end{bmatrix} \tag{3.2.30}$$

The phase 1 voltage of upstream source is assumed as $v_1 = v_m \sin\omega t$. While the approach

used in the above derivation is based on the "average-value" approach described in [91, 92], the expressions derived here include the dynamics of Inv.2 and that of the DG. Furthermore, while the authors of [30, 31] have suggested the concept and configuration of the PQCC, they have not described the PQCC model in such details. (3.2.25) also expresses in a qualitative manner the design of the PQCC considered in [30, 31].

3.2.2 Time-Invariant Solution

It is seen from (3.2.19) – (3.2.24) that d_k and d_n are functions of time, matrix A given in (3.2.29) is therefore time-variant. In order to simplify the analysis, it is desirable to transform the system model into a rotating reference frame, where the matrix A would appear time-invariant. This is known as the Park's transformation. The transformation matrix T and its inverse T^{-1} are

$$T=\frac{2}{3}\begin{bmatrix} \sin\omega t & \sin(\omega t-\frac{2\pi}{3}) & \sin(\omega t+\frac{2\pi}{3}) & 0 & 0 & 0 & 0 \\ \cos\omega t & \cos(\omega t-\frac{2\pi}{3}) & \cos(\omega t+\frac{2\pi}{3}) & 0 & 0 & 0 & 0 \\ \frac{1}{2} & \frac{1}{2} & \frac{1}{2} & 0 & 0 & 0 & 0 \\ 0 & 0 & 0 & \frac{3}{2} & 0 & 0 & 0 \\ 0 & 0 & 0 & 0 & \sin\omega t & \sin(\omega t-\frac{2\pi}{3}) & \sin(\omega t+\frac{2\pi}{3}) \\ 0 & 0 & 0 & 0 & \cos\omega t & \cos(\omega t-\frac{2\pi}{3}) & \cos(\omega t+\frac{2\pi}{3}) \\ 0 & 0 & 0 & 0 & \frac{1}{2} & \frac{1}{2} & \frac{1}{2} \end{bmatrix} \tag{3.2.31}$$

$$T^{-1}=\begin{bmatrix} \sin\omega t & \cos\omega t & 1 & 0 & 0 & 0 & 0 \\ \sin(\omega t-\frac{2\pi}{3}) & \cos(\omega t-\frac{2\pi}{3}) & 1 & 0 & 0 & 0 & 0 \\ \sin(\omega t+\frac{2\pi}{3}) & \cos(\omega t+\frac{2\pi}{3}) & 1 & 0 & 0 & 0 & 0 \\ 0 & 0 & 0 & 1 & 0 & 0 & 0 \\ 0 & 0 & 0 & 0 & \sin\omega t & \cos\omega t & 1 \\ 0 & 0 & 0 & 0 & \sin(\omega t-\frac{2\pi}{3}) & \cos(\omega t-\frac{2\pi}{3}) & 1 \\ 0 & 0 & 0 & 0 & \sin(\omega t+\frac{2\pi}{3}) & \cos(\omega t+\frac{2\pi}{3}) & 1 \end{bmatrix} \tag{3.2.32}$$

Since the upstream power system is a three-wire balanced system, input $\boldsymbol{v}$ shown in (3.2.27) can be transformed into its time-invariant equivalent vector $\boldsymbol{v_r}$,

$$\boldsymbol{v_r}=T\boldsymbol{v}=\begin{bmatrix} v_m & 0 & 0 & E & 0 & 0 & 0 \end{bmatrix}^{\mathrm{T}} \tag{3.2.33}$$

The time-invariant form of the state variable vector $\boldsymbol{x}$ is denoted $\boldsymbol{x_r}$, which is

$$\boldsymbol{x_r}=T\boldsymbol{x}=\begin{bmatrix} i_d & i_q & i_0 & v_{dc} & i_d^{'} & i_q^{'} & i_0^{'} \end{bmatrix}^{\mathrm{T}} \tag{3.2.34}$$

where i_d, i_q and i_0 are the d-axes, q-axes and zero sequence components of i_1, i_2, i_3 respectively. Similarly i_d', i_q' and i_0' are the respective components of SP load side current. The DC side voltage v_{dc} is not affected by the transformation. From (3.2.34), therefore

$$\dot{\boldsymbol{x}} = T^{-1}\dot{\boldsymbol{x}}_{\boldsymbol{r}} + \dot{T}^{-1}\boldsymbol{x}_{\boldsymbol{r}} \tag{3.2.35}$$

Substituting (3.2.35) into (3.2.25), the following equation can be derived

$$Z(T^{-1}\dot{\boldsymbol{x}}_{\boldsymbol{r}} + \dot{T}^{-1}\boldsymbol{x}_{\boldsymbol{r}}) = AT^{-1}\boldsymbol{x}_{\boldsymbol{r}} + BT^{-1}\boldsymbol{v}_{\boldsymbol{r}} \tag{3.2.36}$$

Left multiply by T on both sides,

$$(TZT^{-1})\dot{\boldsymbol{x}}_{\boldsymbol{r}} = (TAT^{-1} - TZ\dot{T}^{-1})\boldsymbol{x}_{\boldsymbol{r}} + (TBT^{-1})\boldsymbol{v}_{\boldsymbol{r}} \tag{3.2.37}$$

Substituting (3.2.26) - (3.2.30) into (3.2.37), the state-space equation of the PQCC model in a rotating frame of reference can then be obtained:

$$\begin{bmatrix} L\dot{i}_d \\ L\dot{i}_q \\ L\dot{i}_0 \\ c_f\dot{v}_{dc} \\ L'\dot{i}_d' \\ L'\dot{i}_q' \\ L'\dot{i}_0' \end{bmatrix} = \begin{bmatrix} -R & \omega L & 0 & -\frac{m_1\sin\varphi_1}{2} & 0 & 0 & 0 \\ -\omega L & -R & 0 & -\frac{m_1\cos\varphi_1}{2} & 0 & 0 & 0 \\ 0 & 0 & -R & 0 & 0 & 0 & 0 \\ \frac{3m_1\sin\varphi_1}{4} & \frac{3m_1\cos\varphi_1}{4} & \frac{3}{2} & -(\frac{1}{r}+\frac{1}{R_d}) & -\frac{3m_2\sin\varphi_2}{4} & -\frac{3m_2\cos\varphi_2}{4} & -\frac{3}{2} \\ 0 & 0 & 0 & \frac{m_2\sin\varphi_2}{2} & -R' & \omega L' & 0 \\ 0 & 0 & 0 & \frac{m_2\cos\varphi_2}{2} & -\omega L' & -R' & 0 \\ 0 & 0 & 0 & 0 & 0 & 0 & -R' \end{bmatrix} \begin{bmatrix} i_d \\ i_q \\ i_0 \\ v_{dc} \\ i_d' \\ i_q' \\ i_0' \end{bmatrix} + \begin{bmatrix} v_m \\ 0 \\ 0 \\ \frac{E}{r} \\ 0 \\ 0 \\ 0 \end{bmatrix} \tag{3.2.38}$$

As the PQCC system is a 3-wire system, the zero sequence components in the above equation should be i_0=0, i_0'=0. Hence the last equation can be simplified further as:

$$\begin{bmatrix} L\dot{i}_d \\ L\dot{i}_q \\ c_f\dot{v}_{dc} \\ L'\dot{i}_d' \\ L'\dot{i}_q' \end{bmatrix} = \begin{bmatrix} -R & \omega L & -\frac{m_1\sin\varphi_1}{2} & 0 & 0 \\ -\omega L & -R & -\frac{m_1\cos\varphi_1}{2} & 0 & 0 \\ \frac{3m_1\sin\varphi_1}{4} & \frac{3m_1\cos\varphi_1}{4} & -(\frac{1}{r}+\frac{1}{R_d}) & -\frac{3m_2\sin\varphi_2}{4} & -\frac{3m_2\cos\varphi_2}{4} \\ 0 & 0 & \frac{m_2\sin\varphi_2}{2} & -R' & \omega L' \\ 0 & 0 & \frac{m_2\cos\varphi_2}{2} & -\omega L' & -R' \end{bmatrix} \begin{bmatrix} i_d \\ i_q \\ v_{dc} \\ i_d' \\ i_q' \end{bmatrix} + \begin{bmatrix} v_m \\ 0 \\ \frac{E}{r} \\ 0 \\ 0 \end{bmatrix} \tag{3.2.39}$$

In this equation, the system state variables are conveniently represented by their equivalent DC quantities.

3.2.3 PQCC Small Signal Model

After applying the Park's transformation, the PQCC model represented by (3.2.39) becomes a time-invariant system. However it is still a nonlinear one. It contains the state variables i_d, i_q, v_{dc}, i_d', i_q', the input variables v_m, E/r and the control variables m_1, m_2, φ_1 and φ_2. The PQCC model described by (3.2.39) can be readily studied through computer simulations but the solution technique is involved and usually requires numerical means. If one intends to gain an insight into the extent how the PQCC could help enhance power system dynamics and quality, one can simplify the analysis by linearzing (3.2.39). The study is then restricted to an operating regime which is within a small area around its steady-state operating point. Let the perturbed state variables be

$$\boldsymbol{x_r} = \boldsymbol{X}_r + \Delta\boldsymbol{x}_r = \begin{bmatrix} I_d + \Delta i_d \\ I_q + \Delta i_q \\ V_{dc} + \Delta v_{dc} \\ I_d^{'} + \Delta i_d^{'} \\ I_q^{'} + \Delta i_q^{'} \end{bmatrix} \tag{3.2.40}$$

Then introduce the small perturbations in the source voltage $v_m = V_m + \Delta v_m$ and the load $R' = R' + \Delta R'$. The control variables are $m_1 = M_1 + \Delta m_1$, $\varphi_1 = \phi_1 + \Delta\varphi_1$, $m_2 = M_2 + \Delta m_2$, $\varphi_2 = \phi_2 + \Delta\varphi_2$. Substitute these perturbation equations into (3.2.39) and omit the second-order terms. Then separating the DC components from the ac variations, both steady-state DC model and the small-signal ac model for the PQCC system can be obtained.

The steady-state DC model is

$$0 = \begin{bmatrix} -R & \omega L & -\frac{M_1 \sin\phi_1}{2} & 0 & 0 \\ -\omega L & -R & -\frac{M_1 \cos\phi_1}{2} & 0 & 0 \\ \frac{3M_1 \sin\phi_1}{4} & \frac{3M_1 \cos\phi_1}{4} & -(\frac{1}{r} + \frac{1}{R_d}) & -\frac{3M_2 \sin\phi_2}{4} & -\frac{3M_2 \cos\phi_2}{4} \\ 0 & 0 & \frac{M_2 \sin\phi_2}{2} & -R^{'} & \omega L^{'} \\ 0 & 0 & \frac{M_2 \cos\phi_2}{2} & -\omega L^{'} & -R^{'} \end{bmatrix} \begin{bmatrix} I_d \\ I_q \\ V_{dc} \\ I_d^{'} \\ I_q^{'} \end{bmatrix} + \begin{bmatrix} V_m \\ 0 \\ \frac{E}{r} \\ 0 \\ 0 \end{bmatrix} \tag{3.2.41}$$

From the DC model, the PQCC steady-state operation solution can be derived,

$$I_d = \frac{-\frac{M_1}{2} V_{dc}(\omega L \cos\phi_1 + R \sin\phi_1) + V_m R}{R^2 + \omega^2 L^2}$$

$$I_q = \frac{\frac{M_1}{2}V_{dc}(\omega L\sin\phi_1 - R\cos\phi_1) - V_m\omega L}{R^2+\omega^2L^2}$$

$$I_d^{'} = \frac{M_2V_{dc}(\omega L^{'}\cos\phi_2 + R^{'}\sin\phi_2)}{2(R^{'2}+\omega^2L^{'2})}$$

$$I_q^{'} = \frac{M_2V_{dc}(R^{'}\cos\phi_2 - \omega L^{'}\sin\phi_2)}{2(R^{'2}+\omega^2L^{'2})}$$

$$V_{dc} = \frac{\frac{E}{r} + \frac{3V_mM_1(R\sin\phi_1 - \omega L\cos\phi_1)}{4(R^2+\omega^2L^2)}}{\frac{3M_1^2R}{8(R^2+\omega^2L^2)} + \frac{1}{r} + \frac{1}{R_d} + \frac{3M_2^2R^{'}}{8(R^{'2}+\omega^2L^{'2})}}$$

It's important to obtain these steady-state solutions not only because they provide knowledge about the relationship between the state variables and system parameters under steady-state but also, the dynamic response of the nonlinear system is dependent of the steady-state operating point.

The small-signal ac model can be written in a compact form as:

$$Z_r\Delta\dot{\boldsymbol{x}}_{\boldsymbol{r}} = A_{ss}\Delta\boldsymbol{x}_{\boldsymbol{r}} + \underbrace{A_{m_1}\boldsymbol{X}_{\boldsymbol{r}}\Delta m_1 + A_{\varphi_1}\boldsymbol{X}_{\boldsymbol{r}}\Delta\varphi_1 + A_{m_2}\boldsymbol{X}_{\boldsymbol{r}}\Delta m_2 + A_{\varphi_2}\boldsymbol{X}_{\boldsymbol{r}}\Delta\varphi_2}_{control} + \underbrace{B_{v_m}\Delta v_m}_{\substack{upstream\ system\\ distrubance}} + \underbrace{A_{R^{'}}\boldsymbol{X}_{\boldsymbol{r}}\Delta R^{'}}_{\substack{SP\ load\\ disturbance}} \tag{3.2.42}$$

where:

$$A_{ss} = \begin{bmatrix} -R & \omega L & -\frac{1}{2}M_1\sin\phi_1 & 0 & 0 \\ -\omega L & -R & -\frac{1}{2}M_1\cos\phi_1 & 0 & 0 \\ \frac{3}{4}M_1\sin\phi_1 & \frac{3}{4}M_1\cos\phi_1 & -(\frac{1}{r}+\frac{1}{R_d}) & -\frac{3}{4}M_2\sin\phi_2 & -\frac{3}{4}M_2\cos\phi_2 \\ 0 & 0 & \frac{1}{2}M_2\sin\phi_2 & -R^{'} & \omega L^{'} \\ 0 & 0 & \frac{1}{2}M_2\cos\phi_2 & -\omega L^{'} & -R^{'} \end{bmatrix}$$

$$A_{m_1} = \begin{bmatrix} 0 & 0 & -\frac{\sin\phi_1}{2} & 0 & 0 \\ 0 & 0 & -\frac{\cos\phi_1}{2} & 0 & 0 \\ \frac{3\sin\phi_1}{4} & \frac{3\cos\phi_1}{4} & 0 & 0 & 0 \\ 0 & 0 & 0 & 0 & 0 \\ 0 & 0 & 0 & 0 & 0 \end{bmatrix} \qquad A_{m_2} = \begin{bmatrix} 0 & 0 & 0 & 0 & 0 \\ 0 & 0 & 0 & 0 & 0 \\ 0 & 0 & 0 & -\frac{3\sin\phi_2}{4} & -\frac{3\cos\phi_2}{4} \\ 0 & 0 & \frac{\sin\phi_2}{2} & 0 & 0 \\ 0 & 0 & \frac{\cos\phi_2}{2} & 0 & 0 \end{bmatrix}$$

$$A_{\varphi_1} = \begin{bmatrix} 0 & 0 & -\frac{M_1 \cos\phi_1}{2} & 0 & 0 \\ 0 & 0 & \frac{M_1 \sin\phi_1}{2} & 0 & 0 \\ \frac{3M_1 \cos\phi_1}{4} & -\frac{3M_1 \sin\phi_1}{4} & 0 & 0 & 0 \\ 0 & 0 & 0 & 0 & 0 \\ 0 & 0 & 0 & 0 & 0 \end{bmatrix} \qquad A_{R'} = \begin{bmatrix} 0 & 0 & 0 & 0 & 0 \\ 0 & 0 & 0 & 0 & 0 \\ 0 & 0 & 0 & 0 & 0 \\ 0 & 0 & 0 & -1 & 0 \\ 0 & 0 & 0 & 0 & -1 \end{bmatrix}$$

$$A_{\varphi_2} = \begin{bmatrix} 0 & 0 & 0 & 0 & 0 \\ 0 & 0 & 0 & 0 & 0 \\ 0 & 0 & 0 & -\frac{3M_2 \cos\phi_2}{4} & \frac{3M_2 \sin\phi_2}{4} \\ 0 & 0 & \frac{M_2 \cos\phi_2}{2} & 0 & 0 \\ 0 & 0 & -\frac{M_2 \sin\phi_2}{2} & 0 & 0 \end{bmatrix} \qquad B_{v_m} = \begin{bmatrix} 1 & 0 & 0 & 0 & 0 \end{bmatrix}^T$$

In (3.2.42), one can readily see that the linearized state variables are related to the control variables $\Delta\varphi_1$, Δm_1, $\Delta\varphi_2$ and Δm_2 through the respective matrices A_{mi}, $A_{\varphi i}$ under the upstream voltage and SP load disturbances.

Laplace transformation of (3.2.42) yields

$$\begin{aligned} \Delta \boldsymbol{x_r} = (SZ_r - A_{ss})^{-1} [& A_{m_1} \boldsymbol{X_r} \Delta m_1(s) + A_{\varphi_1} \boldsymbol{X_r} \Delta\varphi_1(s) \\ & + A_{m_2} \boldsymbol{X_r} \Delta m_2(s) + A_{\varphi_2} \boldsymbol{X_r} \Delta\varphi_2(s) + B_{v_m} \Delta v_m(s) + A_{R'} \boldsymbol{X_r} \Delta R'(s)] \end{aligned} \tag{3.2.43}$$

where,

$$(SZ_r - A_{ss})^{-1} = \begin{bmatrix} sL+R & -\omega L & \frac{M_1 \sin\phi_1}{2} & 0 & 0 \\ \omega L & sL+R & \frac{M_1 \cos\phi_1}{2} & 0 & 0 \\ -\frac{3M_1 \sin\phi_1}{4} & -\frac{3M_1 \cos\phi_1}{4} & sc_f + \frac{1}{r} + \frac{1}{R_d} & \frac{3M_2 \sin\phi_2}{4} & \frac{3M_2 \cos\phi_2}{4} \\ 0 & 0 & -\frac{M_2 \sin\phi_2}{2} & sL'+R' & -\omega L' \\ 0 & 0 & -\frac{M_2 \cos\phi_2}{2} & \omega L' & sL'+R' \end{bmatrix}^{-1} \tag{3.2.44}$$

In (3.2.43) and (3.2.44), the matrices A_{ss}, A_{m1}, $A_{\varphi 1}$, A_{m2}, $A_{\varphi 2}$ can be readily determined as the PQCC steady-state operating conditions $\boldsymbol{X_r}$ are evaluated using (3.2.41). Hence the transfer functions between the state variables Δi_d, Δi_q, Δv_{dc}, $\Delta i_d'$, $\Delta i_q'$ and the control variables $\Delta\varphi_1$, Δm_1, $\Delta\varphi_2$, Δm_2, the load disturbance $\Delta R'$ and upstream source disturbance Δv_m can be easily derived from (3.2.43). These transfer functions are most valuable in the design of the regulators for a closed-loop control system for the PQCC. This model would be used in the next Chapter.

3.3 PQCC System Stability Consideration

The PQCC model derived earlier will now be applied in a power system in which the attempt is to use the PQCC to mitigate power system frequency variations.

Power frequency variation is defined as the deviation of power system fundamental frequency from its specified nominal value. For satisfactory operation of a power system, the frequency should remain nearly constant, which ensures constancy of speed of induction and synchronous motors [47]. In a network, excessive decrease in frequency could result in high magnetizing currents in induction motors and transformers and could be damaging to equipment. Rotational machinery output would also reduce considerably as a result of the frequency decrease. System frequency is dependent on system active power balance. An unbalance between load and generation is reflected by a change in frequency.

Conventionally, a speed governor on each generating unit provides the primary speed control function. The basic concept of speed governor can be illustrated by considering an isolated generating unit supplying a local load, as shown in Figure 3-5 [47]. As shown in the figure, when there is a load change (P_L), it is reflected instantaneously as a change in the electrical output power of the generator (P_e). This causes a mismatch between the mechanical output power (P_m) from the generator turbine and P_e, which in turn results in the speed variation of the generator, i.e., system frequency variation. Under such a case, the speed governor can adjust the turbine valve/gate and in turn change the turbine output mechanical power to bring the frequency back to its nominal value. Generally, the speed governor is a proportional-integral type controller [47].

It is also seen from Figure 3-5 [47] that in the conventional restoration scheme, the system response to a load change is normally determined by the generator inertia constant, the load-damping constant, turbine constant and governor setting [47]. Those time constants are normally quiet large. For example, one of the dominant time constants of a single reheat tandem-compound steam turbine is typically 7 seconds and the load-damping constant could be up to 10 seconds. Moreover, the governor is essentially a mechanical transducer and its dynamic performance is relatively slow. In this situation,

the restoration of the system frequency variations could be of long duration and is undesirable.

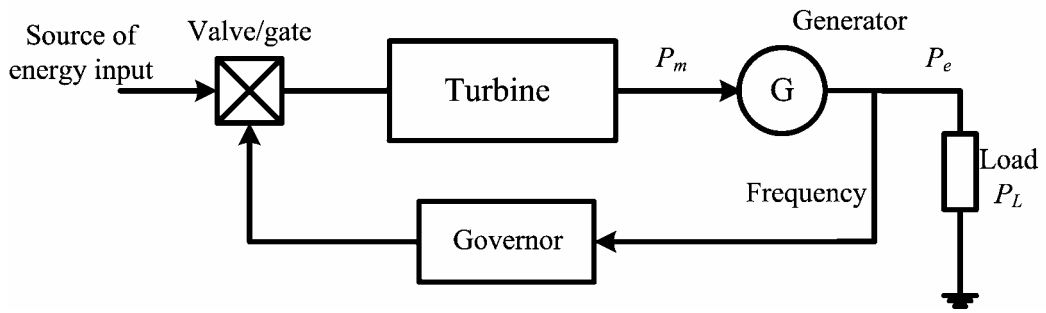

Figure 3-5 Generator supplying isolated load [47]

In this section, a new power system control strategy with the help of the PQCC is proposed. The new scheme attempts to coordinate the operation of the upstream generator and the DG installed in the PQCC. By taking advantage of the flexibility offered by the PQCC, the new scheme is expected to restore system frequency more rapidly than the convention scheme shown in Figure 3-5. It is also an example where the network model developed for the PQCC can be applied for power system studies.

3.3.1 System Description

The system model used to study the proposed control scheme is given in Figure 3-6, which consist of a PQCC connected to a main generator-transmission system. As shown in the figure, the upstream power system is represented by an equivalent generator source in series with an equivalent source impedance of $R+j\omega L$. The generator is also equipped with a speed governor to regulate the system frequency variations. In the PQCC system, the OQ, HQ loads are ignored for the purpose of simplifying the analysis. The system is similar to that used in Section 3.2. The DC and SP loads are assumed as constant impedance type. In the proposed scheme, the DG is to take the form of a micro-turbine. The reason is that in order to achieve a more satisfactory frequency restoration scheme, the dynamic response of the DG should be relatively fast, such that it can regulate its output power rapidly. Compared with other types of distributed generators, such as fuel cell which has a typical time constant of several tens of seconds [67, 68], the time constants associated with the micro-turbine are relatively smaller and its dynamic

response is therefore likely to be rapid. The dynamic model of micro-turbine would be introduced later.

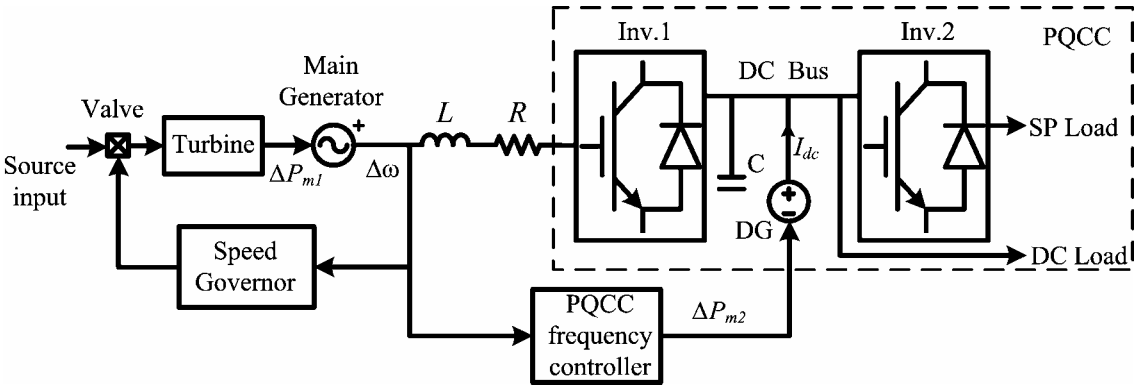

Figure 3-6 Proposed frequency control system model

The proposed frequency control scheme in Figure 3-6 would operate as follows. Under normal state, power flows from the main generator to the DC-link and supplies the DC and SP loads. It is also expected that the micro-turbine in the PQCC provides part of load demands under steady-state. In the scenario examined in this work, suppose a disturbance occurs in the upstream part of the network and causes an immediate imbalance in the generation and load demand. The system frequency will then vary by an amount $\Delta\omega$. In order to restore the frequency deviation $\Delta\omega$, the proposed control scheme attempts to coordinate the action of the main generator and the DG. Under such a scheme, both the main generator and micro-turbine can regulate their output power simultaneously and maintain the active power balance of supply and load. While the main generator is controlled by its speed governor, a PQCC frequency controller is then introduced to regulate the micro-turbine output active power. As the dynamic response of the micro-turbine is much faster than that of the main generator, it is expected that the new control scheme can mitigate $\Delta\omega$ more rapidly than the conventional one. Furthermore there are two generating sources in the system. Then the new control system must also achieve equitable active power sharing between the micro-turbine and the main generator. In other words, the output active power change made by the micro-turbine and the main generator is proportional to the ratio of their capacities. During the disturbances, it is assumed that Inv.1 can maintain constant DC-link voltage so that Inv.2 can maintain constant supply to the SP load.

3.3.2 Model Development

A detailed analysis of the proposed system model will now be described. The two generators in the proposed system would be examined separately.

3.3.2.1 Linear micro-turbine model

As described in Chapter 2, the micro-turbine assumed here has a single rotating shaft, with generator, air compressor, and turbine mounted on air bearings. The shaft operates at high speed of 15,000 ~ 90,000 rpm. The power plant is an air-cooled, 2-pole permanent magnet (PM) generator [65], which generates high frequency AC voltage source. Therefore a power electronic interface is needed between the PM generator and the DC-bus. This interface is an AC/ DC rectifier in the proposed micro-turbine model. Normally the PM generator and rectifier in the micro-turbine can be modeled as a three-phase, full wave, diode-bridge rectifier with the ac source. See Figure 3-7 [93]. L_T is the equivalent inductance for each phase of the generator. It is assumed that the losses can be neglected. For an ideal PM generator, its line-to-line voltage V_{LL} can be expressed as [88]:

$$V_{LL} = k_v \omega_1 \sin(\omega_1 t) \tag{3.3.1}$$

where k_v is the voltage constant and ω_1 is the micro-turbine generator electrical angular frequency. Based on the basic power electronics technique [88], the DC-bus voltage for a full-wave rectifier can be expressed as:

$$V_{dc} = \frac{3|V_{LL}|}{\pi} - \frac{3\omega_1 L_T I_{dc}}{\pi} \tag{3.3.2}$$

(3.3.1) and (3.3.2) allow the DC side voltage to be represented as:

$$E = V_{dc} + rI_{dc} \tag{3.3.3}$$

where it is defined that:

$$\left.\begin{aligned} E &= k_e \omega_1 = 3k_v \omega_1 / \pi \\ r &= k_x \omega_1 = 3L_T \omega_1 / \pi \end{aligned}\right\} \tag{3.3.4}$$

k_e, k_x are both constants. The micro-turbine generator and rectifier therefore can be represented by an equivalent DC internal voltage source E in series with an internal resistance r as described by (3.3.3) and (3.3.4). E and r are both functions of ω_1. Based on this equivalent model, the output power of the micro-turbine can be represented as:

$$P_{e2} = V_{dc} I_{dc}$$

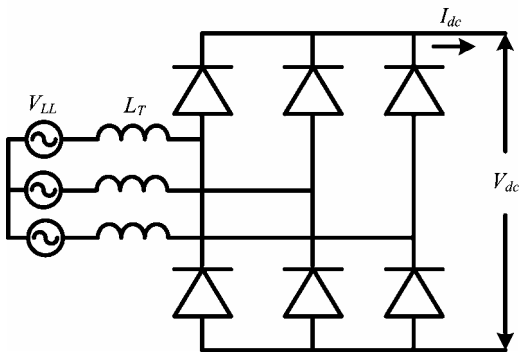

Fig 3-7 Micro-turbine generator and rectifier model [93]

Since

$$I_{dc} = \frac{E - V_{dc}}{r} = \frac{k_e \omega_1 - V_{dc}}{r}$$

From the above two equations, hence

$$P_{e2} = \frac{k_e \omega_1 - V_{dc}}{r} V_{dc} \qquad (3.3.5)$$

Equations (3.3.4) and (3.3.5) therefore provide the basic equations for describing the electrical nature of the micro-turbine.

Based on these equations and the micro-turbine model proposed in [93], a simplified dynamic micro-turbine model is developed. Such model is necessary for investigating the dynamics of the system shown in Figure 3-6. The model includes the micro-turbine mechanical system component as well. See Figure 3-8. The input ω_1* is the reference of the micro-turbine generator speed. The inner loop represents the electrical dynamic of the micro-turbine, described by (3.3.4) and (3.3.5). The output of the electrical part is the micro-turbine output electrical power P_{e2}. The micro-turbine mechanical components are included in the model through the inertia (J) of the shaft, the turbine stage and the speed governor. The governor regulates the turbine of the micro-turbine, which in turn generates the mechanical power P_{m2}. The governor of the micro-turbine in Figure 3-8 is a proportional-integral type controller and it has a different role from the PQCC frequency controller shown in Figure 3-6. The design of the PI controller will be discussed later.

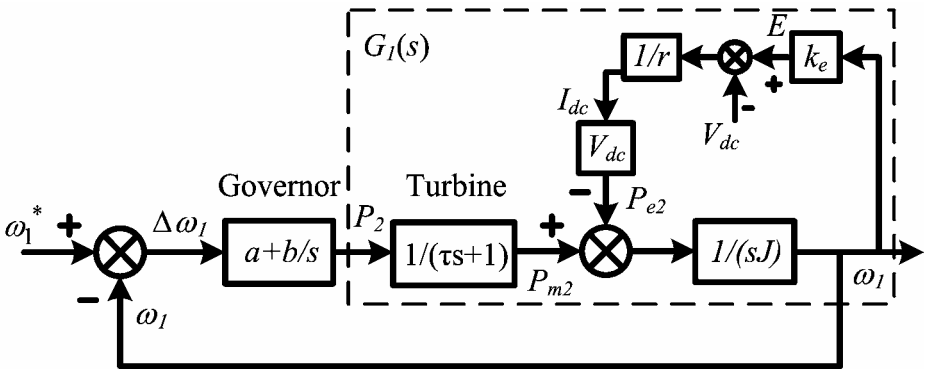

Figure 3-8 Linearized micro-turbine model

3.3.2.2 *Main generator model*

Figure 3-9 shows a classical model for the system main generator, which consists of a speed governor, steam turbine and the system model [47]. The turbine is assumed to be a single reheat tandem-compound steam turbine and is represented by a simplified transfer function derived in [47]. T_{RH} and T_{CH} are the time constants of the main inlet steam chest and reheater respectively. F_{HP} is the fraction of total turbine power generated by the high pressure section. The block 1/(2H) represents the inertia effect of the generator-power system. D is the system damping constant. As pointed out before, the speed governor is a proportional-integral type controller, which has two parameters k_g, k_h. The effect of the excitation system is not considered in the model. This is because of the assumption that the excitation system can react quickly enough to keep the system voltage constant during the disturbances.

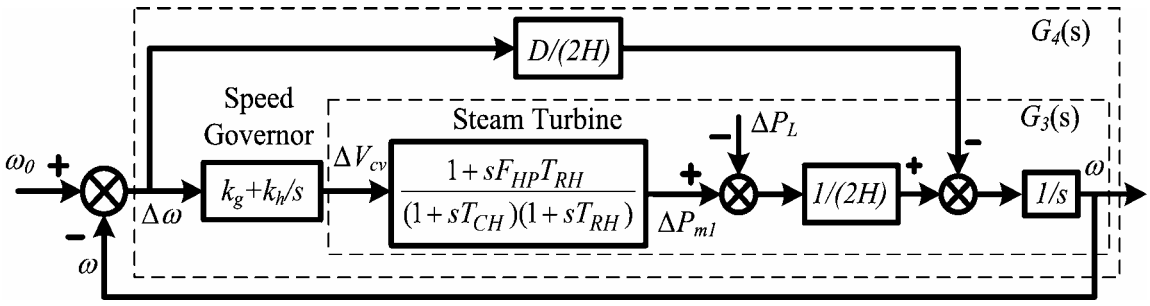

Figure 3-9 Simplified main generator model [47]

3.3.2.3 *Combined system model*

Having examined the micro-turbine and main generator dynamic models separately, it is possible to amalgamate them to form the complete dynamic model for the proposed

system given in Figure 3-6. As the frequency variation is normally quite small around its steady-state operating point, Figure 3-10 then develops the small-signal dynamic model of the whole system. In this model $\Delta\omega$ represents the system frequency change due to load change ΔP_L. As can be seen from the figure, ΔP_L is to be mitigated through regulating the active power of both the main generator (ΔP_{m1}) and the micro-turbine (ΔP_{m2}). The micro-turbine model given in Figure 3-8 is represented by the transfer function G(s). The additional PQCC frequency controller is used to regulate the desired speed of the micro-turbine. It is also assumed to be a proportional-integral type controller.

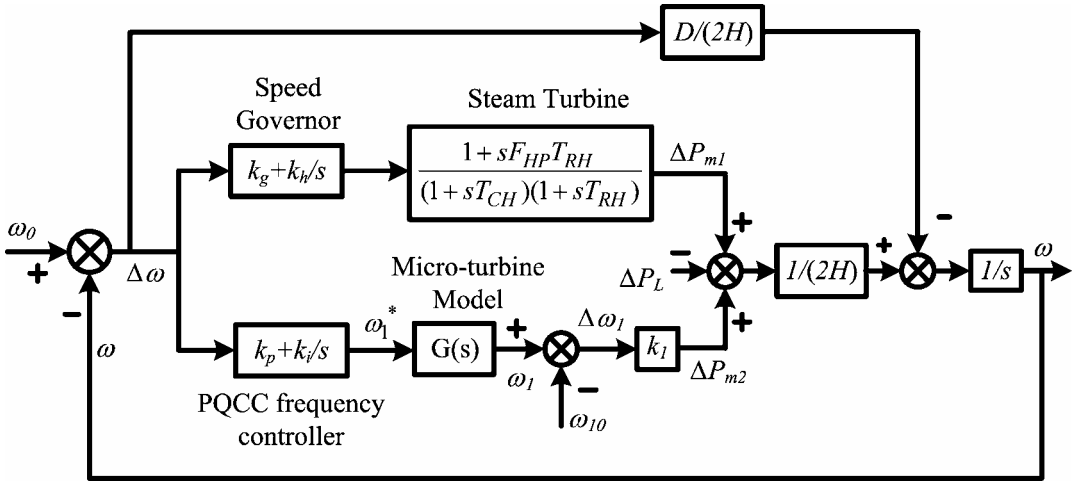

Figure 3-10 Combined model for system frequency regulation

In the micro-turbine loop, k_1 is a constant, which can be derived from (3.3.5) as follows. By introducing small perturbations $P_{m2} = P_{m2}+\Delta P_{m2}$, $\omega_1 = \omega_{10} + \Delta\omega_1$ into (3.3.5), one obtains:

$$P_{m2} + \Delta P_{m2} = \frac{k_e V_{dc}}{k_x} - \frac{V_{dc}^2}{k_x(\omega_{10} + \Delta\omega_1)} \tag{3.3.6}$$

Equation (3.3.6) can be separated into the DC and small-signal models. The small-signal model is:

$$\Delta P_{m2} = \frac{V_{dc}^2 \Delta\omega_1}{k_x \omega_{10}^2} = k_1 \Delta\omega_1$$

Therefore

$$k_1 = \frac{V_{dc}^2}{k_x \omega_{10}^2} \tag{3.3.7}$$

3.3.3 Controller Design

The tuning methods for the controllers are now considered. There are three PI controllers in the combined system model that needs to be designed: the governor of the micro-turbine, the governor of the main generator and the PQCC frequency controller for regulating the micro-turbine speed. Since the two governors only ensure the dynamic performance of the respective generators, their design will not affect significantly the coordination of the main generator and the micro-turbine in term of their power-sharing for frequency regulation. Therefore, these two governors could be designed separately using the models given in Figure 3-8 and Figure 3-9. Frequency response techniques [94], which determine the control parameters based on the open-loop gain and phase margins, could then be used to obtain satisfactory dynamic performance. The details are given as follows.

In Figure 3-8, the open-loop transfer function G_1(s), which is between P_2 and ω_1, can be derived as

$$G_1(s) = \frac{1}{\tau J s^2 + (\tau \frac{k_e V_{dc}}{r} + J)s + \frac{k_e V_{dc}}{r}} \tag{3.3.8}$$

After including the governor into the micro-turbine model, the compensated open loop transfer function between ω_1 and $\Delta\omega_1$ is:

$$G_2(s) = (a + \frac{b}{s}) * G_1(s) = (a + \frac{b}{s}) * \frac{1}{\tau J s^2 + (\tau \frac{k_e V_{dc}}{r} + J)s + \frac{k_e V_{dc}}{r}} \tag{3.3.9}$$

According to the basic frequency response technique, at the crossover point $s = j\omega_{c2}$, the desired gain of G_2(s) should be 1 and the corresponding phase angle should be ($-180^\circ + \phi_2$), where ϕ_2 is the desired phase margin at the crossover point. Thus,

$$G_2(j\omega_{c2}) = (a + \frac{b}{j\omega_{c2}}) * G_1(j\omega_{c2}) = (a + \frac{b}{j\omega_{c2}}) * M_{g1} e^{j\varphi_{g1}} = 1 e^{j(-180^\circ + \phi_2)} \tag{3.3.10}$$

where M_{g1} and φ_{g1} are the gain and phase angle of G_1(s) at the crossover frequency ω_{c2}. M_{g1} and φ_{g1} can be easily obtained from (3.3.8). Separating the above equation into its real and imaginary parts, a and b can be derived from (3.3.10) as:

$$\left.\begin{aligned} a &= -\frac{\cos(\phi_2 - \varphi_{g1})}{M_{g1}} \\ b &= \frac{\omega_{c2}}{M_{g1}}\sin(\phi_2 - \varphi_{g1}) \end{aligned}\right\} \tag{3.3.11}$$

Once the model parameters are given and knowing ω_{c2}, ϕ_2, the values of a, b can be determined from (3.3.11).

The main generator governor is tuned using the model shown in Figure 3-9. The uncompensated open loop transfer function is

$$G_3(s) = \frac{\omega(s)}{\Delta v_{cv}(s)} = \frac{1 + sF_{HP}T_{RH}}{(1 + sT_{CH})(1 + sT_{RH})} * \frac{\omega_0}{2Hs} \tag{3.3.12}$$

The compensated open loop transfer function is

$$G_4(s) = \frac{\omega(s)}{\Delta\omega(s)} = G_3(s)(k_g + \frac{k_h}{s}) - \frac{D}{2Hs} \tag{3.3.13}$$

Again using the frequency response technique, at the new crossover point $s = j\omega_{c4}$, the desired system open-loop gain of G_4(s) should be 1 and the phase angle should be (-180°+ϕ_4), where ϕ_4 is the desired phase margin at the crossover point. Then it yields,

$$G_3(j\omega_{c4})(k_g + \frac{k_h}{j\omega_{c4}}) - \frac{D}{j2H\omega_{c4}} = 1e^{j(-180^\circ + \phi_4)}$$

or,

$$(k_g + \frac{k_h}{j\omega_{c4}}) = \frac{1e^{j(-180^\circ + \phi_4)} - j\dfrac{D}{2H\omega_{c4}}}{M_{g3}e^{j\varphi_{g3}}} \tag{3.3.14}$$

M_{g3} and φ_{g3} are the gain and phase angle of G_3(s) at ω_{c4}. M_{g3} and φ_{g3} can be easily derived from (3.3.12). It is then clear that once ω_{c4} and ϕ_4 are chosen, k_g, k_h can be obtained from (3.3.14).

The PQCC frequency controller parameters k_p, k_i are designed to achieve equitable steady-state power sharing between the main generator and micro-turbine. This means that at the new steady state, it is desirable that:

$$\frac{\Delta P_{m1}}{\Delta P_{m2}} = \frac{S_{MG}}{S_{DG}} \tag{3.3.15}$$

where S_{MG}, S_{DG} are the apparent power capacities of the main generator and the micro-turbine respectively. These are assumed known. From Figure 3-10, it is derived that:

$$\Delta P_{m1}(s) = \Delta P_L * \frac{(k_g s + k_h)(1 + sF_{HP}T_{RH})}{A - BC} \tag{3.3.16}$$

$$\Delta P_{m2}(s) = \Delta P_L * \frac{(1 + sT_{CH})(1 + sT_{RH})(k_p s + k_i)G(s)k_1}{A - BC} \tag{3.3.17}$$

where:

$$A=(k_g s + k_h)(1 + sF_{HP}T_{RH})$$

$$B=[Ds - 2Hs^2 - (k_g s + k_h)G(s)k_1]$$

$$C = (1 + sT_{CH})(1 + sT_{RH})$$

Using final-value theorem, at the new steady-state:

$$\frac{\Delta P_{m1}}{\Delta P_{m2}} = \frac{\lim_{s\to 0} s\Delta P_{m1}(s)}{\lim_{s\to 0} s\Delta P_{m2}(s)} = \frac{k_h}{k_i k_1} = \frac{S_{MG}}{S_{DG}} \tag{3.3.18}$$

As k_h is already determined from (3.3.14) and k_1 is a known constant, k_i can therefore be calculated from (3.3.18).

From Figure 3-10 the closed-loop transfer function of the combined system can be shown to be of the form:

$$G_{com}(s) = \frac{\omega(s)}{\omega_0(s)} = \frac{\sum_{i=1}^{7} b_i s^{i-1}}{\sum_{i=1}^{8} a_i s^{i-1}} \tag{3.3.19}$$

The parameters $a_1 \sim a_8$, $b_1 \sim b_7$ are as defined in the Appendix A. In G_{com}(s), all the coefficients are functions of the known parameters except for k_p. Theoretically, the range of k_p can be determined by applying the Routh's stability criterion to G_{com}(s) [94]. However, as the expression of G_{com}(s) is complex, it is difficult to obtain a general range for k_p in term of the known parameters. In such a case, one can apply Routh's stability criterion based on a numerical example, which will be illustrated in Section 3.3.4. A try and error method is then used to study the dynamic response of G_{com}(s). k_p would be determined once a acceptable dynamic response of G_{com}(s) is reached.

3.3.4 Illustrative Example

A numerical example is used to verify the proposed control scheme described in the previous Sections. The system parameters selected are as given in Table 3-1 [47, 95]. All

the values are then transformed into pu values. The base quantities are: S_b = 131 kVA, V_b = 360 V, ω_b = 377 rad/s.

Table 3-1: System parameters

Micro-turbine				Main generator and system	
P_{m2} [kw]	131	L_T [μH]	28	F_{HP}	0.3
ω_{10}[rpm]	70,000	J [kgm^2]	0.0063	T_{CH} [s]	0.3
V_{rms} [V]	360	τ [s]	5	T_{RH} [s]	7
V_{dc} [V]	600			H [s]	5
				D	2

Using the parameters given above, the open-loop Bode Plot of the micro-turbine model G_1(s) is shown in Figure 3-11. The micro-turbine closed-loop transfer function is G(s) = ω_1/ω_1^* = G_2(s)/(1+G_2(s)). Applying the Routh's stability criterion to the equation of G(s), it is found that in order to ensure stability of G(s), b should be a positive value. In other words, in (3.3.11), it is derived that ϕ_2-φ_{g1} < 180° (i.e., φ_{g1} > ϕ_2-180°). Choosing the desired phase margin ϕ_2 as 15° , it is shown that φ_{g1} < -165°. It is seen from Figure 3-11 that to satisfy the range of φ_{g1}, the new crossover frequency ω_{c2} should not be larger than 1.81 rad/sec. Since a fast dynamic response of the micro-turbine is desirable, the new crossover frequency is chosen as 1.81 rad/sec. The corresponding governor parameters can be calculated from (3.3.11) and they are a = 43.145, b = 1.363. Bode plot of G(s) is also given in Figure 3-12, which shows the designed micro-turbine controller is satisfactory.

The procedure for tuning the main generator governor is similar and would not be described here. Suffice to state that the new crossover frequency ω_{c4} is 0.8 rad/sec and the phase margin ϕ_{c4} is 45°. Based on these parameters, the corresponding governor parameters are k_g = 18.5733, k_h = 6.348. As k_h is determined, k_1 is a constant, which can be easily obtained from (3.3.7).

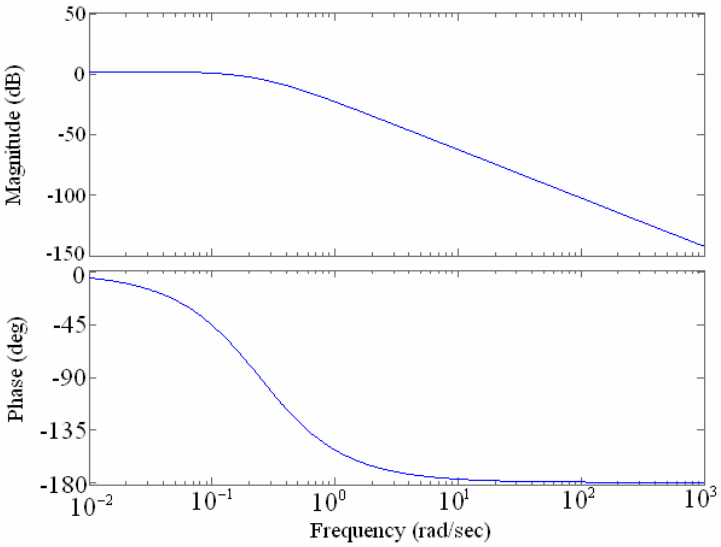

Figure 3-11 Bode plot of the open-loop mocro-turbine model $G_1(s)$

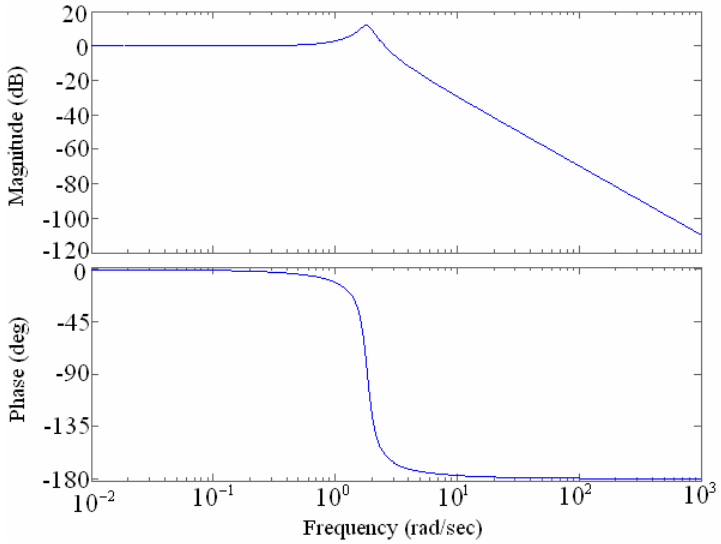

Figure 3-12 Bode plot of closed-loop micro-turbine transfer function $G(s)$

Suppose the capacity of micro-turbine is 30% that of the main generator. Therefore, the desired power-sharing ratio of the main generator to that of the micro-turbine is 3.33. From (3.3.18), $k_i = 2.643$ is obtained.

Substituting all the above parameters into (3.3.19), the closed-loop transfer function of the combined system $G_{com}(s)$ is obtained. The range of k_p is also examined by applying the Routh's stability criterion to $G_{com}(s)$. It is shown that for guaranteed stability, k_p should be within the range: $-6 < k_p < 5.3$. Using a try and error method, it is found that in this example when k_p is 0.1, the system dynamic response is acceptable. The

corresponding Bode plot of G_{com}(s) is given in Figure 3-13 and its bandwidth is 1.66 rad/sec.

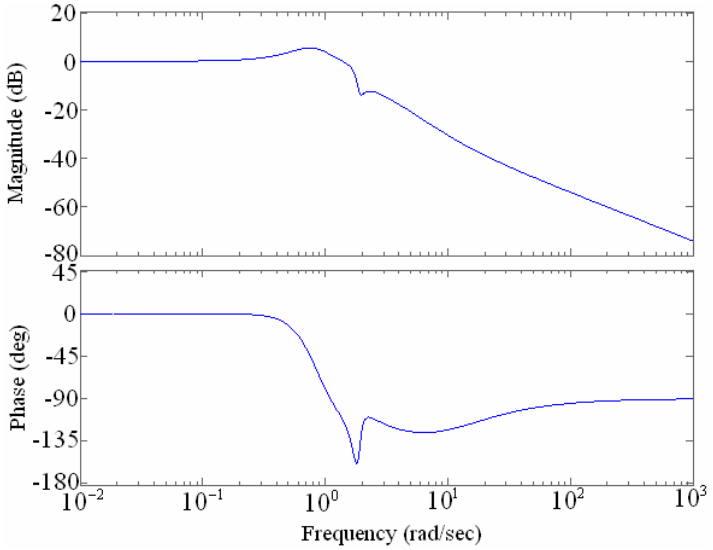

Figure 3-13 Bode plot of closed-loop transfer function of combined system G_{com}(s)

Simulations based on the model of Figure 3-10 have been carried out to demonstrate the proposed control. All the parameters are those given earlier. In the simulation, a step load change (ΔP_L) of 0.5 pu is applied. The plots of ΔP_{m1}, ΔP_{m2}, $\Delta\omega$ and the speed of micro-turbine ω_1 are shown in Figures 3-14 - 3-17.

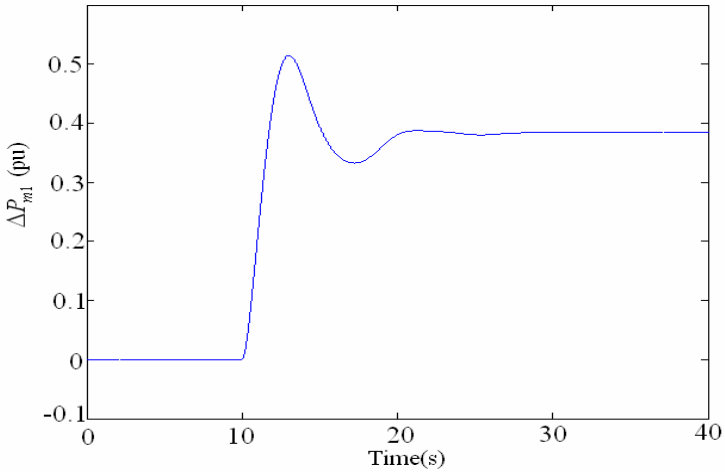

Figure 3-14 Active power change of the main generator (ΔP_{m1})

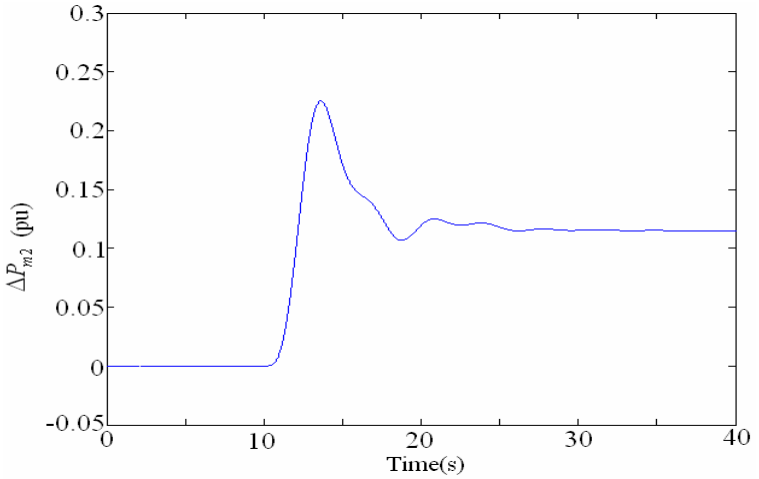

Figure 3-15 Active power change of the micro-turbine (ΔP_{m2})

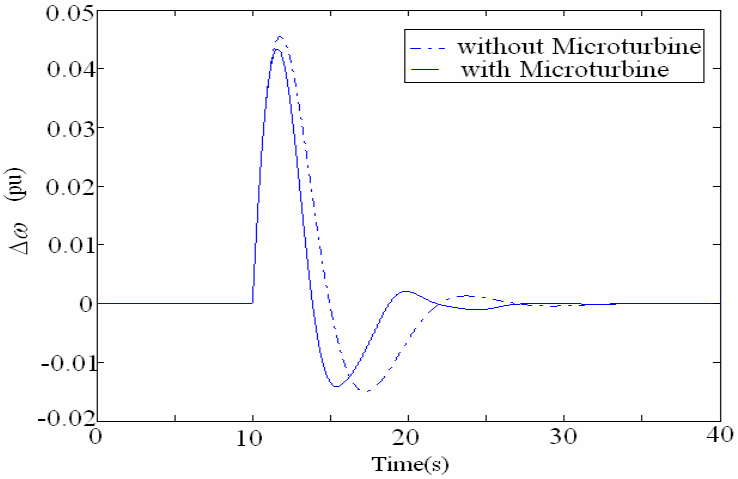

Figure 3-16 System frequency change ($\Delta\omega$)

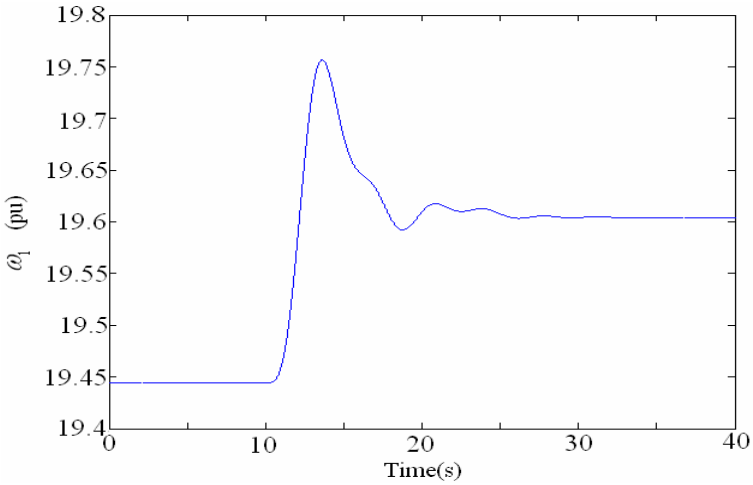

Figure 3-17 Micro-turbine speed (ω_1)

It is seen from Figure 3-14 and Figure 3-15 that at the new steady-state, $\Delta P_{m1}/\Delta P_{m2} \approx 0.385/0.115 = 3.33$. It is the desired load-sharing ratio as it has been assumed that the DG capacity is 30% that of the main generator. Figure 3-16 compares the system frequency change $\Delta\omega$ when the micro-turbine is in service (the new control scheme) and when the micro-turbine is not in service (the conventional control scheme). The conventional scheme is simulated using the model in Figure 3-9, with the same system parameters as that of the earlier design. It is clear that the new scheme reduces the first swing of $\Delta\omega$. The setting time of the new control is also shorter than that of the conventional scheme. Figure 3-17 shows the micro-turbine speed only increases by 0.84% during the speed regulation. It is acceptable for micro-turbine performance.

3.4 Conclusions

The general mathematical model for the UPS-type PQCC has been developed. In developing the model, the analysis includes the upstream power system, the PWM converters and the DG. The derivation of the switching functions of the PWM converters involves the averaging technique and to simplify analysis, Park's transformation and small signal linearization have been used. Both the steady-state DC model and the small signal AC model of the PQCC have been obtained. System steady-state operating conditions and dynamic responses can be examined using the derived model. This model is valuable in term of the design of the control system for the PQCC.

A new frequency stabilization control strategy, which takes advantage of the flexibility offered by the UPS-type PQCC, has also been proposed in this Chapter. Linearized models for micro-turbine and main generator are implemented to study the proposed control scheme. Using the well-known frequency response technique, a simple and useful guide on the design of the generator governors and PQCC frequency controllers has been proposed. The method helps to coordinate the response of the main generator with that of the DG. Simulation results show that the proposed control can effectively mitigate system frequency fluctuation. By comparing the results of the proposed control scheme with that of the conventional control, the PQCC with DG can render improved regulation of the power system frequency.

As reviewed in Chapter 2, the PQCC is expected to be able to mitigate power quality problems. In this Chapter, using the PQCC to mitigate the system frequency variations has been examined. In the next Chapter, application of the PQCC to deal with upstream voltage disturbances would be investigated. The PQCC model developed in this Chapter would form a useful basis for such a study.

Chapter 4

Voltage-Sag Mitigation through Power Quality Control Center

4.1 Introduction

In Chapter 3, the dynamic model of the UPS-type Power Quality Control Center has been derived and its application for power system frequency stability enhancement is also examined. In this Chapter, the use of PQCC to improve system voltage sag ride-through for sensitive loads would be examined.

As was pointed out in Chapter 2, a voltage sag is defined as a momentary voltage decrease and it is one of the most devastating disturbances. Methods to mitigate voltage sags are therefore of great interest and many mitigation techniques have been reported [48]. The method includes re-configuring the power system, increasing equipment immunity or installing mitigation devices, such as the dynamic voltage restorer.

The installation of mitigating devices at the system equipment interface can be a possible solution for customers, who rarely have the chance to request either specific tolerance level for equipment or improved power supply quality. However these devices usually need to be equipped with energy storage facilities in order to compensate for the voltage sags. The amount of stored energy determines the extent of the severity of the sags for which load ride-through can be provided for. Energy storage devices are expensive, and a tradeoff between ride-through capability and cost is required.

Alternatively, by taking full advantages of the flexibility offered by the PQCC and the presence of DG, a new voltage sag mitigation scheme is to be proposed in this Chapter. The proposed scheme is seen to be able to provide, to some extent, similar voltage sag ride-through capability. Also unlike the PQCC ride-through method proposed in [31], the

use of hybrid transfer switches is avoided.

Most of the materials contained in this Chapter have been published in [89].

4.2 PQCC Structure and Distributed Generator Model

4.2.1 Previous PQCC Voltage Sag Ride-through Method

The configuration of the UPS-type PQCC proposed in [30, 31] has been explained in Chapters 2 and 3. Figure 4-1 shows a schematic diagram of the PQCC, including both the structures on high-voltage side as well as low-voltage side of the Center transformer. As introduced in Chapter 2, several levels of power supply quality can be created for customers served by the PQCC. In this investigation, the SP, DC, HQ and OQ loads are assumed to be linear and will not introduce harmonics into the power system. The PQCC also entails a DG connected to the DC-bus. The exact form of the DG for this investigation will be discussed later.

In order to mitigate upstream disturbance effects, the author of [31] proposed that on the high voltage side of the PQCC, the upstream power system is interconnected to the PQCC through two feeders. Each feeder is equipped with hybrid transfer switches (HTS) at the end terminals, as shown in Figure 4-1. The detailed configuration and operation of the HTS can be found in Chapter 2. Under normal operating condition, only one of the two feeders, called the primary feeder, would be used to supply the entire OQ, HQ loads and part of the SP, DC loads. The HTS on the primary feeder are then closed while those on the standby feeder are open. When a fault occurs on the primary feeder, reference [31] proposed that its HTS are opened to isolate the fault from the PQCC and the HTS on the standby feeder are closed. The PQCC is then supplied by the standby feeder. However, over the interval when the power transfer is switched from the primary to the standby feeders, OQ load would be disconnected by the solid-state relay *C* shown in Figure 4-1, which consists of an opposite-poled thyristor pair. The other loads are supplied by the DG. Inv.1 is then operated in the inversion mode during the power transfer.

It is clear that this upstream arrangement is intended to cater for faults which occur on the

primary and standby feeders. In practice, the feeders would only constitute a relatively small part of the upstream system, and the number of fault incidents on the feeders will be small compared to those on the much more extensive upstream transmission-distribution system. Hence, in practice the transfer switches would rarely be called upon to operate. Furthermore, one notes that the DG plays an important role in maintaining the supply to the SP load. Hence, the role of the DG in the PQCC has to be examined more closely. This aspect of the work, and the precise form of the DG and its interaction with the network under system fault conditions, has not been addressed in [30, 31]. In this Chapter, it is proposed that the effects of upstream voltage sag on loads will be mitigated through the use of the DG in conjunction with the control actions of Inv.1. The HTS and the standby supply will not be needed in the proposed scheme.

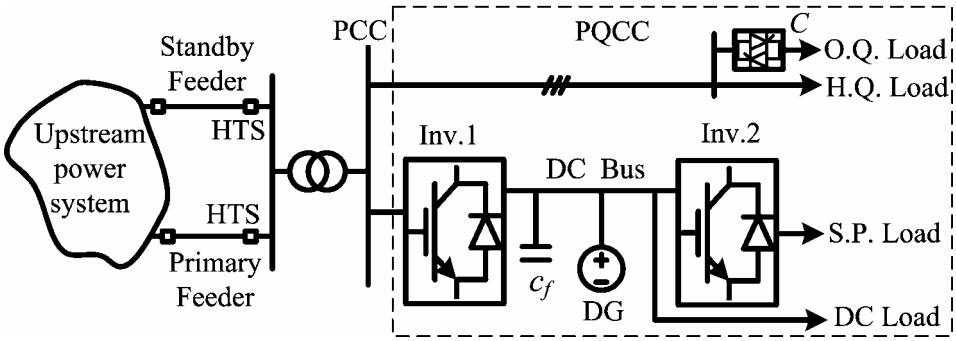

Figure 4-1 Interior structure of the UPS-type PQCC proposed in [31]

4.2.2 Fuel Cell Distributed Generator

As introduced in Chapter 2, in recent years, fuel cells (FC) have emerged as attractive power sources as they are energy-efficient, friendly to the environment and can provide reliable service [67-69]. While there are various kinds of FC, the high temperature solid-oxide fuel cell (SOFC) power plant has been chosen as the form of DG in the present work. The main reason for doing so is because of the impressive service record of a number of demonstration units of SOFC currently in operation [67].

The SOFC internal electrochemical process has been described in Chapter 2. According to the SOFC Nernst Equation given in (2.3.1), it is seen that the ideal SOFC open-circuit EMF E should be constant [13, 67, 68]. However, there are several physical and chemical processes which introduce losses to the performance of fuel cells, such as transport of

reactants to the electrolyte interface and absorption of electro-active species onto the electrode. These losses could result in an operation voltage less than the theoretical values. Figure 4-2 therefore presents a comparison of the ideal and actual voltage versus fuel-cell stack current (I_{FC}) characteristics of a typical fuel cell operation state [13]. It is seen that the ideal voltage of fuel cell is constant. The actual operation voltage is less than the ideal voltage. The differences can be divided into three regions. The region of activation polarization is dominant at lower current densities and is generally a result of losses associated with slow chemical reactions. Ohmic polarization is loss due to the flow of electricity through the fuel cell which resists the flow. It is seen from Figure 4-2 that the region of Ohmic polarization is the linear part of the voltage and varies directly with current. The region of concentration polarization is cause by transport phenomena which lead to lower concentrations of reactants at the electrochemical surface. It is prominent when current densities are large.

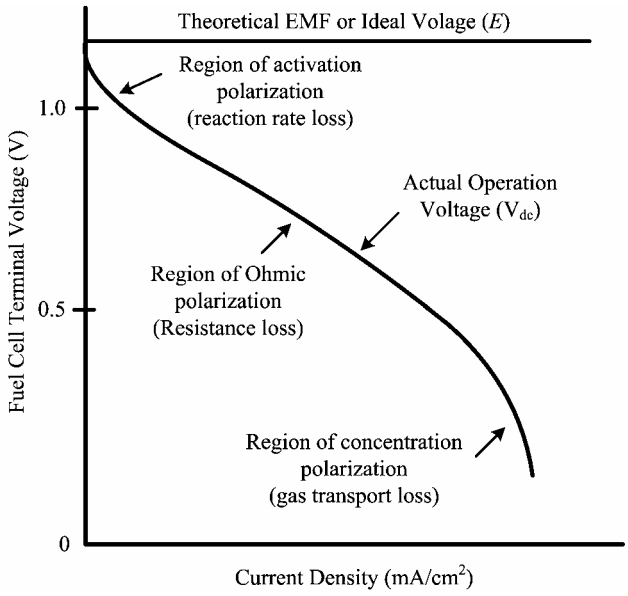

Figure 4-2 Ideal and actual fuel cell current and voltage characteristics [13]

For simplified analysis, SOFC would be assumed always to operate in the linear Ohmic polarization region and the Ohmic loss is the main voltage loss under steady-state. Therefore, the electrical characteristics of the SOFC under steady-state can be expressed as,

$$V_{dc} = E - rI_{FC} \tag{4.2.1}$$

where V_{dc} is the fuel cell steady-state output voltage, E is the ideal constant open-circuit

EMF and I_{FC} is the fuel-cell stack current. In this case r accounts for the Ohmic losses.

The calculation of E is through the application of (2.3.1). It is shown as a highly non-linear function of the hydrogen, oxygen, water partial pressures and cells operating temperature. From the SOFC internal electro-thermodynamics, it is also known that E depends essentially on the rate of the reaction between the input fuel and oxygen. As can be seen in [67, 68], a change in the stack current I_{FC} will typically take tens of seconds for its effect to be fully felt in E. In the context of the problem in-hand, however, it has been recognized that the main considerations is to mitigate the effects of upstream voltage-sag events on loads. Such occurrences have typical duration of the order of one second or less. Hence E can be assumed essentially constant under such a short-duration disturbance condition and (4.2.1) can be used in describing the circuit behavior of the SOFC in the remainder of this Chapter. Furthermore, the SOFC output power (P_{dg}) is then given by

$$P_{dg} = V_{dc} I_{FC} \tag{4.2.2}$$

4.3 Proposed PQCC Voltage Sag Ride-through Scheme

To simplify the analysis, the PQCC is represented by the equivalent circuit model shown in Figure 4-3. Unlike the model shown in Figure 4-1, the HTS and the alternative feeder have been excluded in the proposed scheme. The model developed here is very similar to that shown in Figure 3-1: OQ and HQ loads are ignored at this stage as the SP and DC loads are the main concern for voltage sag ride-through. The upstream power system is represented as a three-phase equivalent voltage source (v_1, v_2, v_3). L is the total upstream line, transformer and inverter reactor inductance. Unlike the model in Figure 3-1, however it is assumed that losses of the upstream line, inverters and transformer are negligible. Furthermore, the simplified SOFC model described by (4.2.1) will be used to represent the DG. The capacitor c_f in the DC-link is included only to indicate the need of a filter. Its energy storage capability tends to be small compared to that of the SOFC. The DC and SP loads are represented by the respective impedances R_d and $R'+j\omega L'$.

Under normal state, while the upstream source supplies the DC and SP loads, it is also expected that the SOFC meets part of these load demands. Inv.1 operates in rectifier

mode and tries to maintain the DC-link voltage (V_{dc}) constant. Furthermore, Inv.1 is controlled to achieve unity power factor at the terminals of the equivalent source in the upstream system, indicated in Figure 4-3 as point 'A'. This is a desirable operating mode as it maximizes the utilization of the upstream transmission-distribution system facility. Inv.2 is used to achieve constant voltage and high level of waveform quality at the SP load terminals.

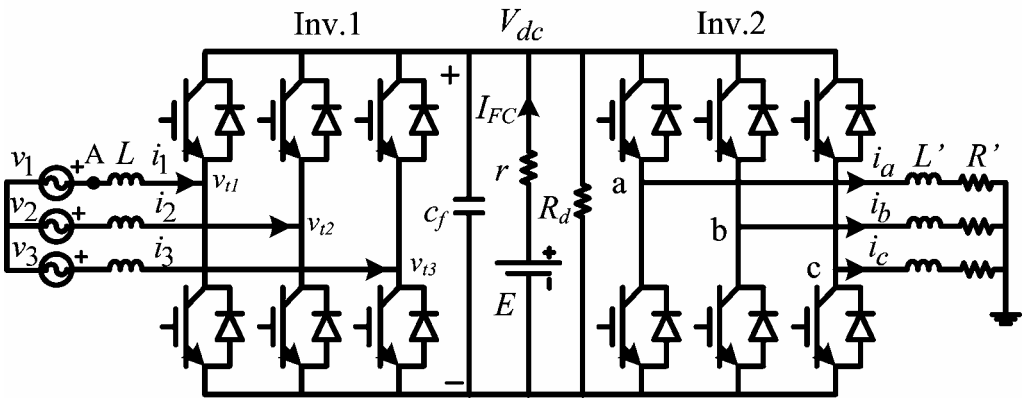

Figure4-3 A simplified PQCC network model

In the proposed scheme, when an upstream sag occurs, the PQCC can achieve high ride-through capability through the appropriate regulation of V_{dc}. The extent of the sags for which the PQCC can ride through must, however, take into consideration the current rating of Inv.1. Such consideration was not given in the previous PQCC designs described in [30, 31]. A detailed explanation of the proposed scheme is given as follows. To simplify the analysis, harmonics and losses due to the inverters are ignored. Due to the complexity and extensiveness of the upstream system, only balanced voltage sag events originated in the upstream power system are considered.

As the upstream AC system and SP load are assumed balanced, it is only necessary to consider one phase (say phase '1') of the three-phase system. With reference to Figure 4-3, suppose under normal state the *rms* value of v_1 is V_{s0} and that of the ac link current i_1 is I_{s0} (*rms*). The subscript '0' is used in this Chapter hereafter to denote the respective pre-sag steady-state quantity. Denote the current rating of Inv.1 as $I_{inv1,rate}$. Hence, the ac line current should be limited to less than $I_{inv1,rate}$. In the event of upstream voltage sag, V_{s0} decreases to V_{sag} and the line current becomes I_{sag}. Suppose Inv.1 is controlled to operate at unity power factor even under a sag condition, i.e. V_{s0} is in phase with I_{s0} as well as

V_{sag} is in phase with I_{sag}. In view of the current limit placed on the interconnection and Inv.1, the proposed scheme is then designed to consist of the following stages, depending on the severity of the voltage sags.

4.3.1 Stage 1

Under this stage, the upstream sag is relatively shallow such that V_{dc} can be controlled to maintain at the same level as before the sag, denoted as V_{dc0}. This is the conventional method for compensating voltage sags, as described in [96]. Under this situation the output power from the SOFC remains constant before and during the sag: the SOFC is undisturbed. The DC and SP load demands are also unaffected as V_{dc} is constant. Therefore the same active power, which is denoted as P_{ac0}, would be supplied from the upstream system to the DC side during the sag as before the sag, i.e.,

$$P_{ac0} = 3V_{s0}I_{s0} = 3V_{sag}I_{sag} \tag{4.3.1}$$

Under the sag condition, $V_{s0} > V_{sag}$. This means that the line current would have to increase during the sag. Since the maximum line current is limited to the current rating $I_{inv1,rate}$, the most severe sag (denoted as $V_{sag,max1}$) the system can ride-through under Stage 1 is therefore given by:

$$V_{sag,\max 1} I_{inv1,rate} = V_{s0}I_{s0}$$

or

$$V_{sag,\max 1} = \frac{V_{s0}I_{s0}}{I_{inv1,rate}} \tag{4.3.2}$$

The above equation shows that any sag which results in a standing voltage at the PCC such that $V_{sag} > V_{sag,max1}$, the resulting line current during sag will still be within the current rating of Inv.1. Inv.1 will not be overloaded. Hence, the PQCC will be able to compensate for the voltage sag by maintaining V_{dc} constant through the control of Inv.1. Equation (4.3.2) shows that the maximum sag that can be accommodated is directly proportional to the ratio between the initial current loading to the current rating of Inv.1. Unfortunately, for sags which result in $V_{sag} < V_{sag,max1}$, Inv.1 could be damaged under such a control strategy. Another control scheme described below is therefore needed to improve on the system ride-through capability.

4.3.2 Stage 2

When $V_{sag} < V_{sag,max1}$, it is still necessary to ensure $I_{sag} < I_{inv1,rate}$. Since the input power from the upstream source is $P_{ac}=3V_{sag}I_{sag}$, and as V_{sag} is not directly controllable, then the only possible way to reduce I_{sag} is to reduce P_{ac}. As it is imperative that the SP load demand (P_{SP}) should not be affected during the sag, reducing P_{ac} necessitates the SOFC to increase its output power contribution (P_{dg}) in order to maintain the load-generation balance. Since E and r of the SOFC are essentially constant under such short-duration sag conditions, then the output power of the DG can only be increased by reducing V_{dc}. Therefore the main control strategy of Stage 2 is to allow V_{dc} to vary from V_{dc0} to a lower level, denoted as $V_{dc}^{'}$.

As the SOFC internal resistance r is relatively small in comparison to the upstream source impedance [67, 68], a small decrease in V_{dc} can realize a large increase in P_{dg}. Therefore one practical limit placed on $V_{dc}^{'}$ is to ensure that there is no reverse power flow from the SOFC back to the upstream power system, i.e. $P_{ac} \geq 0$. Failing to achieve this would mean that the SOFC contributes toward the power flow into the upstream system. There will be an undesirable increase in the fault current. The power supplied by the upstream network can be expressed as

$$P_{ac} = P_{SP} + P_{DC} - P_{dg} = P_{SP} + \frac{V_{dc}^2}{R_d} - \frac{V_{dc}(E - V_{dc})}{r} \tag{4.3.3}$$

As the SP load must not be disturbed by the sag, P_{SP} is therefore constant. Rearranging (4.3.3), therefore

$$P_{ac} = (\frac{1}{R_d} + \frac{1}{r})V_{dc}^2 - \frac{EV_{dc}}{r} + P_{SP} \tag{4.3.4}$$

Equation (4.3.4) is quadratic in V_{dc} and Figure 4-4 shows how P_{ac} varies with V_{dc}. V_1, V_2 in Figure 4-4 are the two roots of (4.3.4), i.e.

$$V_{1,2} = \frac{E/r \pm \sqrt{(E/r)^2 - 4P_{SP}(1/R_d + 1/r)}}{2(1/R_d + 1/r)} \tag{4.3.5}$$

Note that in (4.3.5), a necessary condition for the existence of the two roots is $P_{SP} < E^2/4r$. It places a constraint on E and r of the SOFC for a given P_{SP}. The minimum value of P_{ac} is reached when V_{dc} equals to V_0, which for $R_d >> r$,

$$V_o = \frac{E/r}{2(1/R_d + 1/r)} \approx \frac{E}{2} \tag{4.3.6}$$

Under normal operating state, V_{dc} equals to V_{dc0} and the corresponding active power from the upstream ac source is P_{ac0}. This corresponds to operating point 'b' in Figure 4-4. As the SOFC is injecting power into the DC-link, it is obtained $E > V_{dc0}$. Although point 'a' in Figure 4-4 also yields the same power level P_{ac0}, its corresponding voltage V_a is relatively small ($V_a < E/2$). The SOFC output current would be very large and could exceed the DG current rating. Clearly the feasible range of V_{dc0} has to be such that $V_{dc0} > V_2$ to achieve $P_{ac} \geq 0$.

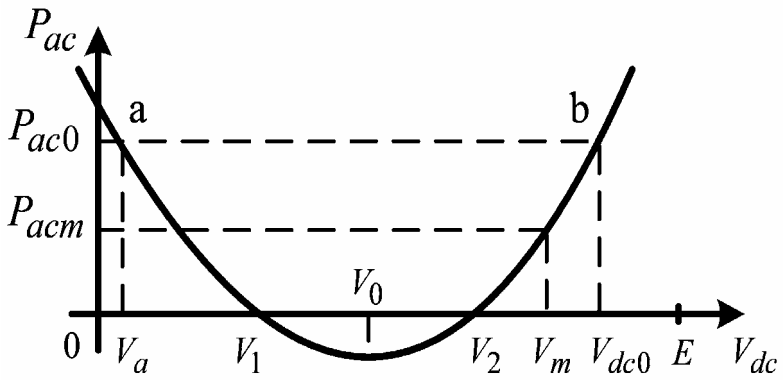

Figure 4-4 P_{ac} vs V_{dc}

Suppose V_{dc} is allowed to decrease from V_{dc0} to $V_{dc}^{'}$ over the sag period. While it is not clear what is a suitable value for $V_{dc}^{'}$, Figure 4-4 shows that in order to ensure $P_{ac} \geq 0$, $V_{dc}^{'}$ should be chosen within the range of V_{dc0} and V_2. When V_{dc} reduces to V_2, there is no power flow on the interconnection and the SOFC meets the entire load requirement (P_{DC}+P_{SP}). This is the critical condition. Once V_{dc} reduces to less than V_2, the active power supplied by the SOFC is more than the load requirements. The surplus power would flow reversely into the upstream power system, corresponding to $P_{ac} < 0$. This condition is undesirable.

Another consideration on $V_{dc}^{'}$ is that it should be within a reasonable lower bound from its nominal value, for example $V_{dc}^{'} > 0.9V_{dc0}$. It is quite conceivable that if this condition is not satisfied, the DC load may not be able to maintain normal operation. Inv.2 may also be in danger of running out of its control margin and therefore cannot achieve constant

voltage at the SP load terminals. As it is known that a small decrease in V_{dc} can realize a large increase in P_{dg}, hence it is most likely that $V_2 > 0.9V_{dc0}$. Taking all these into consideration, a reasonable bound for $V_{dc}^{'}$ is therefore $V_2 < V_{dc}^{'} < V_{dc0}$.

From Figure 4-4, it can be seen that a lower value of $V_{dc}^{'}$ results in a reduced P_{ac}. It is desirable because the PQCC can then provide increased output power to support the loads during sag. However, due to the complexity and intricacy of the SOFC power plant, it is also desirable to maximize the amount of power that can be drawn from the upstream system and therefore minimizes the disturbance to the SOFC during the sag. A compromise has to be sought. It is proposed that under Stage 2, $V_{dc}^{'}$ is set at the mid-point value between V_{dc0} and V_2, denoted as V_m in Figure 4-4, i.e.

$$V_m = \frac{V_{dc0} + V_2}{2} \tag{4.3.7}$$

Substituting (4.3.7) into (4.3.3) and re-organizing terms, the active power supplied by the upstream system under Stage 2 is

$$P_{acm} = P_{SP} + 0.25(1 + \frac{V_2}{V_{dc0}})[\frac{V_{dc0}^2}{R_d} - \frac{(E - V_{dc0})V_{dc0}}{r}] + 0.25(1 + \frac{V_{dc0}}{V_2})[\frac{V_2^2}{R_d} - \frac{(E - V_2)V_2}{r}] \tag{4.3.8}$$

Note that when $V_{dc} = V_{dc0}$, from (4.3.3) the active power supplied by the upstream system is:

$$P_{ac0} = P_{SP} + \frac{V_{dc0}^2}{R_d} - \frac{V_{dc0}(E - V_{dc0})}{r}$$

or

$$\frac{V_{dc0}^2}{R_d} - \frac{V_{dc0}(E - V_{dc0})}{r} = P_{ac0} - P_{SP} \tag{4.3.9}$$

When $V_{dc} = V_2$, $P_{ac} = 0$. Then

$$0 = P_{SP} + \frac{V_2^2}{R_d} - \frac{V_2(E - V_2)}{r}$$

or

$$\frac{V_2^2}{R_d} - \frac{V_2(E - V_2)}{r} = -P_{SP} \tag{4.3.10}$$

Substituting (4.3.9), (4.3.10) into (4.3.8), one obtains

$$P_{acm} = 0.5P_{SP} + 0.25P_{ac0} + \frac{0.25V_2}{V_{dc0}}(P_{ac0} - P_{SP}) - \frac{0.25V_{dc0}P_{SP}}{V_2} \tag{4.3.11}$$

Since in practice $V_2 > 0.9V_{dc0}$, then $V_2/V_{dc0} \approx 1$. Substituting this into (4.3.11), one obtains,

$$P_{acm} \approx 0.5P_{ac0} \tag{4.3.12}$$

Equation (4.3.12) shows that under Stage 2 when V_{dc} is reduced to V_m, the active power supplied by the upstream system decreases to nearly half of its pre-sag value. It then follows that during the sag,

$$3V_{sag}I_{sag} \approx 0.5P_{ac0}$$

or

$$V_{sag}I_{sag} \approx 0.5V_{s0}I_{s0} \tag{4.3.13}$$

The condition when Inv.1 will not be overloaded is when $I_{sag}=I_{inv1,rate}$. Substituting this into (4.3.13), the most onerous sag which can be mitigated under Stage 2 is when $V_{sag} = V_{sag,max2}$, i.e.

$$V_{sag,\max 2} = \frac{0.5V_{s0}I_{s0}}{I_{inv1,rate}} = 0.5V_{sag,\max 1} \tag{4.3.14}$$

In summary, therefore, Stage 2 is seen to be capable of handling any upstream fault event which is twice as severe as that can be accommodated under Stage 1. This is achieved by allowing the DC-bus voltage to decrease to V_m. Power compensation is through the support provided by the SOFC. Reverse power flow will be prevented as V_{dc} is not reduced to less than V_2.

4.3.3 Stage 3

In the unfortunate event when the upstream voltage sag is even more severe than that considered earlier, it is impossible to apply the Stage 2 control scheme. It is proposed that the DG would supply all the SP and DC loads over the short duration of the sag. This is the basic requirement of Stage 3 and P_{ac} would decrease to 0. One could of course rely on the upstream circuit protection system to isolate the PQCC from the faulted upstream network. However, the typical circuit breaking system would take at least several cycles to take effect. Once the disturbance is over, moreover, the PQCC has to be reconnected to the upstream system by reclosing the switching device. There is then the attendance risk of large in-rush current if the reclosure process is not properly coordinated [50]. Instead of using the switches to disconnect the PQCC from the upstream system, the proposed scheme uses Inv.1 to realize the same objective, as follows.

From Figure 4-4, it is known that P_{ac} is 0 when $V_{dc} = V_2$. Therefore, as soon as it has been determined that $V_{sag} < V_{sag,max2}$, the reference value of V_{dc} for the control of Inv.1 will be set to V_2 immediately. The active power supplied by the upstream system is then forced to reduce. When V_{dc} reaches the value of V_2, P_{ac} would be 0. At this precise condition, the power supplied by the SOFC satisfies the total DC and SP load requirements. Note that in order to ensure constant E of the SOFC, Stage 3 can only be used to ride through short duration sags. The case of prolonged sags would need further examination where the internal dynamics of the SOFC would have to be taken into consideration.

From the above scheme, it is also clear that the minimum power rating for the SOFC in order to sustain the proposed operation is

$$P_{dg,rate} = P_{SP} + (\frac{V_2}{V_{dc0}})^2 P_{DC0} \tag{4.3.15}$$

Once the disturbance is over, the reference value of V_{dc} can be restored to its nominal value V_{dc0}. As no circuit breaker is used in the proposed scheme, no in-rush current would occur when the PQCC is restored to the normal state.

4.4 Control System Design

A closed-loop control system necessary for the implementation of the above proposed sag mitigation scheme is developed. The design of the control system would be based on the dynamic model of the PQCC derived in Chapter 3. As Inv.1 plays a central role in the scheme, attention is therefore directed toward the design of the controller of Inv.1. The controller design for Inv.2 is not described as its control scheme is well known [88]. Its main function is to maintain the terminal voltage of the SP load. The main functions of Inv.1 are to regulate V_{dc} and to maintain unity power factor on the ac side. As introduced in Chapter 2 and 3, Inv. 1 is a PWM converter. Many control strategies for this type of converters have been proposed [97, 98]. The voltage-oriented control strategy described in [98] would be adopted here because it has a fixed switching frequency and the controller structure is simpler. The proposed controller is given in Figure 4-5.

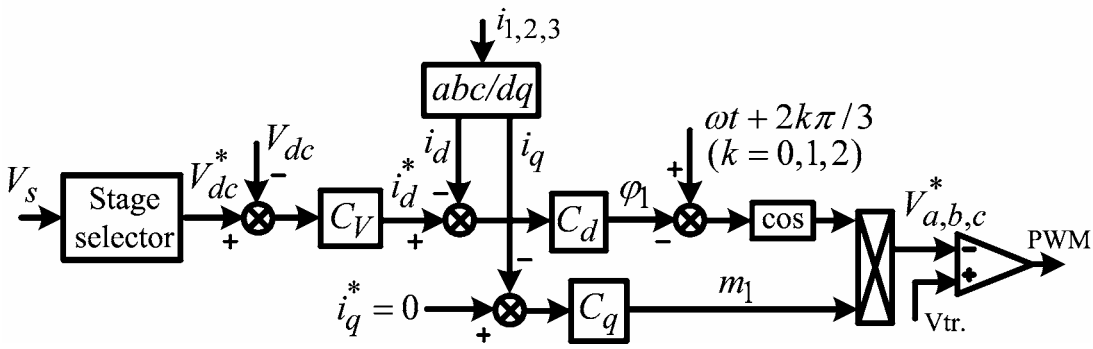

Figure 4-5 Proposed control scheme for Inv.1

It is seen in the controller, an inner current control loop is used to achieve fast dynamic response and unity power factor. Unity power factor is realized by setting the reference value of the line current to be in phase with the source voltage, hence $i_q^* = 0$. Two PI controllers, C_d and C_q, are used in the inner loop to regulate the d-axis and q-axis current components respectively. The outer loop, and its associated controller C_V, is used to regulate V_{dc}. A voltage sensor is used to measure the upstream voltage and convert it into its *rms* value, denoted here as V_s. This information is sent to the "Stage Selector" block, which would output the appropriate reference value (V_{dc}^*) for V_{dc}. Following the sag mitigation scheme described in Section 4.3, the Selector operates in the following way:

Stage 1: If $V_{sag,\max 1} < V_s \le V_{s0}$, then $V_{dc}^* = V_{dc0}$;

Stage 2: If $V_{sag,\max 2} < V_s \le V_{sag,\max 1}$, then $V_{dc}^* = V_m$;

Stage 3: If $V_s \le V_{sag,\max 2}$, then $V_{dc}^* = V_2$.

It is seen from Figure 4-5 that the inverter-switching pattern is obtained from a comparison of the reference voltage $V_{a,b,c}^* = m_1 \cos(\omega t - 2k\pi/3 - \varphi_1)$, ($k$ = 0, 1, 2) with a fixed high-frequency triangular waveform V_{tri}. This is based on the PWM scheme described in Chapter 3. It is also noticed that in the controller Δi_d is used to regulate the phase angle φ_1 while Δi_q is to manipulate the modulation index m_1. The reason is as follows. In Chapter 3, the dynamic model of the PQCC has been developed and the transfer functions between the system state variables and the control variables can be similarly derived. Therefore one can obtain the transfer functions $\Delta i_d(s)/\Delta m_1(s)$ and $\Delta i_q(s)/\Delta m_1(s)$ from (3.2.43) by setting the upstream line resistance R = 0. Since the control system is to be designed over a frequency range much below the bandwidth of

$\Delta i_d(s)/\Delta m_1(s)$ and $\Delta i_q(s)/\Delta m_1(s)$, the magnitude of the transfer functions can be approximated by:

$$\lim_{S\to 0}\left|\frac{\Delta i_d(s)}{\Delta m_1(s)}\right| = A_1\omega L\left|\cos\phi_1\right| \tag{4.4.1}$$

$$\lim_{S\to 0}\left|\frac{\Delta i_q(s)}{\Delta m_1(s)}\right| = A_1\omega L\left|\sin\phi_1\right| \tag{4.4.2}$$

where A_1 is a constant value and ϕ_1 is the steady-state value of φ_1. It is seen that the relative size of above equations depends on the value of ϕ_1 and its value can be derived as follows.

It is known that Inv.1 terminal voltage V_{t1} can be regulated through modifying the modulation index and phase angle of Inv.1. As the reference voltage for the PWM pattern is $V^*_{a,b,c} = m_1\cos(\omega t - 2k\pi/3 - \varphi_1)$ and from the basic PWM technique [88], the steady-state Inv.1 terminal voltage (phase '1') can be represented as $V_{t10} = 0.5V_{dc0}M_1\cos(\omega t - \phi_1)$. It is also known that the ac source voltage is $v_1 = \sqrt{2}V_{s0}\sin\omega t$. Under unity power factor condition, the phasor diagram of upstream source side voltage and line current is as shown in Figure 4-6. u_L is the voltage drop across the inductor L. Unity power factor means that i_1 is in phase with v_1 and the following equation will be satisfied:

$$0.5V_{dc0}M_1\cos(\frac{\pi}{2} - \phi_1) = \sqrt{2}V_{s0} \tag{4.4.3}$$

Therefore under steady-state in order to achieve unity power factor, the modulation index of Inv.1 must be set as,

$$M_1 = \frac{2\sqrt{2}V_{s0}}{V_{dc0}\cos(\phi_1 - \frac{\pi}{2})} \tag{4.4.4}$$

To achieve sufficient margin of the modulation index, it is then desirable to set the steady-state value of ϕ_1 very close to 90° [91]. Hence $\cos\phi_1 \approx 0$, $\sin\phi_1 \approx 1$. Therefore over the frequency band for which the controller should be effective and from (4.4.1) and (4.4.2), one note that $\left|\Delta i_d/\Delta m_1\right| << \left|\Delta i_q/\Delta m_1\right|$. Using the same method, it can also be shown that $\left|\Delta i_q/\Delta\varphi_1\right| << \left|\Delta i_d/\Delta\varphi_1\right|$. These two inequality equations show that $\Delta\varphi_1$ will play a more dominant role than Δm_1 in affecting Δi_d while Δm_1 is the dominant factor in affecting Δi_q.

This explains the control scheme shown in Figure 4-5 where φ_1 is used as the control variable to correct the error signal $(i_d^* - i_d)$ while m_1 is used for controlling $(i_q^* - i_q)$.

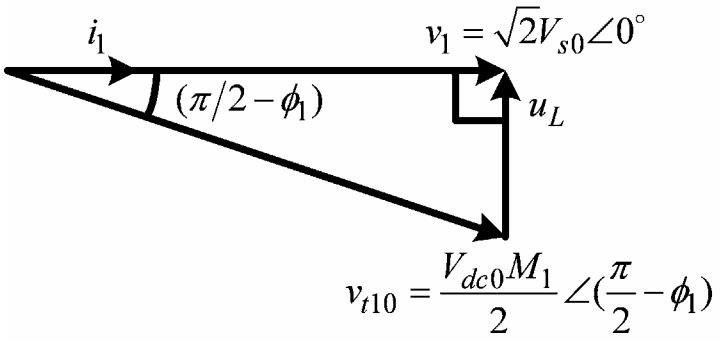

Figure 4-6 Inv.1 voltage and current phasor diagram under unity power factor

Based on the above description, a simplified small-signal model describing the PQCC closed-loop control system is obtained, as shown in Figure 4-7. In the figure, the dynamics of Inv.1 is represented by the transfer functions $G_1(s) = \Delta i_d(s)/\Delta\varphi_1(s)$, $G_2(s) = \Delta i_q(s)/\Delta m_1(s)$, $G_3(s) = \Delta V_{dc}(s)/\Delta\varphi_1(s)$ and $G_4(s) = \Delta V_{dc}(s)/\Delta m_1(s)$. These transfer functions are determined from (3.2.43). The inner current loops and the outer voltage loop of the control system are clearly revealed in the figure. In this investigation, proportional-integral control has been used. Therefore $(k_{p1}+k_{i1}/s)$ and $(k_{p2}+k_{i2}/s)$ correspond respectively to the two inner loop PI controllers C_d and C_q in Figure 4-5. The outer loop PI controller C_V has the form (k_p+k_i/s).

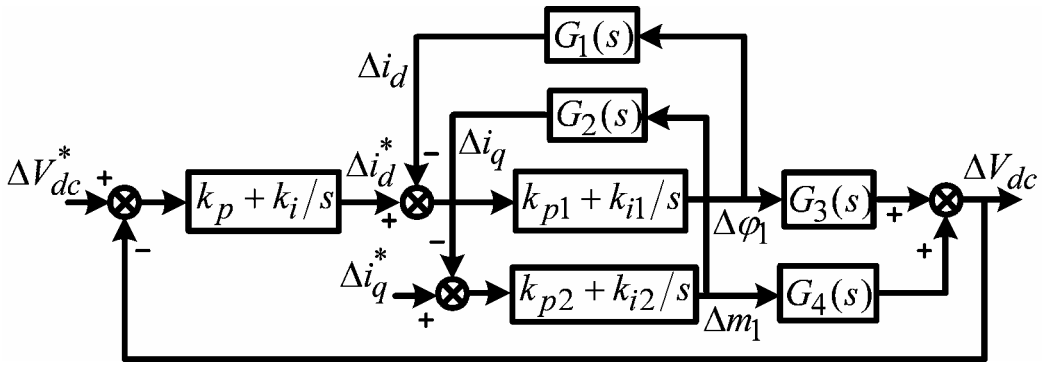

Figure 4-7 Simplified controller block diagram

The parameters of the PI controllers can then be determined based on this simplified model. The frequency response tuning technique, similar to that used in Chapter 3, may

be adopted. Focusing firstly on the d-axis inner current loop, the compensated loop should give a pre-specified desirable bandwidth ω_c and phase margin ϕ_c. The parameters k_{p1} and k_{i1} are therefore derived to meet those requirements. The PI controller in the q-axis inner loop is normally set in the same manner as that for the d-axis loop. The outer loop controller is then tuned to achieve the desired outer loop bandwidth ω_0 and phase margin ϕ_0. When tuning the outer loop, the inner loop is replaced by its closed-loop transfer function, for ease of the analysis.

4.5 Simulation

A numerical example may now be used to demonstrate the proposed control scheme. The system parameters used are as given in Table 4-1, which were calculated according to the following assumed active power distribution. Under normal steady-state, P_{ac0} = 100 kW, P_{DC0} = 50 kW, P_{SP} = 150 kW and P_{dg0} = 100 kW. The SOFC rating is 200 kW and its parameters were obtained from [99]. The inductance L is chosen to provide a fault level of approximately 400 kVA at the PQCC terminals. The capacitor in the DC-bus is for filtering purpose and its value is therefore chosen to be relatively small. Note that the PWM rectifier is a boost converter. Therefore V_{dc0} should be larger than V_{s0}. In this example, V_{dc0} is selected to be 800 V.

Table 4-1: Parametric values of the PQCC and power system

V_{s0} [V]	220	R_d [Ω]	12.8
L [mH]	1	R' [Ω]	0.472
c_f [μF]	200	L' [mH]	1.277
E [V]	815.75	V_{dc0} [V]	800
r [Ω]	0.126	ω [Hz]	60

Using the above parameters, the PI controllers can be tuned. The inner current loop transfer function is examined firstly. Its desired bandwidth and phase margin are selected as ω_c = 150 rad/sec, ϕ_c = 45°. The corresponding PI controller parameters are therefore determined as $k_{p1} = k_{p2}$ = 2.5, $k_{i1} = k_{i2}$ = 1200. It is known that the outer-loop bandwidth should be much smaller than the inner loop bandwidth. In this example, the bandwidth ω_0

is set at 30 rad/sec and the phase margin ϕ_0 is 45°. The outer loop PI controller is then determined as $k_p = 4$, $k_i = 200$.

Under this load condition, the steady-state upstream line current can be obtained as $I_{s0} = P_{ac0}/3V_{s0} = 152$ A. Suppose Inv.1 is loaded to 80% of its rating. Therefore, $I_{s0} = 0.8I_{inv1,rate}$ and $I_{inv1,rate} = 190$ A. From (4.3.2) and (4.3.14), therefore one obtains $V_{sag,max1} = 0.8V_{s0}$ and $V_{sag,max2} = 0.4V_{s0}$. Substituting $V_{dc0} = 800$ V and the relevant parameters into (4.3.5) and (4.3.7), hence $V_2 = 784$ V and $V_m = 792$ V. The PQCC sag ride-through scheme can therefore be divided into the three stages shown in Table 4-2 with the respective reference voltage for V_{dc}.

Table 4-2: PQCC stage selector settings

Stage	Sag ride-through range	V_{dc}^* [V]
1	$V_{sag} > 0.8V_{s0}$	800
2	$0.4V_{s0} < V_{sag} \leq 0.8V_{s0}$	792
3	$V_{sag} \leq 0.4V_{s0}$	784

Simulations using the model in Figure 4-3 have been carried out to verify the proposed voltage sag ride-through scheme. The simulation software used is Matlab/Simulink. The cases examined include those when the upstream voltage is depressed to 90%, 60% and 30% of its nominal value. Each sag event lasts for 0.2 s. Results are shown in Figures 4-8 – 4-10.

Figure 4-8 shows the system response under the 90% sag condition. It shows that the DC-link voltage is constant before and during the sag. Active power supplied by the upstream network and the SOFC (P_{ac}, P_{dg}) are almost unchanged over the sag duration. Line current increases under sag condition but is well within Inv.1 current rating. The upstream network is operating at unity power factor as Q_{ac} is negligible throughout the interval.

Figure 4-9 shows the ride-through situation under Stage 2 when the 60% sag occurs. In order to improve the system ride-through capability and based on Table 4-2, V_{dc} is

allowed to reduce slightly to 792 V as shown in the figure. P_{ac} is reduced to about one half of its original value during the sag. P_{dg} therefore increases correspondingly to achieve active power balance. The upstream line current decreases as P_{ac} reduces over the sag state. Unity power factor is again achieved, except for the short instants at the beginning and the end of the sag.

For those more severe sags, such as the 30% voltage sag shown in Figure 4-10, the PQCC supplies all the downstream loads. Upon the detection of the sag, V_{dc} is controlled to decrease to 784 V (i.e. V_2). Both P_{ac} and the upstream line current reduce to 0 almost instantaneously. When the sag is over, the DC-link voltage is restored to its steady-state value. No large in-rush current is seen at the end of the sag.

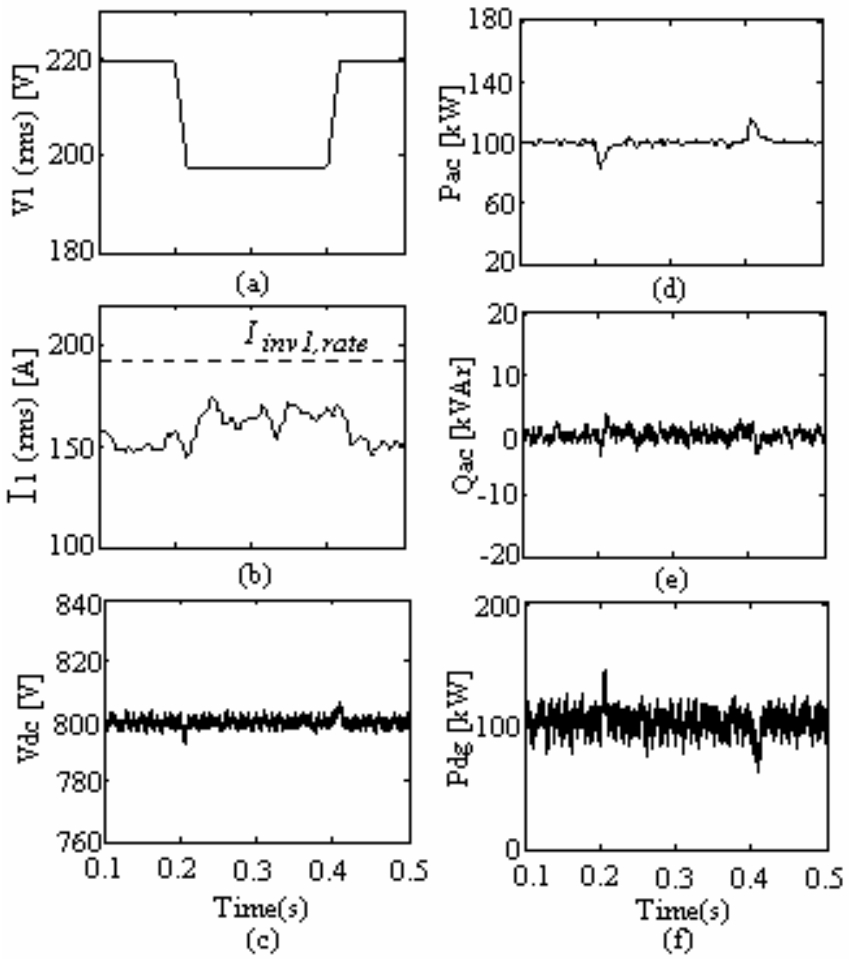

Figure 4-8 Ride-through for a 90% voltage sag (Stage 1): (a) Phase '1' source voltage; (b) Upstream line current I_1 (rms); (c) DC-link voltage; (d) Active power supplied by the upstream source; (e) Reactive power supplied by the upstream source; (f) Active power supplied by the DG.

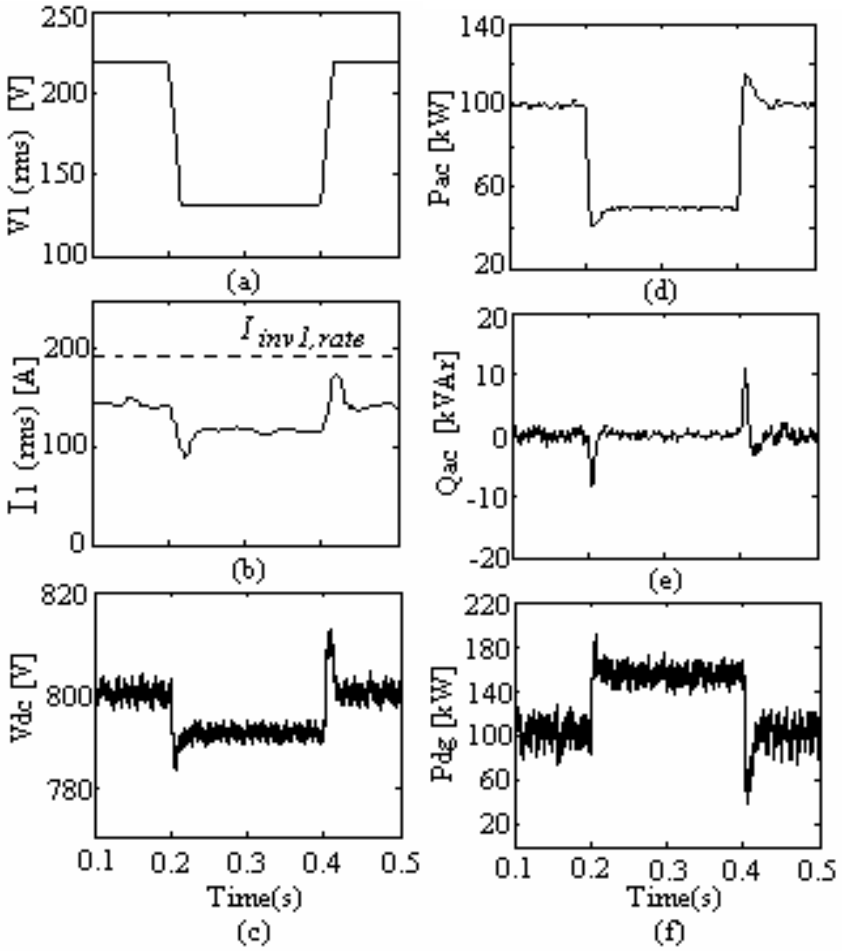

Figure 4-9 Ride-through for a 60% voltage sag (Stage 2): (a) Phase '1' source voltage; (b) Upstream line current I_1 (rms); (c) DC-link voltage; (d) Active power supplied by the upstream source; (e) Reactive power supplied by the upstream source; (f) Active power supplied by the DG.

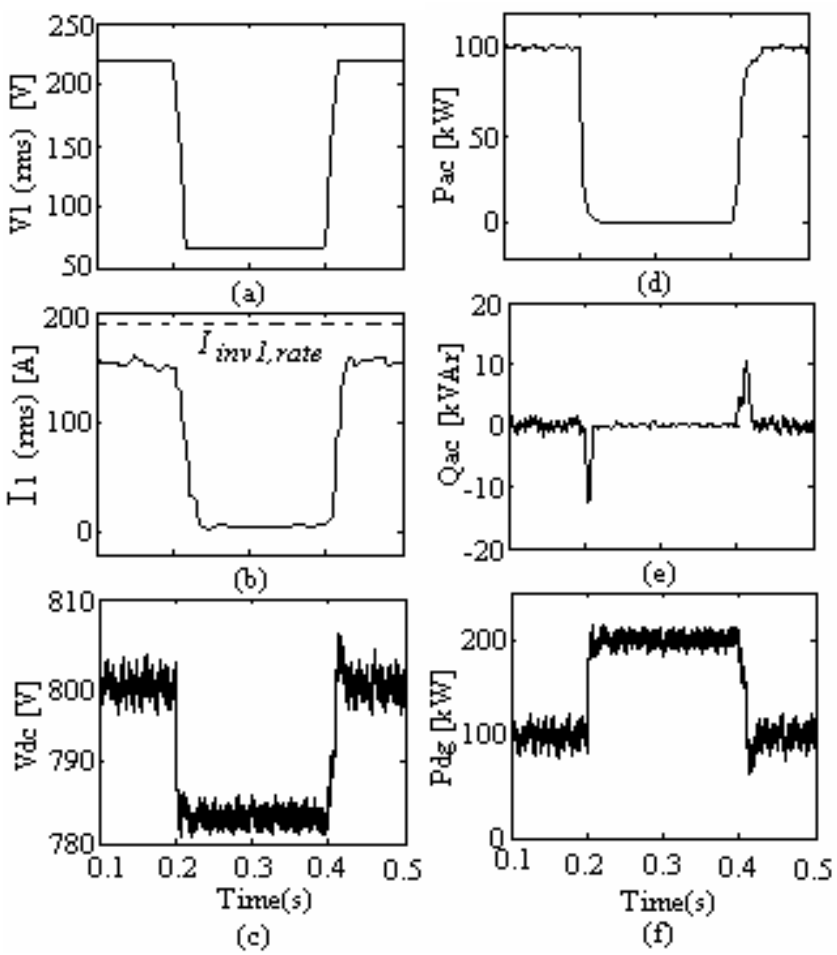

Figure 4-10 Ride-through for a 30% voltage sag (Stage 3): (a) Phase '1' source voltage; (b) Upstream line current I_1 (rms); (c) DC-link voltage; (d) Active power supplied by the upstream source; (e) Reactive power supplied by the upstream source; (f) Active power supplied by the DG.

In all cases considered, the Inv.1 controllers appear to be well tuned, and have performed satisfactorily in that the transient responses of the PQCC are well damped.

4.6 Conclusions

A new voltage sag mitigation scheme, which takes advantage of the flexibility offered by the Power Quality Control Center, has been proposed. A three-stage operation scheme has been incorporated into the control of the inverters and the fuel cell in the PQCC. Analysis shows that the system ride-through capability can be extended considerably to cater for upstream voltage sags. Unlike previous schemes associated with the PQCC, the present scheme has the advantage of not requiring the use of standby feeders and the

associated hybrid transfer switches. The scheme exploits more fully the flexible control features offered by the inverter and the ability of the distributed generator in the PQCC. From the system mathematical model developed for the PQCC, the control system of the inverters to realize the proposed scheme has been developed. The efficacy of the scheme is borne out by the simulation results.

Although the above results appear promising, the proposed voltage sag ride-through scheme has not included the OQ and HQ loads. Unbundled power quality service, which is the most desirable feature of the PQCC system, has not been examined under upstream voltage sag condition. Furthermore, the DG, which is in the form of a SOFC, is only represented as a constant EMF with a series resistance. Many functional characteristics of the SOFC have not been considered in this simplified model. These issues would be investigated in the next Chapter.

Chapter 5

Fuel Cell-Based PQCC to Realize Unbundled Power Quality Supply

In Chapter 4, using a fuel cell-based PQCC to improve the voltage sag ride-through capability of sensitive loads has been examined. Although the scheme proposed there offers some degrees of flexibility in term of the operations of the PQCC, unbundled power quality supply has not been addressed as the OQ and HQ loads are ignored when examining the upstream system voltage sag effects. Since unbundled power quality supply is one of the most important functions for the distribution systems of the future, additional operation scheme of the PQCC should be included to achieve the objective.

As introduced in Chapter 2, the authors of [30, 31] have suggested the interior structure of the PQCC and the corresponding operational scheme. Although the operation scheme given there achieves unbundled power quality supply, one also notices that there are still a number of technical issues that warrant deeper investigation. For instance, as the exact form of the DG is not reported in [30, 31], the DG is expected to meet any of the power shortfall in the HQ, SP and DC load demands during the upstream fault condition. In adopting this operating scheme, however, it is important to consider firstly the dynamic response capability of the DG. Depending on the relative sizes of the HQ, SP and DC loads in comparison with the DG capacity, the DG output power would have to change rapidly and at the precise output level when the upstream power system transits from a healthy into a faulted state. In the reported work, it is not clear to what extent the DG can accommodate such a power change while maintaining the desired supply quality. Moreover, the scheme proposed in [30, 31] have not considered the impacts of upstream or downstream fault on the PQCC, in term of the manner by which the DG and the power converters are controlled so as to maximize the potential benefits that can be extracted from the flexible distribution system.

In view of the above, the present investigation re-examines the work reported in [30, 31],

with the intention to develop a more realistic operational scheme for the PQCC under both steady-state and system fault conditions. Similar to Chapter 4, the DG will assume the form of a SOFC. The SOFC is only represented as a constant EMF in series with a resistance in that Chapter because the study is focused on short-duration disturbances. This simplified model may not be sufficient over the time interval when there are unavoidable interactions between the DG and the upstream system. The SOFC functional characteristic needs further examination before its integration into the PQCC system can be considered.

In summary, therefore the operational scheme proposed in this Chapter would strive for unbundled power quality supply, while certain operational constraints on the DG will be included. A dynamic model of the PQCC system is also presented and from which the control system for the proposed PQCC operation scheme is derived. Most of the materials contained in this Chapter have been reported in [100].

5.1 Additional Considerations on SOFC Characteristics

In Chapter 4, the SOFC has been represented as a constant EMF in series with a resistor as its internal electrochemical and fuel processor time constants are large compared to the duration of typical voltage sag events. However as the intention of this Chapter is to realize unbundled power quality services, the interactions between SOFC and PQCC have to be examined in greater details. The simplified SOFC model given in Chapter 4 may not be sufficient for the present study. The internal dynamics and the functional characteristics of SOFC have to be considered.

FC converts chemical energy in hydrogen (H_2) and oxygen (O_2) directly into electrical energy. The detailed energy conversion process is highly complex and, for the purpose of the present investigation, it would be sufficient to consider the schematic diagram of the SOFC shown in Figure 5-1 [99, 101]. Two main parts of the DG can be readily identified. The part called the balance of plant (BOP) consists of the natural gas fuel storage, fuel valve and the fuel processor. The fuel processor reforms the natural gas, of input flow rate N_f, to the hydrogen-rich fuel with flow rate of $N_{H_2}^{in}$. The processor dynamic can be

approximated by a first-order lag model of time constant τ_f [99]. The part labeled as the FC stack is where the complex thermodynamic and electrochemical processes take place. A general introduction of the process has been given in Chapter 2 and [67, 68].

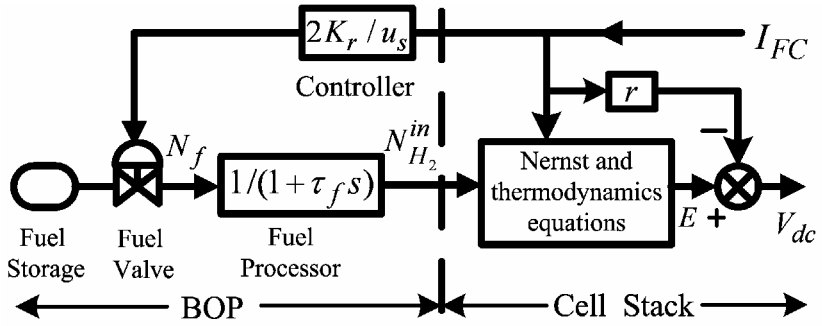

Figure 5-1 Schematic diagram of a SOFC [99]

Based on the information contained in Chapters 2 and 4, it is known that under steady-state and short duration voltage sag events, the electrical characteristics of the SOFC can be expressed as,

$$V_{dc} = E\text{-}rI_{FC} \tag{5.1.1}$$

where, V_{dc} is the SOFC terminal voltage, E is the SOFC open-circuit EMF, which is assumed to be essentially constant under steady-state and short-duration disturbance condition. r accounts for the Ohmic loss. Furthermore, the SOFC output power (P_{dg}) is then given by

$$P_{dg} = V_{dc}I_{FC} \tag{5.1.2}$$

According to [67, 68], it is known that the operation of SOFC has to take into account two practical constraints. The first is pertaining to the fuel utilization factor u. It is the most important operating variable affecting the performance of SOFC and is defined as

$$u \equiv \frac{N_{H_2}^{in} - N_{H_2}^{o}}{N_{H_2}^{in}}$$

where $N_{H_2}^{in}$ and $N_{H_2}^{o}$ are the input and output flow rates of hydrogen in the FC stack. It is shown in [99] that u can also be expressed in term of I_{FC} as

$$u = \frac{2K_r I_{FC}}{N_{H_2}^{in}} \tag{5.1.3}$$

where K_r is a modeling parameter. Typical desirable range of u, expressed as $u_{min} \leq u \leq$

u_{max}, is from 0.7 to 0.9. Overused-fuel condition (u > 0.9) could lead to permanent damage to the cells due to fuel starvation whereas underused-fuel situation (u < 0.7) results in undesirably high cell voltages.

The second constraint concerns the fuel cell output power P_{dg}. It should be maintained within the range

$$P_{min} \le P_{dg} \le P_{max} \tag{5.1.4}$$

The minimum power constraint is necessary in order to maintain stable stack operating temperature and acceptable power plant efficiency [102]. P_{max} denotes the design power rating of the SOFC.

Due to the above constraints, a steady-state feasible operating area (FOA) of the SOFC using the typical data given in Appendix B can be derived. This is shown in Figure 5-2. The detailed construction of the FOA has been described in [49, 101]. The operating temperature of the FC stack has been assumed constant in deriving the FOA. In arriving at this diagram, the FC rated power and output voltage are used as the base quantities. The constraints placed on u are represented by the horizontal lines AD and BC. The limits on P_{dg} are shown by the curves AB and CD. The FOA of the SOFC would correspond to the area 'ABCDA'. The SOFC must operate within the FOA as operation outside of FOA will reduce cell life and is unacceptable. Also shown in Figure 5-2 is the curve XY describing the operational characteristic of the SOFC under a constant V_{dc} condition. It shows V_{dc} operating within the voltage limits $V_{dc,\,max}$ and $V_{dc,\,min}$.

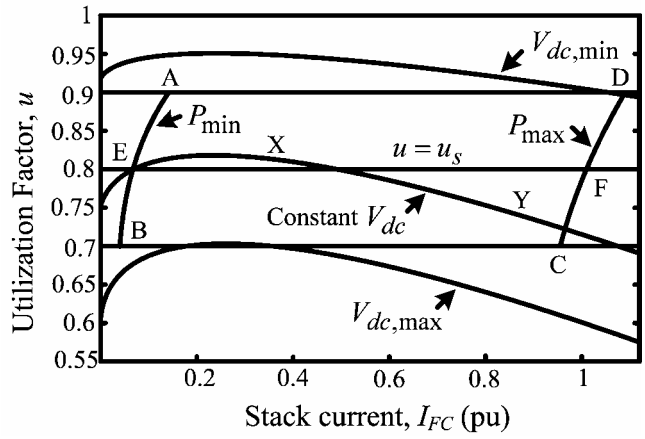

Figure 5-2 Feasible operation area of a SOFC [101]

From (5.1.3), it is found that the operation of the FC stack with a fuel input $N_{H_2}^{in}$ proportional to the stack current I_{FC} results in a constant utilization factor under steady-state. Such a constant utilization factor operation in turn brings on very small deviations in V_{dc} due to changes in stack current, as can be seen in Figure 5-2. However, such small voltage changes can be easily handled through a DC/DC converter at the terminals of the SOFC. Thus, the FC stack can be controlled to operate with a constant steady-state utilization factor by controlling the natural gas input to the stack in the following manner:

$$N_f = \frac{2K_r I_{FC}}{u_s} \tag{5.1.5}$$

where u_s is the desired utilization factor under steady-state. Such an input fuel control scheme produces a characteristic which can also be seen in Figure 5-1 and Figure 5-2. By adopting a constant u operational scheme such as described by the line EF in Figure 5-2, where u_s is shown as 0.8, V_{dc} would vary as I_{FC} changes.

Furthermore, with the adoption of this fuel input control strategy and in conjunction with the fuel processor dynamics described in Figure 5-1, the relationship between a small change of stack current ΔI_{FC} and a small change of hydrogen input $\Delta N_{H_2}^{in}$ fed to the FC stack can be derived as

$$\Delta N_{H_2}^{in} = \frac{2K_r}{u_s(1+\tau_f s)} \Delta I_{FC} \tag{5.1.6}$$

From (5.1.3), the small-signal equation relating Δu, ΔI_{FC} and $\Delta N_{H_2}^{in}$ about the initial steady-state $N_{H_{2,0}}^{in}$ and u_s can be written as

$$\Delta I_{FC}(s) = \frac{N_{H_{2,0}}^{in}}{2K_r} \Delta u(s) + \frac{u_s}{2K_r} \Delta N_{H_2}^{in}(s) \tag{5.1.7}$$

The subscript '0' is used herewith in this Chapter to denote the respective steady-state quantity. Substituting (5.1.3) and (5.1.6) into (5.1.7), one obtains

$$\Delta u(s) = \frac{u_s \tau_f s}{I_{FC,0}(1+\tau_f s)} \Delta I_{FC}(s) \tag{5.1.8}$$

where $I_{FC,0}$ is the initial stack current. It is governed by the initial value of N_f (i.e., $N_{H_{2,0}}^{in}$) through (5.1.5). Suppose the disturbance is due to an external power variation and has resulted in a step change in I_{FC} of magnitude ΔI_{FC} pu. Expressed in the s-domain, it yields $\Delta I_{FC}(s) = \Delta I_{FC}/s$. Substituting it into (5.1.8), one obtains the SOFC step response in u as

$$\Delta u(t) = \frac{u_s \Delta I_{FC}}{I_{FC,0}} \exp(-t/\tau_f) \tag{5.1.9}$$

Equation (5.1.9) shows that $\Delta u(t)$ will experience a maximum change of magnitude ($u_s \Delta I_{FC}/I_{FC,0}$) initially, and then $\Delta u(t)$ will decay in an exponential manner. The rate of decay corresponds to the time constant of the fuel processor. One may now define a new variable ε in term of the upper and lower limits on u

$$\varepsilon = \begin{cases} (u_{\max} - u_s)/u_s & \text{for positive } I_{FC} \text{ step} \\ (u_{\min} - u_s)/u_s & \text{for negative } I_{FC} \text{ step} \end{cases} \tag{5.1.10}$$

From the definition of ε shown in (5.1.10), clearly the maximum change in u should be constrained such that

$$u_s \Delta I_{FC}/I_{FC,0} \le u_s |\varepsilon|$$

i.e.,

$$\Delta I_{FC} \le |\varepsilon| I_{FC,0} \tag{5.1.11}$$

Hence, the maximum step change in I_{FC} which can be accommodated by the SOFC is described by (5.1.11). This is to ensure that $u_{min} \le u \le u_{max}$.

Conversely, the maximum allowable instantaneous real power change imposed on the cell can also be approximately calculated based on the above discussion. Over the initial period in which E is constant in (5.1.1) and applying the small-signal analysis to (5.1.2), the real power change ΔP_{dg} can be expressed as,

$$\Delta P_{dg} = V_{dc,0} \Delta I_{FC} + I_{FC,0} \Delta V_{dc} \approx (V_{dc,0} - r I_{FC,0}) \Delta I_{FC}$$

Substituting (5.1.11) into the above equation, therefore one obtains the constraint equation

$$\Delta P_{dg} \le |\varepsilon| (V_{dc,0} - r I_{FC,0}) I_{FC,0} \approx |\varepsilon| P_{dg,0}$$

or

$$\Delta P_{dg} \le |\varepsilon| P_{dg,0} \tag{5.1.12}$$

where $P_{dg,0} = V_{dc,0} I_{FC,0}$ is the initial operating power level. In arriving at the last approximation, one makes use of the observation that the internal voltage drop term $rI_{FC,0}$ is much smaller than $V_{dc,0}$. Hence, (5.1.12) shows that the instantaneous power change (ΔP_{dg}) imposed on the SOFC should be less than $|\varepsilon| P_{dg,0}$, in order to maintain operation within the FOA [49].

Consider the typical values of $u_s = 0.8$, $u_{min} = 0.7$ and $u_{max} = 0.9$. From (5.1.10), it yields $\varepsilon = 0.125$. Therefore, the maximum instantaneous power change that can be accommodated by the SOFC is 12.5% of its initial loading, i.e., $0.125P_{dg,0}$. Demand for an instantaneous power change of less than 12.5% of $P_{dg,0}$ can be met by the SOFC instantaneously in a single step change in the output power. For a larger power change demand, however, the SOFC would require several tens of seconds for the fuel processor to adjust the fuel input, and that through the internal electro-chemical process, before the targeted power level can be reached.

In summary, it is clear that there is a practical limit in term of the magnitude and the speed by which the SOFC can respond to a power change demand. Due to the inherent slow dynamics of the SOFC, a buffer energy storage device, such as a super-capacitor or battery, is often used in conjunction with the SOFC system [103]. However, in this Chapter an alternative scheme is proposed in which the buffer energy storage device would not be included. Instead, the intention is to investigate to what extent the PQCC can meet the need of providing unbundled power quality supply for loads.

5.2 Proposed Scheme

Recognizing the short-comings and practical problems faced in implementing the PQCC scheme described in [30, 31] and Chapter 4, a new PQCC operation scheme is now proposed. The design is based on the consideration of normal system conditions as well as that pertaining to the upstream faults or outages of the various components in the power system.

5.2.1 Steady-State Operations

To facilitate the description of the scheme, the simplified equivalent circuit PQCC model shown in Figure 5-3 is used. In a scheme similar to that proposed in Chapter 4, the standby feeder and the HTS in the high voltage side have been excluded in the present system. The SP, DC, HQ and OQ loads are also assumed to be linear and will not introduce harmonics into the power system. In the figure, all the AC voltages shown are measured phase-ground whereas the power flows are three-phase quantities.

The upstream system is represented simply as an equivalent voltage source $\vec{V}_s$ with its equivalent series impedance $R+j\omega L$, where ω is the AC system frequency. The Point of Common Coupling (PCC) voltage phasor is treated as the reference quantity and is denoted as $\vec{V_p}$. $\vec{V_p}$ is assumed measurable. The SP, DC, HQ and OQ loads are represented by the respective impedances for convenience, although in the analysis to follow, the load model used is a more general static-type. L_f represents the total inductance which links the PCC to Inv.1 inverter. It also acts as a filter for high-frequency harmonics produced by the inverter and therefore the inverter harmonics are considered negligible in the following analysis. Although in Figure 5-3 the SOFC is shown as a DC source, its functional characteristic described in Section 5.1 would be taken into consideration. As introduced in Chapter 4, the capacitor c_f is only used for filtering purposes and is not sufficiently large as to be an effective energy storage device.

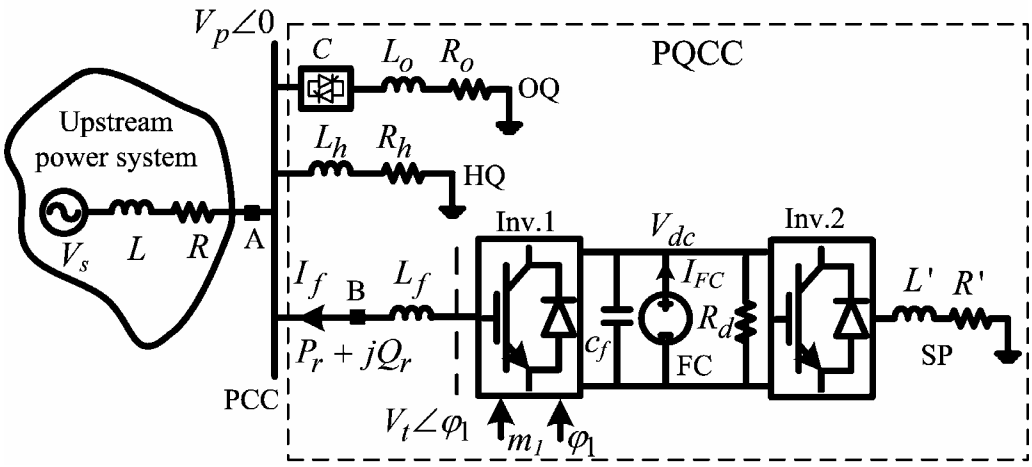

Figure 5-3 A simplified PQCC model

Within Inv.1, the two control variables are the modulation index m_1 and the phase angle φ_1. By controlling them, Inv.1 front-end voltage $V_{t\angle}\varphi_1$ as shown in Figure 5-3 can be regulated and the power flow P_r+jQ_r is therefore controlled. The role of Inv.2 is to ensure a high AC waveform quality at the terminals of the SP load, again through the control of the Inv.2 modulation index and phase for a given V_{dc}.

As pointed out in Chapter 2, the authors of [30, 31] proposed that the DG supplies part of the DC and SP load under steady-state and in the event of a decrease of upstream in-feed at point 'A', the SOFC has to increase its output power instantaneously to satisfy the

balance of the load demand. However, (5.1.12) shows that the SOFC has only a limited ability to react instantaneously to a real power change. Hence, the scheme in [30, 31] has to be modified, as follows.

In the scheme proposed here, the SOFC is to supply the entire power demand of DC and SP loads under the normal steady-state. As the DC and SP load demands vary, the output power of the SOFC would vary correspondingly. This load-tracking feature of the SOFC is possible, as one would expect normal load variations would be slow compared to the response of the SOFC power plant. Clearly, the rating of the SOFC will have to be at least that of the maximum of the total DC and SP load demands. This is a reasonable requirement because in an event of a complete loss of the upstream system, i.e., 'A' opens, the SOFC will then be called upon to meet the total demand of the DC and SP loads.

Having met the total DC and SP load demands, the SOFC could also inject any surplus active power (P_r) to the PCC bus. P_r is then used to meet part of the OQ and HQ load demands. Under such an arrangement, the SOFC and downstream loads are always connected to the upstream grid, by having Inv.1 operating in the inversion mode. The upstream power system therefore acts as a backup source for the SP and DC loads, in the event of the loss of the SOFC. Hence, the SP and DC loads enjoy a supreme-level of supply reliability, as intended.

While the above operating scenario can be expected to prevail under almost all instances, one has to consider the possibility of the loss of the connection between Inv.1 and the PCC (i.e., circuit breaker 'B' open). This is a necessary consideration for this incident will result in the output of the SOFC being decreased suddenly by an amount equaled to P_r. In order to safeguard the FC stack, the steady-state pre-disturbance value of P_r, i.e. $P_{r,0}$, must therefore be constrained to within the range

$$0 \le P_{r,0} \le |\varepsilon| P_{dg,0} \tag{5.2.1}$$

Equation (5.2.1) is obtained as a consequence of (5.1.12) so as to satisfy the FOA constraint. However,

$$P_{dg,0} = P_{SD} + P_{r,0} \tag{5.2.2}$$

where P_{SD} is the total demand of the SP and DC loads. The output power of SOFC, $P_{dg,0}$, should also satisfy the output power limit constraint (5.1.4) during steady-state operation. Combining the requirements (5.2.1) and (5.2.2), one arrives at the condition

$$(1-|\varepsilon|)P_{dg,0} \le P_{SD} \le P_{dg,0} \tag{5.2.3}$$

Yet another steady-state consideration concerns the possibility of reverse power flow into the upstream power system. In the event the total demand of the HQ and OQ loads is less than $P_{r,0}$, the surplus portion of $P_{r,0}$ would flow reversibly back to the upstream system. Perhaps due to contractual reasons, assume such reverse power flow is prohibited. Therefore, it is proposed that active power flow in the upstream feeder (point 'A') is continuously monitored. Once reverse power flow is detected, the output power (P_{dg}) of the SOFC is to be reduced until the reverse power flow ceases and (5.2.3) is also satisfied.

Apart from supplying active power to the OQ and HQ loads, it is also proposed that the control on Inv.1 is set so that Inv.1 supplies all the reactive power required by the OQ and HQ loads under steady-state, i.e.,

$$Q_{r,0} = Q_{OQ,0} + Q_{HQ,0} \tag{5.2.4}$$

Power factor at 'A' is therefore maintained at unity. The voltage drop across the equivalent upstream impedance is therefore minimized. This is desirable as it will ensure efficient power transfer through the upstream system.

Finally, the current rating of Inv.1, denoted as $I_{inv1,rate1}$, needs be examined. Under this normal steady-state condition, Inv.1 must be rated to supply the proportion of the total maximum HQ and OQ load demands. Thus,

$$I_{inv1,rate1} = \frac{\sqrt{\left(P_{r,0}^2 + Q_{r,0}^2\right)_{\max}}}{3V_{p,0}} \tag{5.2.5}$$

5.2.2 Operation under the Loss of SOFC

Next consider the loss of all or part of the SOFC output power. This incident could be due to an internal fault or mal-operation of the fuel cell system. In order to protect the DC and SP loads from the impact of the loss of P_{dg}, the upstream system must be forced to supply

the balance of the active power to meet the downstream load demands as rapidly as possible. Inv.1 is therefore to operate in rectifier mode to transfer active power from the upstream system to the DC-bus.

The most severe condition under this contingency scenario would be the total loss of power from the SOFC. The upstream system must have sufficient capacity to supply the maximum DC and SP total real power demand ($P_{SD,max}$). Hence, one arrives at another Inv.1 current rating:

$$I_{inv1,rate2} = \frac{P_{SD}}{3V_{p,0}} \tag{5.2.6}$$

Combining with (5.2.5), the current rating of Inv.1 is therefore the larger value of $I_{inv1,rate1}$ and $I_{inv1,rate2}$.

5.2.3 Operation under Upstream Voltage Sag

PQCC operation under upstream voltage-sag conditions is also examined. As in Chapter 4, only balanced voltage sag will be considered due to the complexity and extensiveness of the upstream system. The sag magnitude is assumed constant over the duration of the disturbance. The SP and DC loads could be shielded from the effects of the decrease in the PCC voltage by the corrective actions of Inv.2. However, as the OQ and HQ loads are connected directly to the PCC, they will experience the full impact of the sag. Thus special consideration must be given to improve the ride-through capability of the HQ and OQ loads during the voltage disturbance.

Electrical equipment manufacturers often provide information describing the withstand voltage vs. time characteristics of their products. A well-known and typical example is the ITI (CBEMA) curve described in Chapter 2. As seen from Figure 2-3, a load is capable of continuous operation only for a limited duration under a depressed voltage condition. The duration depends on the sag magnitude. The more severe the sag is, the shorter the tolerable duration T. The lower boundary of the ITI curve describes this relationship. T would be infinite for those sags which result in a standing voltage above a minimal level $V_{\min}$: $V_{\min}$ is the lowest acceptable voltage level for prolonged operation of the load. Suppose HQ and OQ loads have such voltage/time characteristics. Therefore if

the sag duration were less than the specified T, it is expected that the HQ and OQ loads would not be adversely affected. Conversely, if the sag duration exceeds T the loads could malfunction unless corrective actions are taken.

5.2.3.1 Scenario 1

This scenario is pertaining to sags that have duration less than the specified T for HQ and OQ loads. Under such a situation, the HQ and OQ load would not malfunction and they can still be connected to the upstream system. Thus, the system continues to be operated as for the normal steady-state.

5.2.3.2 Scenario 2

If the sag duration were to exceed T, it is proposed that the solid-state circuit breaker C shown in Figure 5-3 of the OQ load would operate at the first available instance to disconnect the OQ load from the network. The OQ load only requires the lowest level of supply quality amongst all the loads. Thus, it is chosen to be the first to be disrupted due to the severe sags. After the shedding of the OQ load, if the PCC voltage recovers to above V_{min}, the PQCC would revert to the scenario 1 control scheme described earlier but without the OQ load. Otherwise, the switch shown as 'A' in Figure 5-3 in the upstream inter-connection link is opened at the earliest possible instant. The PQCC system is then operating in an islanding mode.

Although the OQ load can be shed, the HQ load would still be supplied by the PQCC under this islanding stage. The initial power supplied by the SOFC to the upstream load, $P_{r,0}$, is unlikely to match the HQ load requirement exactly. Thus the output power of the SOFC has to be regulated subsequent to the islanding. From (5.1.12), it is shown that the instantaneous power change imposed on the SOFC must be kept at less than $|\varepsilon|P_{dg,0}$. Hence, following the islanding, the HQ load will draw power $P_{HQ,iso}$ at a level that should be limited to:

$$0 \le P_{HQ,iso} \le P_{r,0} + |\varepsilon| P_{dg,0} \tag{5.2.7}$$

While Inv.1 still operates in inversion mode, it is proposed that its role is changed from controlling P_r+jQ_r to controlling the PCC bus voltage (V_p) and maintaining the bus

frequency. The objective is to maintain V_p at V_{min}. Combining (5.2.7) and (5.2.1), the possible power range of HQ load in the islanding mode can be determined as,

$$0 \le P_{HQ,iso} \le 2|\varepsilon| P_{dg,0} \tag{5.2.8}$$

However, as the initial operating condition is governed by (5.2.3), it can be combined with (5.2.8) to yield

$$0 \le P_{HQ,iso} \le \left(\frac{2|\varepsilon|}{1-|\varepsilon|} \right) \cdot P_{SD} \tag{5.2.9}$$

One must also limit the power output of the DG to the range specified by (5.1.4), i.e.

$$P_{\min} \le P_{SD} + P_{HQ,iso} \le P_{\max} \tag{5.2.10}$$

It is seen that in order for the power change to be met by the SOFC instantaneously and without violating the u and the output power limits, the post-fault HQ, SP and DC load levels must comply with (5.2.9) and (5.2.10). The result of the above derivation can be summarized graphically in Figure 5-4. Equation (5.2.9) is shown by the boundary line 'RS', (5.2.10) is shown by the line 'ST' and 'UR'. Clearly, in order for the SOFC to meet any instantaneous power change when point 'A' is opened, the only feasible load regime is within the area 'RSTUR'.

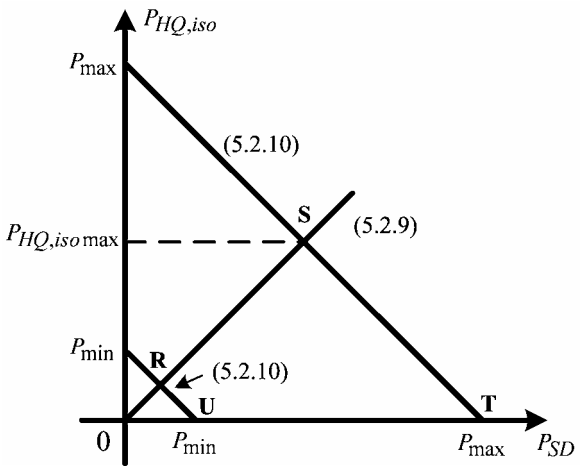

Figure 5-4 PQCC feasible operating zone under Scenario 2

From Figure 5-4, the maximum HQ load that can be supplied in the islanding mode corresponds to point 'S'. It can be determined by solving (5.2.9) and (5.2.10) simultaneously to yield

$$P_{HQ,iso\max} = \frac{2|\varepsilon| P_{\max}}{1+|\varepsilon|} \tag{5.2.11}$$

The HQ load in the isolated mode as obtained from Figure 5-4 can then be translated to its pre-fault value by applying

$$P_{HQ,0} = \frac{P_{HQ,iso}}{V_{\min}^{\beta}} \tag{5.2.12}$$

where $P_{HQ,0}$ and $P_{HQ,iso}$ denote the pre-fault and post-fault HQ load power demands respectively and β is the real power- voltage index [104] of the HQ load. Typically, $0 \le \beta \le 2$.

Based on the above consideration, it can be seen that the loads are to be served by a power supply system with varied quality levels. Table 5-1 summarizes the levels enjoyed by the OQ, HQ, SP and DC loads under the proposed arrangement.

Table 5-1: Power quality levels of loads

Loads	Waveform quality	Voltage sag ride-through attribute
OQ	Not improved	Low
HQ	Not improved	High
SP	Very high	Very high
DC	Improved	Very high

5.3 Control System Design

Control scheme for the varied PQCC operating conditions is considered next. As described earlier with reference to Figure 5-3 when the PQCC is connected to the upstream system, Inv.1 is used to control the power flow P_r+jQ_r. This can be realized by regulating the Inv.1 current i_f through the control of Inv.1 phase angle (φ_1) and modulation index (m_1). Since this power flow control is applied under the interconnected state, which includes normal steady-state, SOFC outage state and upstream voltage sag (Scenario 1), Inv.1 controller configuration is therefore the same under all the above-mentioned operating conditions. The only difference is in the reference value of i_f. Similar as that in Chapter 4, the function of Inv.2 is to maintain the SP load voltage. Its control scheme is not described as it is well known [88].

5.3.1 Control Scheme under Interconnected State

Consider firstly the AC link between the PCC and Inv.1. From Figure 5-3, the link voltage-current relationship can be written as

$$L_f \frac{d}{dt}\vec{i}_f = \vec{V}_t - \vec{V}_p \tag{5.3.1}$$

where $\vec{i}_f$, $\vec{V}_t$ are the vectors of the AC link phase currents and Inv.1 front-end phase voltages. They are defined as,

$$\vec{V}_p = \sqrt{2}V_p \begin{bmatrix} \sin\omega t \\ \sin(\omega t - 2\pi/3) \\ \sin(\omega t + 2\pi/3) \end{bmatrix} \tag{5.3.2}$$

$$\vec{V}_t = \sqrt{2}V_t \begin{bmatrix} \sin(\omega t + \varphi_1) \\ \sin(\omega t + \varphi_1 - 2\pi/3) \\ \sin(\omega t + \varphi_1 + 2\pi/3) \end{bmatrix} \tag{5.3.3}$$

where V_p and V_t are *rms* value of the PCC voltage and Inv.1 front-end line voltages respectively. Similar to that given in Chapter 4, it is known that $V_t = m_1 V_{dc}/(2\sqrt{2})$ [88]. It is also assumed that no mutual coupling exists between phases. Equation (5.3.1) can then be transformed into the d-q frame through Park transformation. The transformation matrix is,

$$T = \sqrt{\frac{2}{3}} \times \begin{bmatrix} \sin\omega t & \sin(\omega t - \frac{2\pi}{3}) & \sin(\omega t + \frac{2\pi}{3}) \\ \cos\omega t & \cos(\omega t - \frac{2\pi}{3}) & \cos(\omega t + \frac{2\pi}{3}) \\ \frac{1}{\sqrt{2}} & \frac{1}{\sqrt{2}} & \frac{1}{\sqrt{2}} \end{bmatrix} \tag{5.3.4}$$

Applying the above transformation matrix to (5.3.1), it can be shown that

$$L_f \frac{d}{dt}\begin{bmatrix} i_d \\ i_q \end{bmatrix} = \begin{bmatrix} 0 & \omega L_f \\ -\omega L_f & 0 \end{bmatrix}\begin{bmatrix} i_d \\ i_q \end{bmatrix} + \begin{bmatrix} V_{td} - \sqrt{3}V_p \\ V_{tq} \end{bmatrix} \tag{5.3.5}$$

where $[i_d, i_q]^T$ and $[V_{td}, V_{tq}]^T$ contain the d-q components of $\vec{i}_f$ and $\vec{V}_t$ respectively. In this investigation, the fundamental components are the main focus and the switching harmonics due to Inv.1 are not considered. Such simplification is reasonable as the cross-over frequency of the control system to be designed for Inv.1 would be much below Inv.1 switching frequency. V_{dc}, V_{td} and V_{tq} relationship can then be described by the algebraic equations

$$\left.\begin{aligned} V_{td} &= k_m m_1 V_{dc}\cos\varphi_1 \\ V_{tq} &= k_m m_1 V_{dc}\sin\varphi_1 \end{aligned}\right\} \tag{5.3.6}$$

where $k_m = \sqrt{3}/(2\sqrt{2}) = 0.612$ [88].

It is can be seen from (5.3.5) and (5.3.6) that the system dynamics is nonlinear. Cross-coupling exists between the state variables i_d, i_q and the control variables m_1, φ_1. Therefore it is necessary to seek a method to facilitate analysis. The decoupled control scheme described in [60] can be used to overcome these design problems. Accordingly, the reference voltage of Inv.1 is defined as $V_t^* = [V_{td}^* \; V_{tq}^*]^T$. From (5.3.6), the control variables of Inv.1 can be derived as,

$$\left.\begin{aligned} m_1 &= \frac{\sqrt{(V_{td}^*)^2 + (V_{tq}^*)^2}}{k_m V_{dc}} \\ \varphi_1 &= \arctan\left(\frac{V_{tq}^*}{V_{td}^*}\right) \end{aligned}\right\} \tag{5.3.7}$$

On the RHS of (5.3.5), it is known that i_d, i_q, V_p, V_{td} and V_{tq} can be measured or determined on-line. One can therefore achieve decoupled control if the following reference voltages are generated,

$$\left.\begin{aligned} V_{td}^* &= V_{td} - \sqrt{3}V_p + \omega L_f i_q \\ V_{tq}^* &= V_{tq} - \omega L_f i_d \end{aligned}\right\} \tag{5.3.8}$$

Substituting (5.3.8) into (5.3.5), one observes that

$$\left.\begin{aligned} L_f \frac{di_d}{dt} &= V_{td}^* \\ L_f \frac{di_q}{dt} &= V_{tq}^* \end{aligned}\right\} \tag{5.3.9}$$

Hence the reference voltage signals can be generated through a current control loop as,

$$\left.\begin{aligned} V_{td}^*(s) &= G(s)(i_d^* - i_d) \\ V_{tq}^*(s) &= G(s)(i_q^* - i_q) \end{aligned}\right\} \tag{5.3.10}$$

where $G(s) = k_{p1} + k_{I1}/s$ is a proportional-integral (PI) type controller whose parameters are yet to be determined. The proposed control scheme is as shown in Figure 5-5. By assuming that Inv.1 is capable of tracking the reference voltage exactly at its output, the block representing the inverter in Figure 5-5 can be omitted from this diagram. It should be noted that the small time delay of the inverter and the harmonics at its output have been neglected in this process. With the inverter block omitted, the cross-coupling terms on the two sides of the inverter cancel out, leaving only the two single-input single-output decoupled closed-loop systems shown in Figure 5-6.

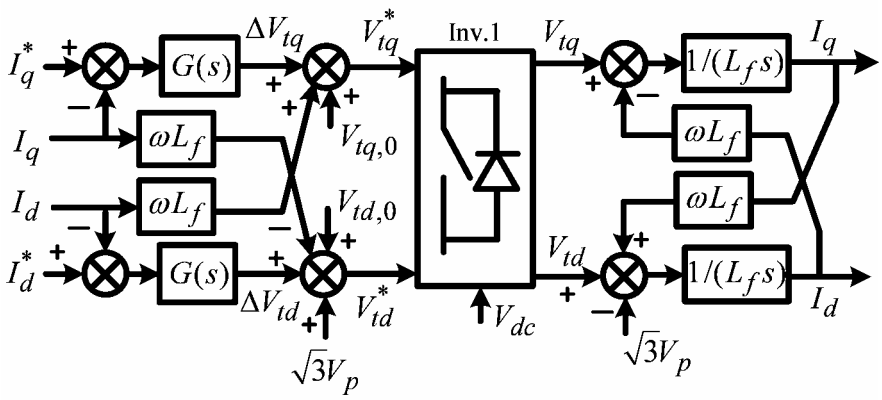

Figure 5-5 Control scheme of Inv.1under interconnected state

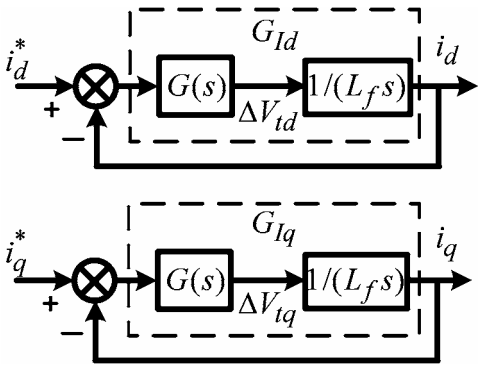

Figure 5-6 Equivalent d-q current control schemes for Inv.1

In Figure 5-6, Inv.1 and the AC link is represented by the first order model $1/(L_f s)$. In order to track the current references properly, the closed-loop systems must achieve satisfactory speed of response (wide bandwidth) with adequate stability (sufficient phase margin). However, as the switching actions of Inv.1 may affect the dynamic performance of the PQCC, it is then proposed that the bandwidth (ω_c) of the compensated system in Figure 5-6 is set at 1/5 ~ 1/2 of the switching frequency. The open-loop transfer functions of Figure 5-5 can be set to provide the desired phase margin (ϕ_c) at ω_c, i.e.

$$G(j\omega_c) = (k_{P1} + \frac{k_{I1}}{j\omega_c})\frac{1}{jL_f\omega_c} = \exp[j(-180^0 + \phi_c)] \tag{5.3.11}$$

Solving for the real and imaginary parts of (5.3.11), the PI controller parameters can then be determined:

$$\left.\begin{aligned} k_{P1} &= \omega_c L_f \cos\phi_c \\ k_{I1} &= \omega_c L_f \sin\phi_c \end{aligned}\right\} \tag{5.3.12}$$

5.3.2 Control Scheme under Islanding Mode (Scenario 2)

Under Scenario 2, the PQCC is disconnected from the upstream power system. Inv.1 is used to maintain V_p at V_{min} at the rated frequency. Under this islanding mode, a phase angle φ_1 cannot be defined as the isolated system has only one voltage source connected to the AC link. Thus, φ_1 can be set to 0 under this mode. Inv.1 front-end voltage is still represented as $V_t = m_1 V_{dc} / (2\sqrt{2})$.

Under isolated condition, the relationship between the steady state P_{HQ} and V_p is assumed to satisfy (5.2.12). Therefore, V_p variation will result in P_{HQ} change such that

$$\Delta P_{HQ,iso} = \beta V_p^{\beta-1} P_{HQ,0} \Delta V_p \tag{5.3.13}$$

Neglecting the relatively small voltage difference across L_f, it yields $V_t \approx V_p = m_1 V_{dc}/(2\sqrt{2})$. Therefore

$$\Delta V_p \approx \Delta V_t = \frac{1}{2\sqrt{2}} (M_1 \Delta V_{dc} + V_{dc,0} \Delta m_1) \tag{5.3.14}$$

As the SP and DC load are kept constant, the FC real power variation will be equal to the AC side real power change, i.e.,

$$\Delta P_{dg} = \Delta P_{HQ,iso} = V_{dc,0} \Delta I_{FC} + I_{FC,0} \Delta V_{dc} \approx (I_{FC,0} - V_{dc,0}/r) \Delta V_{dc} \tag{5.3.15}$$

Substituting (5.3.13) and (5.3.14) into (5.3.15), it is seen that,

$$\Delta P_{dg} = \Delta P_{HQ,iso} = (I_{FC,0} - V_{dc,0}/r) \Delta V_{dc} = \frac{1}{2\sqrt{2}} \beta V_p^{\beta-1} P_{HQ,0} (M_1 \Delta V_{dc} + V_{dc,0} \Delta m_1)$$

Rearranging the above equation, the relationship between ΔV_{dc} and Δm_1 is,

$$\Delta V_{dc} = \frac{\beta V_p^{\beta-1} V_{dc,0} P_{HQ,0} \Delta m_1}{2\sqrt{2}(I_{FC,0} - \frac{V_{dc,0}}{r} - \frac{\beta V_p^{\beta-1} M_1 P_{HQ,0}}{2\sqrt{2}})} \tag{5.3.16}$$

Substituting (5.3.16) into (5.3.14), the relationship between ΔV_p and Δm_1 can then be represented by the transfer function

$$G_{is} = \Delta V_p / \Delta m_1 = k_{iso} \tag{5.3.17}$$

where

$$k_{iso} = \frac{V_{dc,0}}{2\sqrt{2}} + \frac{\beta V_p^{\beta-1} M_1 V_{dc,0} P_{HQ,0}}{8(I_{FC,0} - \frac{V_{dc,0}}{r} - \frac{\beta V_p^{\beta-1} M_1 P_{HQ,0}}{2\sqrt{2}})} \tag{5.3.18}$$

According to (5.3.17), it is found that even an open-loop control is sufficient to control V_p. However, as V_{dc} is expected to change as a result of sudden change in P_{dg}, it is prudent to employ closed-loop feedback control of the output voltage of Inv.1. Figure 5-7 shows the proposed control scheme and a PI-type controller $G_v(s) = k_{P2} + k_{I2}/s$ is again used to yield the desired bandwidth of ω_{c1} and phase margin $\phi_{c1,}$ i.e.,

$$G_v G_{is}(j\omega_{c1}) = k_{iso}(k_{P2} + \frac{k_{I2}}{j\omega_{c1}}) = \exp[j(-180^\circ + \phi_{c1})] \tag{5.3.19}$$

Whence by solving (5.3.19), the control parameters are

$$\left.\begin{aligned} k_{P2} &= -\cos\phi_{c1} / k_{iso} \\ k_{I2} &= \omega_{c1} \sin\phi_{c1} / k_{iso} \end{aligned}\right\} \tag{5.3.20}$$

Since $k_{iso} > 0$, a necessary condition to achieve $k_{P2} > 0$ is that the phase margin $\phi_{c1} > \pi/2$. Also, a larger value of $V_{dc,0}$ will lead to a smaller phase margin, i.e., a more onerous operating condition. Therefore one can design the PI-controller by selecting the largest possible $V_{dc,0}$. The controller designed under this condition will guarantee closed-loop stability at any other operating conditions under Scenario 2.

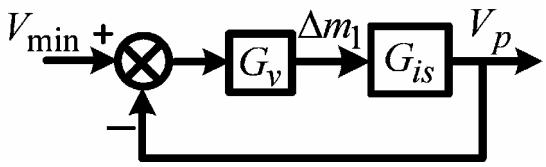

Figure 5-7 Control scheme for Scenario 2

The case of the loss of the AC interconnection between the PCC bus and Inv.1 would not require the control action of Inv.1. Rather Inv.2 will be called upon to regulate the SP load terminal voltage.

5.3.3 Current References

Having examined the controller design, the current references for the different operation states will now be given.

- ❖ Under normal state

Under steady-state, the PCC phase voltage is $V_{p,0}$. Inv.1 transfers active power $P_{r,0}$ from the DC side to the AC system and also supplies all the reactive power required by the HQ

and OQ load. Therefore, the current reference is given by

$$\left.\begin{aligned} i_d^* &= \frac{P_{r,0}}{3V_{p,0}} \\ i_q^* &= \frac{Q_{OQ,0} + Q_{HQ,0}}{3V_{p,0}} \end{aligned}\right\} \tag{5.3.21}$$

❖ Under sudden loss of SOFC

Under the SOFC outage condition, Inv.1 changes from inversion mode to rectifier mode. Inv.1 carries the total active power demand of the DC and SP loads, with $Q_r = 0$. Thus,

$$\left.\begin{aligned} i_d^* &= \frac{-P_{SD}}{3V_{p,0}} \\ i_q^* &= 0 \end{aligned}\right\} \tag{5.3.22}$$

❖ Under voltage sag (Scenario 1)

Under this scenario, suppose the PCC voltage drops to $V_{p,sag}$. Inv.1 transfers the same amount of active power ($P_{r,0}$) as before the sag from the DC to the AC system while at the same time, provides all the reactive power needs of the OQ and HQ loads. Therefore,

$$\left.\begin{aligned} i_d^* &= \frac{P_{r,0}}{3V_{p,sag}} \\ i_q^* &= \frac{Q_{OQ,sag} + Q_{HQ,sag}}{3V_{p,sag}} \end{aligned}\right\} \tag{5.3.23}$$

Note that in generating the current references, the PQCC loads would vary as part of the normal operating condition. Hence, i_d^* and i_q^* will have to be adjusted continuously to track the load changes.

5.4 Illustrative Examples

5.4.1 System Description

In order to ascertain the effectiveness of the proposed operating scheme, a series of simulation studies has been performed. The example system used for the simulation study is as shown in Figure 5-3, with the corresponding system data given in Table 5-2. The SOFC rating is P_{max}=100 kW. The SOFC schematic dynamic model shown in Figure 5-1 is incorporated into the PQCC in the simulation. Its parameters are given in the Appendix B. Fuel utilization factor under steady-state is assumed to be 0.8, with u_{min} = 0.7 and u_{max} = 0.9. From (5.1.10), it is then established that $\Delta P_{dg} \leq 0.125 P_{dg,0}$.

Table 5-2: Parametric values of the PQCC and power system

Power system and Loads: ω = 50 Hz.					
$V_{p,0}$ [V]	86.6	$V_{dc,0}$[V]	330	R' [Ω]	0.2205
R [Ω]	1.364e-4	c_f [uF]	200	L' [mH]	0.716
L [mH]	1.737e-3	R_d [Ω]	3.63	L_f[mH]	0.0358
R_0 [Ω]	0.1158	R_h [Ω]	0.8224		
L_0[mH]	0.121	L_h[mH]	0.86		

The HQ and OQ loads are assumed to be of constant impedance type, i.e. β = 2. Their withstand voltage-time characteristic is assumed to be governed by the ITI curve with V_{min} = 0.9 pu. Therefore, the maximum HQ load power that can be supported by the PQCC under islanding mode at the minimum voltage can be calculated from (5.2.11), viz. $P_{HQ,iso,max}$ = 22.22 kW. From (5.2.12), this corresponds to a maximum pre-fault power of $P_{HQ,0,max}$ = 27.43 kW. Therefore in the illustrative example, the initial HQ load power demand could be chosen up to 27.43 kW.

System and loads parameters are then calculated according to the following assumed active power distribution: under initial steady-state, $P_{dg,0}$ = 90 kW, P_{DC} = 30 kW, P_{SP} = 50 kW, $P_{r,0}$ = 10 kW, P_{OQ} = 175 kW and P_{HQ} = 25 kW. The power factor of the OQ and HQ loads is considered as 0.95 lagging. Inv.1 is represented by six on-off switches with small finite series resistances. The switching frequency of Inv.1 is 4 kHz.

Inv.1 current rating can be determined using the approach described in Section 5.2. In the example, it is seen that $I_{inv1,rate1} < I_{inv1,rate2}$.Therefore $I_{inv1,rated}$ = 308 A. Inv.1 controller bandwidth is selected to be 1/4 of the switching frequency, i.e. $\omega_c = \omega_{c1} = 2000\pi$ rad/sec. By selecting ϕ_c = 45°, the corresponding PI controllers for Inv.1 when the PQCC is operating under interconnected condition can be obtained from (5.3.12) as $G(s) = 0.05 + 0.05/s$. In designing the PI controller for the isolated operating condition, the maximum $V_{dc,0}$ was found to be 344 V when P_{dg} = 28 kW and u = 0.8 [101]. If one selects ϕ_{c1} = 100°, from (5.3.20) the corresponding PI controller is $G_v(s) = 5\times10^{-4} + 6/s$.

5.4.2 Simulation

Simulation studies have been carried out to verify the effectiveness of the proposed scheme. The simulation software used is Matlab/Simulink. Results of four cases are described: that of voltage sag to 90% and 60% of its nominal value, under the sudden loss of the SOFC and under the sudden loss of the AC link (circuit breaker 'B') open. As both the hydrogen input and stack current can be measured on line, real-time u can therefore be determined using (5.1.3). The corresponding simulation results are shown in Figures 5-8 – 5-11.

Figure 5-8 shows the system response under the 90% sag condition. Since the HQ and OQ loads are assumed capable of sustained operation at this voltage level, the PQCC system would therefore remain connected to the upstream power system during the sag. Inv.1 transfers an almost constant 10 kW throughout the duration of the disturbance. This can be seen in Figure 5-8 (d). However, due to the voltage dependency of the reactive power demand of HQ and OQ loads, Q_r supplied by the PQCC reduces as shown in Figure 5-8 (d). As the output power of SOFC is unchanged, Figure 5-8 (a) and (b) confirm that the FC fuel utilization factor and the terminal voltage are undisturbed during the sag. As the real power demand of the HQ and OQ loads decreases, the power drawn from the upstream power system reduces as shown in Figure 5-8 (c) while the reactive power from this source remains at zero since the PQCC supplies all the reactive power required by these loads.

Figure 5-9 shows the consequence of a voltage sag (60%) for which the PQCC needs to operate in the islanding mode. From the ITI curve, the maximum duration (T) of the HQ and OQ loads that could tolerate the 60% sag is about 20 ms. Therefore in Figure 5-9, the OQ load is assumed successfully disconnected by the action of the solid-state circuit breaker C 10 ms after the incipient of the sag. Since the PCC voltage (V_p) remains below V_{min} after the load shed, the PQCC system is then disconnected from the upstream power system half a cycle later. Thereafter, $P_s = Q_s = 0$ as shown in Figure 5-9 (c). The operating mode of Inv.1 is changed from controlling the power flow to regulating V_p and frequency. Figure 5-9 (a) shows that V_p can indeed be restored to 0.9 pu during this islanding mode operation. The SOFC output power increases by 10 kW as evident from

Figure 5-9 (d) and the step power change is within the FOA of the SOFC. The SOFC fuel utility factor u_s increases but does not exceed u_{max}. The DC-link voltage decreases slightly following the islanding stage.

Figure 5-10 shows the system response under the sudden loss of the SOFC. In order to protect the DC and SP loads, the upstream system has to meet all the active power load demand rapidly and Inv.1 is therefore changed from inversion to rectification operating mode. It is seen that V_{dc} decreases at the instance of the DG disconnection. However, it recovers rapidly because of the support from the upstream system. The loads are almost unaffected. Inv.1 current would increase to its rated value during the fault as can be seen from Figure 5-10 (b).

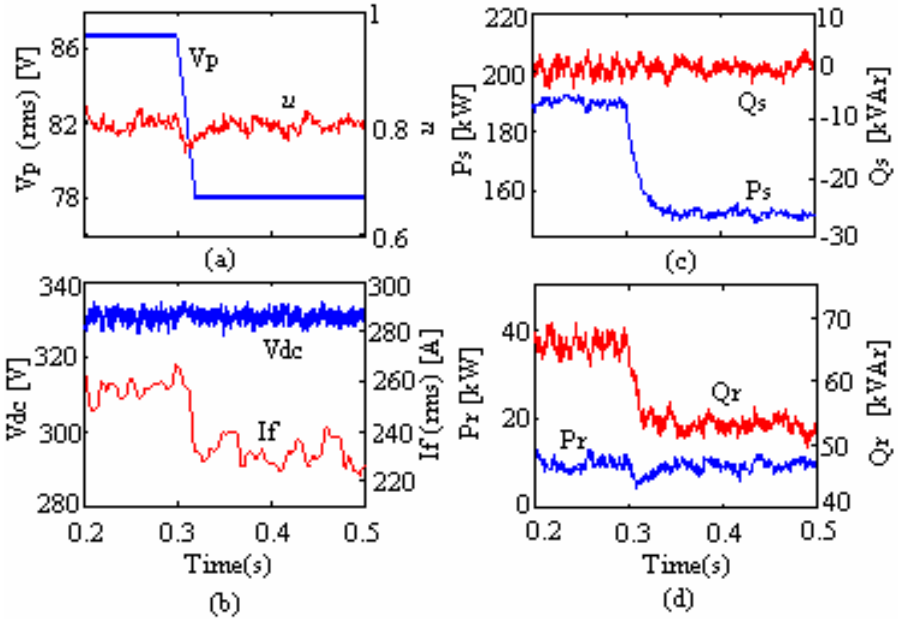

Figure 5-8 System operation under a 90% voltage sag (scenario 1). (a) PCC voltage (phase a) and utilization factor of SOFC. (b) DC-link voltage and Inv.1 current (phase a). (c) Active and reactive power supplied by upstream source. (d) Active and reactive power supplied by Inv.1.

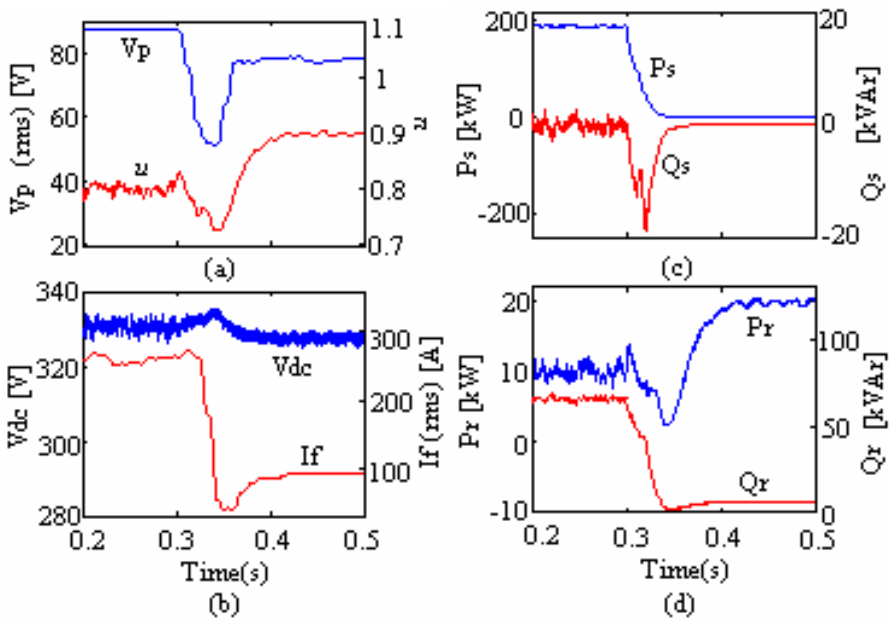

Figure 5-9 System operation under a 60% voltage sag (scenario 2). (a) PCC voltage (phase a) and utilization factor of SOFC. (b) DC-link voltage and Inv.1 current (phase a). (c) Active and reactive power supplied by upstream source. (d) Active and reactive power supplied by Inv.1.

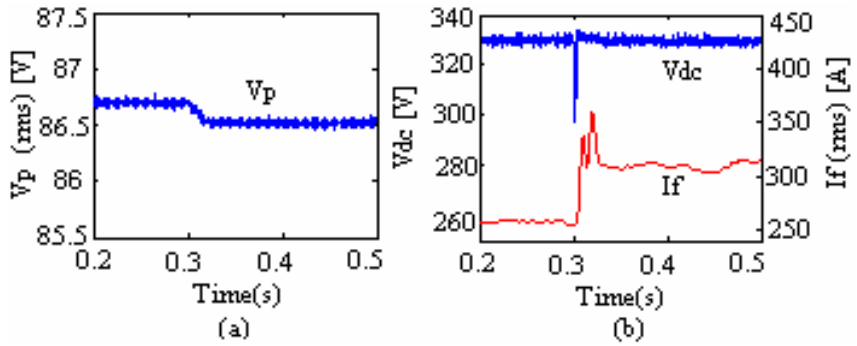

Figure 5-10 System operation under sudden loss of SOFC: (a) PCC voltage (phase a). (b) DC-link voltage and Inv.1 current (phase a).

The simulation results under the sudden loss of the AC link (point 'B' open) are given in Figure 5-11. Both real and reactive power supplied by the upstream system shown in Figure 5-11 (a) increase as the loads are totally supplied by the upstream system. Since $P_{r,0}$ was chosen to satisfy (5.2.1), the sudden power change would not damage the SOFC, as can be seen from Figure 5-11 (b). The utilization factor is within its limit during the fault event. The DC-link voltage V_{dc} increases slightly due to the reduced output power of the SOFC.

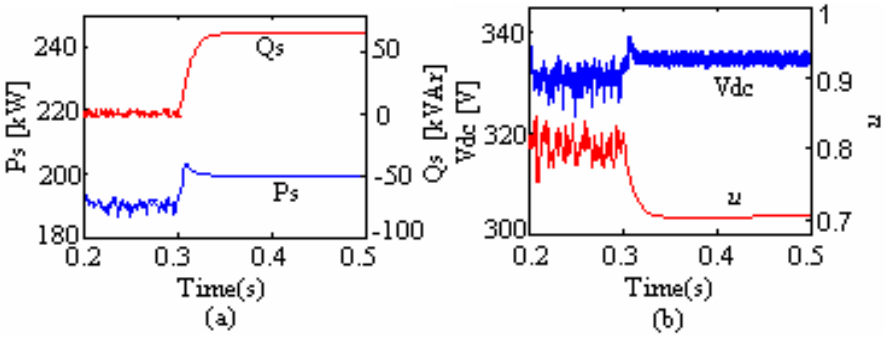

Figure 5-11 System operation under sudden loss of AC link (circuit breaker 'B' open). (a) Active and reactive power supplied by upstream source. (b) DC-link voltage and utilization factor of SOFC.

5.5 Conclusions

Operation scheme of a fuel cell-based Power Quality Control Center under steady-state, upstream voltage sag or AC interconnection outage states has been presented. Unbundled power quality services are realized in the proposed scheme. The DG considered is in the form of a SOFC. Unlike previous works on the PQCC, the role of the DG and the inverters in the PQCC is examined with regard to mitigating the impacts of the fault disturbances on loads. By taking into consideration the ability of the SOFC to track load changes, it is proposed that the SOFC supplies all the downstream loads under steady-state. Upstream voltage sag is dealt with in accordance to the severity of the sag. Two possible scenarios have been considered in which the design criteria is to provide maximum support for load ride-through while maintaining the unbundled power supply feature of the PQCC. Analysis of the system dynamics and the design of the control system of the PQCC have also been presented. The efficacy of the scheme is borne out by simulation results.

Although in the proposed PQCC operation scheme, the dynamic response of the SOFC has been considered and unbundled power quality supply has been realized, it is seen that under upstream voltage sag condition, the voltage sag ride-through capability of the PQCC is relatively low. The PQCC is more likely to be disconnected from the upstream network and operated under Scenario 2. Such islanding operation mode of the PQCC is not entirely satisfactory as it may lead to, for example, large current surges during the disconnection/reconnection of the PQCC. The analysis in Scenario 2 also shows that

there is a severe constraint on the size of the HQ load that can be supported by the PQCC under the islanding mode. Chapter 6 therefore would attempt to address the above problems and to improve the voltage sag ride-through capability of the fuel-cell based PQCC.

Chapter 6

A New PQCC with Series Compensation Capability

Chapter 5 has proposed a practical scheme for the fuel cell-based PQCC system under both steady-state and upstream system voltage sag condition. The scheme attempts to overcome some of the technical problems encountered in the PQCC scheme described in [30, 31]. The difficulties are mainly pertaining to the functional constraints of the DG, which in the present investigation is a SOFC. Unbundled power quality service has also been achieved in the proposed scheme. However, the analysis in Chapter 5 shows that due to the constraints of the SOFC described there, the voltage sag ride-through capability of the HQ load appears to be rather restricted. In order to protect the HQ load, the PQCC would have to be disconnected from the upstream grid and operate in an islanding mode (Scenario 2) under some severe upstream voltage sag conditions. Such an outcome is not entirely satisfactory. For example, during the disconnection process, when the turnoff signal is given to the circuit breaker 'A', the DC-link voltage will vary and in turn regulate the output power of the SOFC. The transition time from the instant when the turnoff signal is given to the new islanding steady-state will depend on the discharging speed of the DC-link capacitor c_f. During the reconnection process, large in-rush currents may occur as the voltage levels on the two sides of the circuit breaker 'A' are different when the turnon signal is given [50]. Re-synchronization with the upstream source is also inconvenient [105]. Furthermore, after the PQCC has been disconnected from the upstream system, there is also a severe constraint on the size of the HQ load that can be supported by the PQCC under the islanding mode, as shown in Figure 5-4.

The research work to be described in this Chapter is an attempt to extend the scheme shown in Chapter 5. The aim is to lessen the need of disconnecting the PQCC from the upstream system during upstream sag conditions, by introducing a Series Compensator (SC) into the PQCC structure. The new scheme, denoted as PQCC-SC, can also realize unbundled power quality supply.

As introduced in Chapter 2, the basic function of a SC is to insert a voltage of required magnitude and frequency in series with the protected load terminal voltage such that it can help restore the load voltage to the desired value [74]. SC has been shown to be particularly effective in overcoming voltage sag problems [57, 58]. Unlike previous works on SC, however, the SC in this Chapter would be incorporated with the PQCC and the DG, in order to realize unbundled power quality service of specified levels.

Two possible PQCC-SC structures would be proposed in this Chapter. Their respective voltage sag ride-through capabilities are analyzed and their performances compared. Harmonics introduced by the power electronics devices and loads are not considered in the analysis, as the main focus is on the fundamental frequency components of the voltages/currents. Similar as in the previous Chapters, all the loads are assumed to be of constant impedance type. Most of the materials contained in this Chapter have been reported in [106, 107].

6.1 PQCC-SC Scheme 1

The configuration of the PQCC-SC Scheme 1 is shown in Figure 6-1. Similar in approach as in the previous work, the complex upstream system is represented simply by the Thevenin equivalent voltage source $\vec{V}_s$ and an inductor L. In this way, an upstream voltage disturbance due to a fault or load switching event could therefore be approximated as the corresponding change in the magnitude and phase angle of $\vec{V}_s$. The survey in [5] indicates that most distribution system sag magnitudes are within the range 0.7 – 0.9 pu and the phase angle changes, often called phase angle jump, are within -20° and 20°.

It is also seen from Figure 6-1 that in addition to the original PQCC structure, the present scheme includes a series compensator (SC), which is installed just upstream of the HQ/OQ load. As explained in Chapter 2, the SC consists of a DC/AC converter, an injection transformer and a DC-link. During an upstream voltage disturbance, the SC is to introduce a voltage component ($\vec{V}_{inj1}$) in series with the HQ/OQ load terminal voltage $\vec{V}_L$. The injected voltage is regulated with the view to control the real and reactive power

(P_{inj1}, Q_{inj1}) exchange between the compensator and the system through the converter. By doing so, the compensator attempts to assist in restoring the HQ load voltage $\vec{V}_L$ to above V_{min} during the upstream sag. In order to differentiate the power quality levels which would be offered to the HQ and SP loads, the SC would be designed only to compensate for up to a specified level of severity of the upstream sag. As a general observation, the extent of the severity of the sags which will be catered for would depend on the potential benefit that can be obtained by the load ride-through versus the cost of the SC.

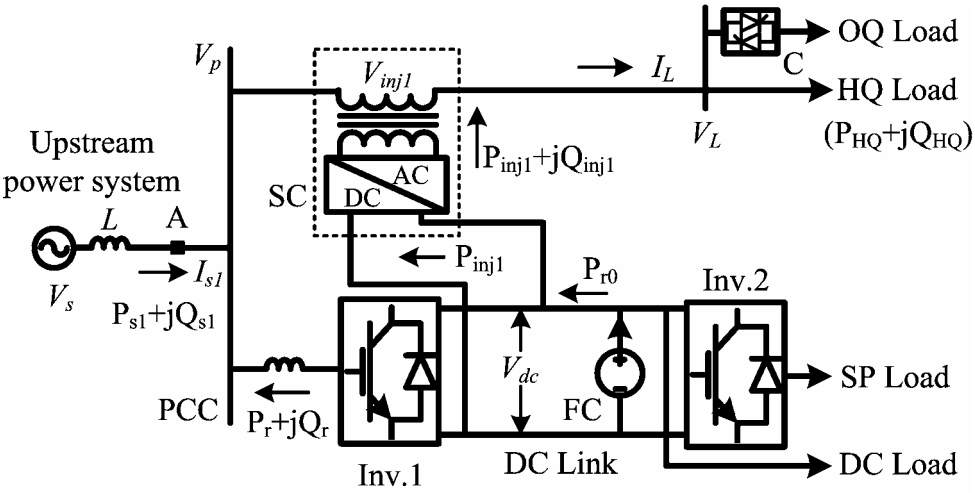

Figure 6-1 PQCC-SC Scheme 1: single-phase representation

Under normal operating conditions of the PQCC-SC scheme, the SC will play no role and its converter will be in off state. The rest of the PQCC will operate as proposed in Chapter 5. This means that SOFC would supply all the DC and SP loads, and also injects a surplus power P_{r0} to the PCC. The steady-state output power of SOFC $P_{dg,0}$ is therefore the same as that given in (5.2.2). The power factor at point 'A' is maintained at unity, thus ensuring that the upstream system supplies only real power to the PCC.

When a sag occurs, the magnitude of the source voltage $\vec{V}_s$ reduces while its phase angle may also undergo a sudden change. The OQ load would be disconnected by the solid-state circuit breaker C if the PCC voltage consequently decreases to below V_{min}. If the load voltage remains below V_{min} after the shedding of the OQ load, the SC will attempt to maintain supply to the HQ load by helping to restore its voltage to V_{min}. The DC and SP loads would still be supplied by the SOFC and would not be affected by the sag as long as V_{dc} is in a reasonable range. During the sag, it is proposed that Inv.1 is also controlled to

maintain unity power factor at point 'A'.

During the restoration stage, the SC has to inject a certain amount of active power (P_{inj1}). Due to the complexity and intricacy of the SOFC power plant, it is desired that the SOFC power plant remains undisturbed at a power level of $P_{dg,0}$ during the sag. Therefore it is proposed that the DC-link voltage is controlled to remain constant before and during the sag through the adjustments of Inv.1. The injected active power by the SC is

$$P_{inj1} = P_{r0} + P_r \tag{6.1.1}$$

where P_r is the active power absorbed by Inv.1 from the PCC. During severe sags where $P_{inj1} > P_{r0}$, active power P_r will be absorbed from the PCC through Inv.1. However, for shallow sags where $P_{inj1} < P_{r0}$, surplus active power P_r will be supplied to the PCC through Inv.1. The changes to the power flow through Inv.1 can be easily achieved by using its switch control signals.

As pointed out in Chapter 2, there are three strategies in achieving voltage restoration through series compensation [77-79]: pre-sag compensation, in-phase injection and energy-saving injection. For the convenience of analysis, a modified pre-sag voltage injection strategy would be considered here. Conventional pre-sag compensation calls for the injection of $\vec{V}_{inj1}$ which is the phasor difference between the pre-sag and sag voltages. In this way, the restored voltage will be identical to the pre-sag voltage. However, in the present scheme the magnitude of the load voltage would only need to be restored to V_{min} instead of the pre-sag magnitude. This is in order to obtain the maximum ride-through potential for the PQCC-SC scheme. The relationship between the voltage quantities during the restoration is described by the phasor diagram in Figure 6-2. The ride-through capability of the scheme can be analyzed as follows. The purpose of the following analysis is to determine the maximum voltage sag Scheme 1 can provide load ride-through when the apparent power rating of SC is pre-determined through economic or other considerations.

As shown in Figure 6-2, the PCC voltage phasor before the voltage sag is chosen as the reference quantity and is denoted as $\vec{V}_{p0}$. Under normal operating conditions, this would be equal to rated load voltage. The subscript '0' denotes pre-sag quantity in this Chapter. The corresponding pre-sag load voltage $\vec{V}_L$ is $\vec{V}_{p0}$ and that of $\vec{V}_s$ is $\vec{V}_{s0}$. The phase

angle of $\vec{V}_{s0}$ is denoted as φ_0. Using the basic electric circuit theory, φ_0 can be easily determined if the HQ, OQ load demands and the upstream system inductor L are known.

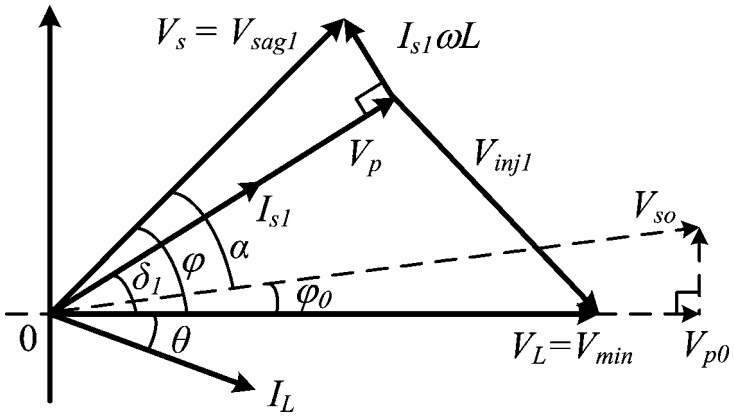

Figure 6-2 Phasor diagram of the proposed Scheme 1

Due to an upstream sag, the magnitude of $\vec{V}_s$ suddenly decreases to V_{sag1} and its phase angle jumps by angle α so that $\varphi = \alpha + \varphi_0$. $\vec{V}_s$ can therefore be expressed as

$$\vec{V}_s = V_{sag1}\cos\varphi + jV_{sag1}\sin\varphi \tag{6.1.2}$$

It is intended that through the modified pre-sag compensation method, the HQ load voltage is restored to

$$\vec{V}_L = V_{\min} + j0 \tag{6.1.3}$$

The HQ load power factor cosθ is assumed lagging and its current $\vec{I}_L$ is therefore

$$\vec{I}_L = I_L\cos\theta - jI_L\sin\theta \tag{6.1.4}$$

The upstream line current $\vec{I}_{s1}$ during the sag would be of the form

$$\vec{I}_{s1} = I_{s1}\cos\delta_1 + jI_{s1}\sin\delta_1 \tag{6.1.5}$$

According to the proposed scheme, the power factor at point 'A' is always unity. Therefore the PCC voltage $\vec{V}_p$ is in phase with $\vec{I}_{s1}$. From Figure 6-2 and at the power frequency ω, the PCC voltage can be represented as:

$$\vec{V}_p = V_{sag1}\cos(\varphi-\delta_1)\cos\delta_1 + jV_{sag1}\cos(\varphi-\delta_1)\sin\delta_1 \tag{6.1.6}$$

and also

$$I_{s1} = \frac{V_{sag1}\sin(\varphi-\delta_1)}{\omega L} \tag{6.1.7}$$

From (6.1.3) and (6.1.6), the injected voltage by the SC during the sag is:

$$\begin{aligned}\vec{V}_{inj1} &= \vec{V}_L - \vec{V}_p \\ &= V_{\min} - \left(V_{sag1}\cos(\varphi-\delta_1)\cos\delta_1 + jV_{sag1}\cos(\varphi-\delta_1)\sin\delta_1\right)\end{aligned} \tag{6.1.8}$$

Under Scheme 1, the current flowing through the primary winding of the injection transformer of the SC is $\vec{I}_L$. Therefore from (6.1.4) and (6.1.8), the power rating of the SC under Scheme 1 is:

$$|S_1| = 3I_L\left|\vec{V}_{inj1}\right| \tag{6.1.9}$$

Let S_{HQ} be the apparent power drawn by the HQ load during the sag. Therefore

$$I_L = \frac{S_{HQ}}{3V_{\min}}$$

Substituting the above equation into (6.1.9), it yields

$$|S_1| = \frac{S_{HQ}\left|\vec{V}_{inj1}\right|}{V_{\min}} \tag{6.1.10}$$

Applying active power balance for the HQ load, one obtains

$$P_{HQ} = P_{s1} + P_{r0} \tag{6.1.11}$$

P_{HQ} is the active power drawn by the HQ load during the sag. P_{s1} is the active power supplied by the upstream source. They are given as

$$P_{HQ} = 3V_{\min}I_L\cos\theta = S_{HQ}\cos\theta \tag{6.1.12}$$

$$P_{s1} = 3V_{sag1}I_{s1}\cos(\varphi-\delta_1) = \frac{3V_{sag1}^2\sin[2(\varphi-\delta_1)]}{2\omega L} \tag{6.1.13}$$

Equation (6.1.11) can be rewritten as

$$S_{HQ}\cos\theta = \frac{3V_{sag1}^2\sin[2(\varphi-\delta_1)]}{2\omega L} + P_{r0} \tag{6.1.14}$$

Thus, if the system parameters L, P_{r0}, θ, S_{HQ}, α and the power rating of the SC S_1 are known or are specified, by solving (6.1.10) and (6.1.14) it is possible to determine the minimum source voltage V_{sag1} that the Scheme 1 is capable of riding-through and the unknown parameter δ_1. Unfortunately these two equations are complex trigonometric equations. It is difficult to obtain general expressions for δ_1 and V_{sag1} in term of the known or specified quantities. In which case, one can resort to numerical means to evaluate δ_1 and V_{sag1}. The results of the computation allow one to observe how the system parameters would affect $\vec{V}_{sag1}$, which in turn reflects the ride-through capability afforded by the PQCC-SC. This aspect of the analysis will be illustrated later.

6.2 PQCC-SC Scheme 2

Figure 6-3 shows an alternative PQCC-SC scheme. The configuration and operation of Scheme 2 is very similar to that of Scheme 1. The only difference is in the location of the voltage injection of the SC. In Scheme 2, the compensator is installed immediately upstream of the PCC. The compensator injects a voltage in series with $\vec{V}_A$ so as to restore $\vec{V}_p$ to V_{min}. Similar to the case in Scheme 1, the active power injected by the SC is:

$$P_{inj2} = P_{r0} + P_r \tag{6.2.1}$$

If $P_{inj2} > P_{r0}$, Inv.1 will absorb active power P_r from the PCC. However, if $P_{inj2} < P_{r0}$, surplus active power P_r will be transferred to the PCC through Inv.1. As in Scheme 1, the SOFC is to remain undisturbed during the sag and V_{dc} is also maintained constant. The power factor at point 'A' is controlled to unity during the sag. The ride-through capability of Scheme 2 is then analyzed. Again the modified pre-sag restoration strategy such as that in Scheme 1 is utilized and the phasor diagram of Scheme 2 is similar to that shown in Figure 6-2. The purpose of the following analysis is to determine the most severe voltage sag that can be compensated by Scheme 2 for a given SC capacity.

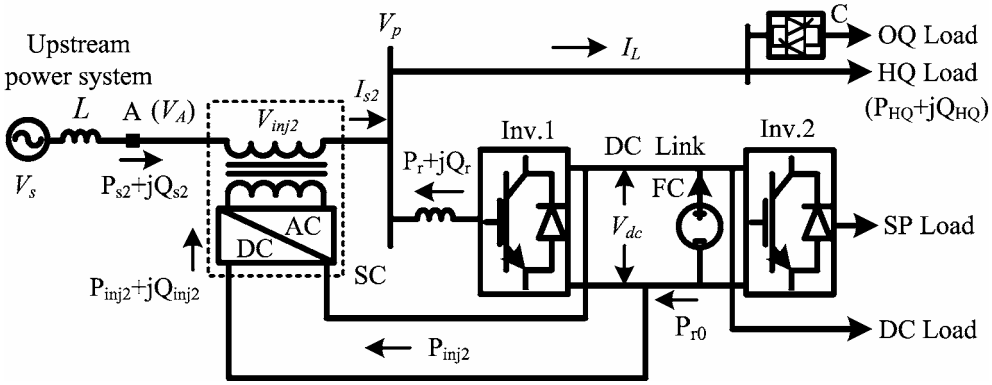

Figure 6-3 PQCC-SC Scheme 2: single-phase representation

As in Scheme 1, the upstream sag voltage $\vec{V}_s$ is denoted as

$$\vec{V}_s = V_{sag2}\cos\varphi + jV_{sag2}\sin\varphi \tag{6.2.2}$$

The PCC voltage is to be restored to V_{min}, that is

$$\vec{V}_p = V_{\min} + j0 \tag{6.2.3}$$

For the same HQ load as that in Scheme 1, the load current is the same as that given in (6.1.4). The upstream line current in Scheme 2 is denoted as $\vec{I}_{s2}$, which is

$$\vec{I}_{s2} = I_{s2}\cos\delta_2 + jI_{s2}\sin\delta_2 \tag{6.2.4}$$

As the power factor at point 'A' is also maintained at unity, then similar relationships as that in Scheme 1 can be derived:

$$I_{s2} = \frac{V_{sag2}\sin(\varphi-\delta_2)}{\omega L} \tag{6.2.5}$$

$$\vec{V}_A = V_{sag2}\cos(\varphi-\delta_2)\cos\delta_2 + jV_{sag2}\cos(\varphi-\delta_2)\sin\delta_2 \tag{6.2.6}$$

Therefore, the injected voltage by the SC is

$$\vec{V}_{inj2} = V_{\min} - \vec{V}_A \tag{6.2.7}$$

The current flowing through the SC in Scheme 2 is $\vec{I}_{s2}$. Therefore the power rating of the SC is,

$$|S_2| = 3\left|\vec{I}_{s2}^{*}\right|\left|\vec{V}_{inj2}\right| = 3\left|\vec{V}_{inj2}\right|V_{sag2}\sin(\varphi-\delta_2)/(\omega L) \tag{6.2.8}$$

Similar to Scheme 1 and according to active power balance, the following relationship would be obtained:

$$P_{HQ} = P_{s2} + P_{r0} \tag{6.2.9}$$

P_{HQ} is the active power demanded by the HQ load and it is the same as (6.1.12). P_{s2} is the active power supplied by the upstream system. It can be represented as:

$$P_{s2} = 3V_{sag2}I_{s2}\cos(\varphi-\delta_2) = \frac{3V_{sag2}^2\sin[2(\varphi-\delta_2)]}{2\omega L} \tag{6.2.10}$$

Substituting (6.1.12) and (6.2.10) into (6.2.9), it yields

$$S_{HQ}\cos\theta = \frac{3V_{sag2}^2\sin[2(\varphi-\delta_2)]}{2\omega L} + P_{r0} \tag{6.2.11}$$

As in Scheme 1, the unknown parameters δ_2 and V_{sag2} can only be calculated from (6.2.8) and (6.2.11) through numerical method as analytical solutions for them are difficult to arrive at.

6.3 Comparison of the Two Schemes under an Extremely Stiff Upstream Supply Condition

As the two schemes are intended to enhance power supply quality, it is necessary to compare the two schemes in term of their ride-through capabilities when the power ratings of the series compensators are the same i.e., $S_1 = S_2 = S_{max}$. However previous

analysis shows that it is difficult to compare the two schemes in general because the resulting equations are complex. Simplification is possible once the following assumption is made: if the fault level of the upstream system is much larger than the capacity of the PQCC, the system series inductance L in the network model can be ignored. This assumption is reasonable so long as the PQCC system is deemed to be connected to an upstream network of relatively large capacity.

Under this special condition, for Scheme 1, it yields $\vec{V}_p = \vec{V}_s$ and therefore $\varphi_0 = 0$, $\varphi = \delta_1 = \alpha$. Equation (6.1.10) becomes

$$|S_1| = S_{HQ} \left| (V_{\min} - V_{sag1}\cos\alpha - jV_{sag1}\sin\alpha) \right| \Big/ V_{\min}$$

or,

$$(V_{\min} - V_{sag1}\cos\alpha)^2 + V_{sag1}^2 \sin^2\alpha = (S_1 V_{\min} / S_{HQ})^2 \qquad (6.3.1)$$

It is seen that (6.3.1) is quadratic in V_{sag1}. Therefore V_{sag1} can be obtained as:

$$V_{sag1} = \frac{2V_{\min}\cos\alpha - \sqrt{4V_{\min}^2\cos^2\alpha - 4[V_{\min}^2 - (S_1 V_{\min}/S_{HQ})^2]}}{2}$$

As only voltage sags are considered here, it should satisfy $V_{sag1} < V_{min}$. The other root of (6.3.1) is then ignored because it could be larger than V_{min}, or even result in a voltage swell. The above equation shows that if S_1 is equal to its maximum value, S_{max}, the most severe sag Scheme 1 can compensate is obtained. This is denoted as $V_{sag1,max}$

$$V_{sag1,\max} = \frac{2V_{\min}\cos\alpha - \sqrt{4V_{\min}^2\cos^2\alpha - 4[V_{\min}^2 - (S_{\max} V_{\min}/S_{HQ})^2]}}{2} \qquad (6.3.2)$$

Similar derivation can also be applied to Scheme 2. If L= 0 for Scheme 2, it yields $\varphi_0 = 0$, $\varphi = \delta_2 = \alpha$. Therefore (6.2.8) can be simplified as

$$|S_2| = 3I_{s2} \left| (V_{\min} - V_{sag2}\cos\alpha - jV_{sag2}\sin\alpha) \right|$$

or,

$$(V_{\min} - V_{sag2}\cos\alpha)^2 + V_{sag2}^2\sin^2\varphi = (\frac{S_2}{3I_{s2}})^2 \qquad (6.3.3)$$

From (6.2.9), it is seen that

$$3V_{sag2}I_{s2} = P_{HQ} - P_{r0}$$

or

$$I_{s2} = \frac{S_{HQ}\cos\theta - P_{r0}}{3V_{sag2}} \tag{6.3.4}$$

Substituting (6.3.4) into (6.3.3) and rearranging (6.3.3), it yields

$$[1 - \frac{S_2^2}{(S_{HQ}\cos\theta - P_{ro})^2}]V_{sag2}^2 - 2V_{\min}V_{sag2}\cos\alpha + V_{\min}^2 = 0 \tag{6.3.5}$$

Equation (6.3.5) is quadratic in V_{sag2}. The most severe sag Scheme 2 can compensate, denoted as $V_{sag2,max}$, can be derived from (6.3.5) when the power rating of the SC is S_{max}.

$$V_{sag2,\max} = \frac{2V_{\min}\cos\alpha - \sqrt{4V_{\min}^2\cos^2\alpha - 4V_{\min}^2[1 - \frac{S_{\max}^2}{(S_{HQ}\cos\theta - P_{ro})^2}]}}{2[1 - \frac{S_{\max}^2}{(S_{HQ}\cos\theta - P_{ro})^2}]} \tag{6.3.6}$$

One can define a ratio k, which compares the VA capacity of the SC to that of the HQ load under sag condition, i.e.,

$$k = S_{\max}/S_{HQ} \tag{6.3.7}$$

Then (6.3.2) and (6.3.7) can be rewritten as

$$V_{sag1,\max} = \frac{2V_{\min}\cos\alpha - \sqrt{4V_{\min}^2\cos^2\alpha - 4V_{\min}^2(1-k^2)}}{2} \tag{6.3.8}$$

$$V_{sag2,\max} = \frac{2V_{\min}\cos\alpha - \sqrt{4V_{\min}^2\cos^2\alpha - 4V_{\min}^2[1 - \frac{(kS_{HQ})^2}{(S_{HQ}\cos\theta - P_{ro})^2}]}}{2[1 - \frac{(kS_{HQ})^2}{(S_{HQ}\cos\theta - P_{ro})^2}]} \tag{6.3.9}$$

It is seen from (6.3.8) and (6.3.9) that the ride-through capabilities of the two schemes can be compared when the system parameters, the rated power capacity of the HQ load S_{HQ} and k are given. For example, using the typical values of V_{min} = 0.9 pu and P_{r0} = 0.1 pu, the relationships of $V_{sag1,max}$ and $V_{sag2,max}$ as functions of the phase angle jump (α) have been plotted under different HQ load power factors and k in Figure 6-4 and Figure 6-5. The phase angle jump has been considered only between the typical range of -20° and 20°.

Figure 6-4 shows the variation of the ride-through capabilities of the two schemes with phase angle jump (α) and HQ load power factor (cosθ). S_{HQ} and k, i.e., S_{max}, are constant in the figure. The figure shows that the ride-through capability of both schemes would

decrease when the absolute value of α increases. Unlike Scheme 2, Scheme 1 ride-through capability is not affected by the HQ load power factor. This is obvious from (6.3.8) and (6.3.9). When cosθ increases, Scheme 2 ride-through capability decreases. Therefore for the given power rating of the HQ load and the SC, if the HQ load power factor is above 0.8 in this example, Scheme 1 would be preferable over Scheme 2.

Figure 6-5 shows the relationship of the system ride-through capabilities under varied SC rating. S_{HQ} and cosθ are fixed when evaluating these curves and hence k is varied. It is seen from the figure that when k increases, i.e. when the power rating of the SC increases, the ride-through capabilities of both schemes would also increase. In Figure 6-5, it also shows that for the given load power factor when k is relatively small (≤ 0.35), the ride-through capability of Scheme 2 is superior compared to that of Scheme 1. However when k becomes larger, the ride-through capability of Scheme 1 could exceed that of Scheme 2, e.g., when $k = 0.7$.

In summary therefore, when the short-circuit ratio at the PCC is very large, a comparison of the two schemes has been given in term of their ride-through capabilities for given power ratings of the HQ load and the SC. It is found that the preference of one scheme over the other depends on the HQ load power factor and the power rating of the SC relative to that of the HQ load.

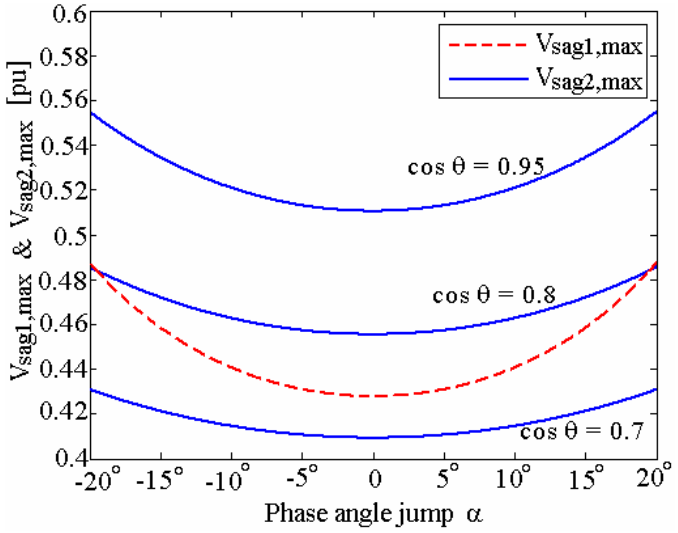

Figure 6-4 Variations of $V_{sag1,max}$ and $V_{sag2,max}$ with phase jump α and HQ load power factor cosθ for $k = 0.52$, $S_{HQ} = 0.38$ pu, L=0

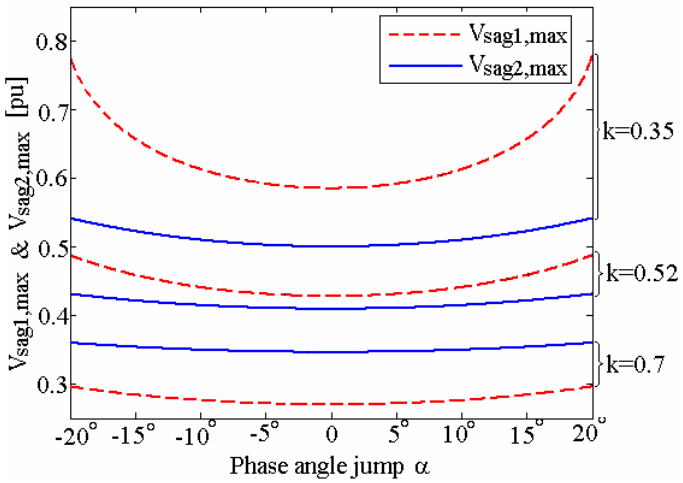

Figure 6-5 Variations of $V_{sag1,max}$ and $V_{sag2,max}$ with α and k for HQ load power factor of 0.7 (lag), S_{HQ} = 0.38 pu, L=0

6.4 Numerical Example and Simulation

In section 6.3, the two PQCC-SC schemes have been compared by assuming the upstream power system is an extremely stiff system. However, such an assumption is not always the case and the two schemes need to be compared under more realistic condition. This Section would give such a comparison based on numerical examples. Simulation results are also given to verify the proposed schemes.

6.4.1 Numerical Example

The system parameters of the numerical example are given in Table 6-1. The upstream inductance X_L is obtained by assuming the upstream fault level is 20 times that of the total PQCC loads. This is a typical value for distribution systems. The SOFC parameters are the same as that given in the Appendix B. The SOFC has a rated DC-link voltage of 330 V and a rated power of 100 kW. Hence the power and voltage base values are chosen to be S_b=100 kVA and V_{dc} = 330 V. From the basic PWM theory [88], it is readily obtained that the corresponding voltage base at the PCC bus is 86.6 V, when the Inv.1 is operated under sinusoidal PWM technique with a nominal modulation index of 0.74. The parametric values in Table 6-1 are expressed in pu on this base. The pre-sag SOFC output is assumed to be 0.9 pu, of which 0.1 pu is diverted to the PCC. V_{min} is assumed to be 0.9 pu, based on the well-known ITI curve.

Table 6-1: Parametric values of the PQCC and power system

V_{p0}	1	V_{min}	0.9
X_L	0.0179	ω [Hz]	50
V_{dc}	1	P_{OQ}	1.6
S_{HQ}	0.38	P_{r0}	0.1
P_{dg0}	0.9	P_{SP}	0.5
P_{DC}	0.3	S_{max}	0.2

As system parameters and the power rating of SC S_{max} are given, V_{sag1} and δ_1 corresponding to Scheme 1 can be determined from (6.1.10) and (6.1.14). Figure 6-6 shows the relationship between the sag magnitudes V_{sag1} and the power rating of the SC under different phase angle jump. It shows in Figure 6-6 that as S_1 increases, V_{sag1} decreases for a given α. Therefore the maximum sag Scheme 1 can compensate, $V_{sag1,max}$, is obtained when S_1 is at its maximum value. In this example, it corresponds to the extreme right-hand value on the V_{sag1} curve in Figure 6-6 when $S_1 = S_{max} = 0.2$ pu. Similar conclusion can also be drawn for Scheme 2 using (6.2.8) and (6.2.11), as shown in Figure 6-7.

In this example, $S_1 = S_2 = S_{max} = 0.2$ pu, $S_{HQ} = 0.38$, i.e. $k = 0.52$. Therefore the most severe sags the two schemes can provide ride-through can be calculated from (6.1.10), (6.1.14) and (6.2.8), (6.2.11). Plotting $V_{sag1,max}$ and $V_{sag2,max}$ under different phase angle jump and HQ load power factors onto the same figure, the ride-through capabilities of the two schemes can be readily compared.

Figure 6-8 and Figure 6-9 compare the ride-through capabilities of the two schemes under different phase angle jump α, HQ load power factor cosθ and k. it is found the relationships shown in the two figures are very similar to that shown in Figure 6-4 and Figure 6-5. Therefore, the above analysis based on this more realistic condition ($L \neq 0$) gives similar conclusion as in the case when $L = 0$. This is because the upstream system is of much higher capacity than that of the PQCC-SC.

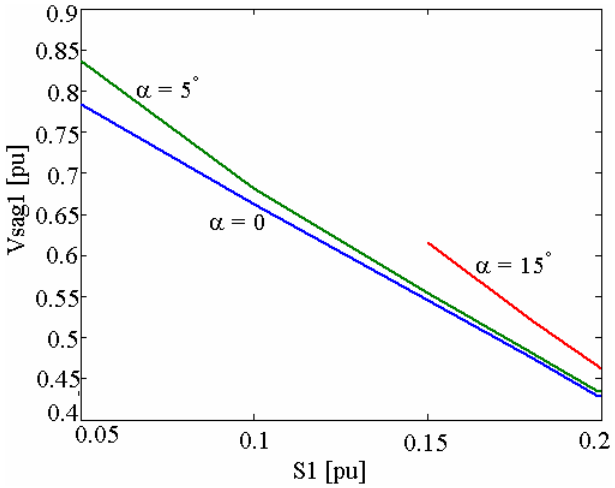

Figure 6-6 Variations of V_{sag1} with α and S_1 for S_{HQ} = 0.38 pu: Scheme 1

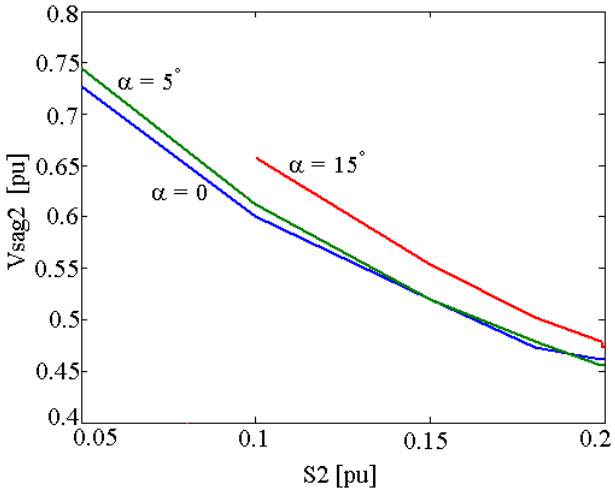

Figure 6-7 Variations of V_{sag2} with α and S_2 for S_{HQ} = 0.38 pu and cosθ = 0.8: Scheme 2

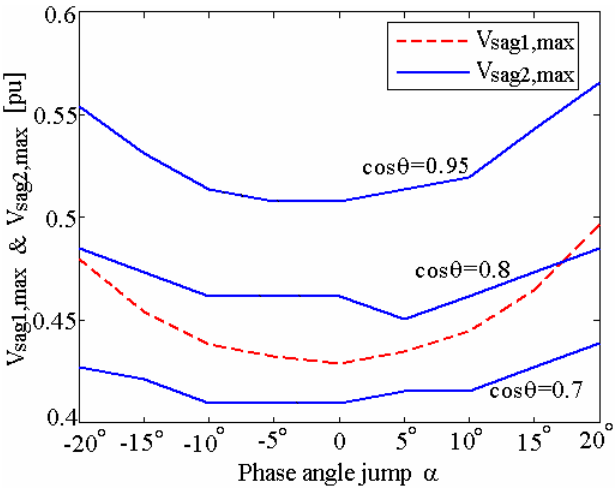

Figure 6-8 Variations of $V_{sag1,max}$ and $V_{sag2,max}$ with phase jump α and HQ load power factor cosθ for k = 0.52, S_{HQ} = 0.38 pu, $L \neq 0$

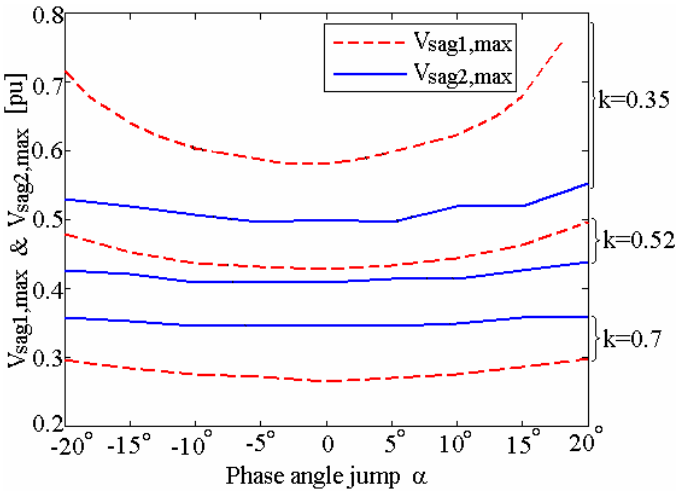

Figure 6-9 Variations of $V_{sag1,max}$ and $V_{sag2,max}$ with α and k for HQ load power factor of 0.7 (lag), S_{HQ} = 0.38 pu, $L \neq 0$

6.4.2 Simulation

Simulation studies have been carried out to verify the proposed schemes. The simulation software used is Matlab/Simulink. The example systems used for simulation study are as shown in Figure 6-1 and Figure 6-3. The SOFC dynamic model shown in Figure 5-1 is also applied in the simulation. The system parameters are the same as that shown in Table 6-1 and cosθ = 0.95, S_{max} = 0.2 pu. From Figure 6-7 and 6-8 or using (6.1.10), (6.1.14) and (6.2.8), (6.2.11), it is established that when the phase angle jump is 0, the most severe sag Scheme 1 can compensate is $V_{sag1,max} \approx 0.42$ pu and for Scheme 2, $V_{sag2,max} \approx 0.51$ pu Simulation results under these sag conditions are shown in Figures 6-10 – 6-11.

Figure 6-10 shows Scheme 1 operation under a 42% sag. It is the most severe sag Scheme 1 can compensate when $\alpha = 0$. Figure 6-10 (b) shows that indeed the HQ terminal voltage has been restored essentially to the required level. Inv.1 transfers P_{r0} from the SOFC to the PCC under steady-state. However, during the sag, Inv.1 attempts to absorb active power from the upstream system. Therefore P_r becomes negative during the sag, as is shown in Figure 6-10 (c). The active power absorbed by Inv. 1 is then transferred to the SC, as intended by the design. The injected active power by the SC P_{inj1} is then equal to ($P_r + P_{r0}$) and the power factor of the upstream line is also unity as $Q_{s1} = 0$, shown in Figure 6-10 (d). The DC-link voltage is kept constant, as can be seen from Figure 6-10 (f). It ensures the normal operation of the SOFC and DC and SP loads. Also in Figure 6-

10 (f), S_1 is seen to be at its maximum value during the sag. This shows that Scheme 1 is indeed providing the maximum sag ride-through support under this disturbance condition.

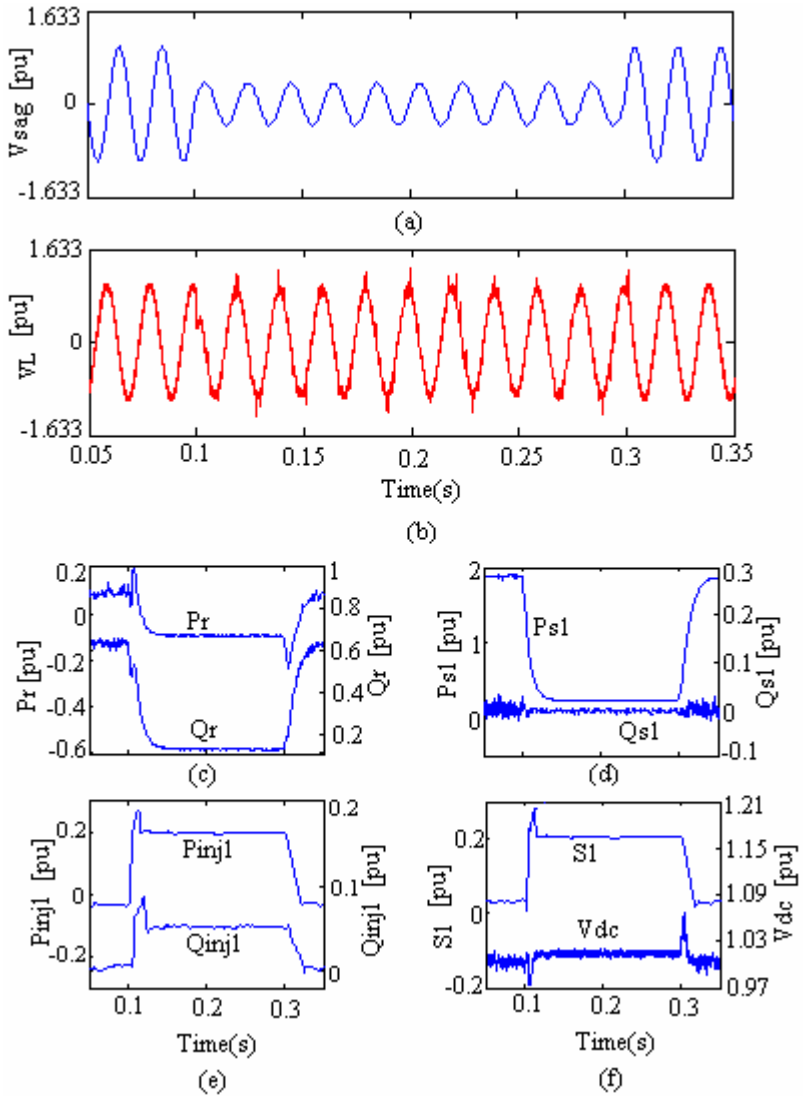

Figure 6-10 Simulation results for Scheme 1 under a 42% sag. (a) source voltage (phase a); (b) HQ load voltage; (c) Active and Reactive power supplied by Inv.1; (d) Active and Reactive power supplied by the upstream system; (e) Active and Reactive power injected by the series compensator; (f) Apparent power of the SC and DC-link voltage.

A 51% sag is then applied to Scheme 2. It is the most severe sag Scheme 2 can compensate when $\alpha = 0$. The simulation results are shown in Figure 6-11. It is seen that during the sag, the sag effect has been mitigated at the PCC as its voltage has been restored to 0.9 pu. See Figure 6-11 (b). The power rating of the SC reaches its maximum value 0.2 pu during the sag which indicates this is the limit of ride-through capability that

can be obtained from this scheme. The power flows in the upstream system, SC and Inv.1 are similar to that shown for Scheme 1.

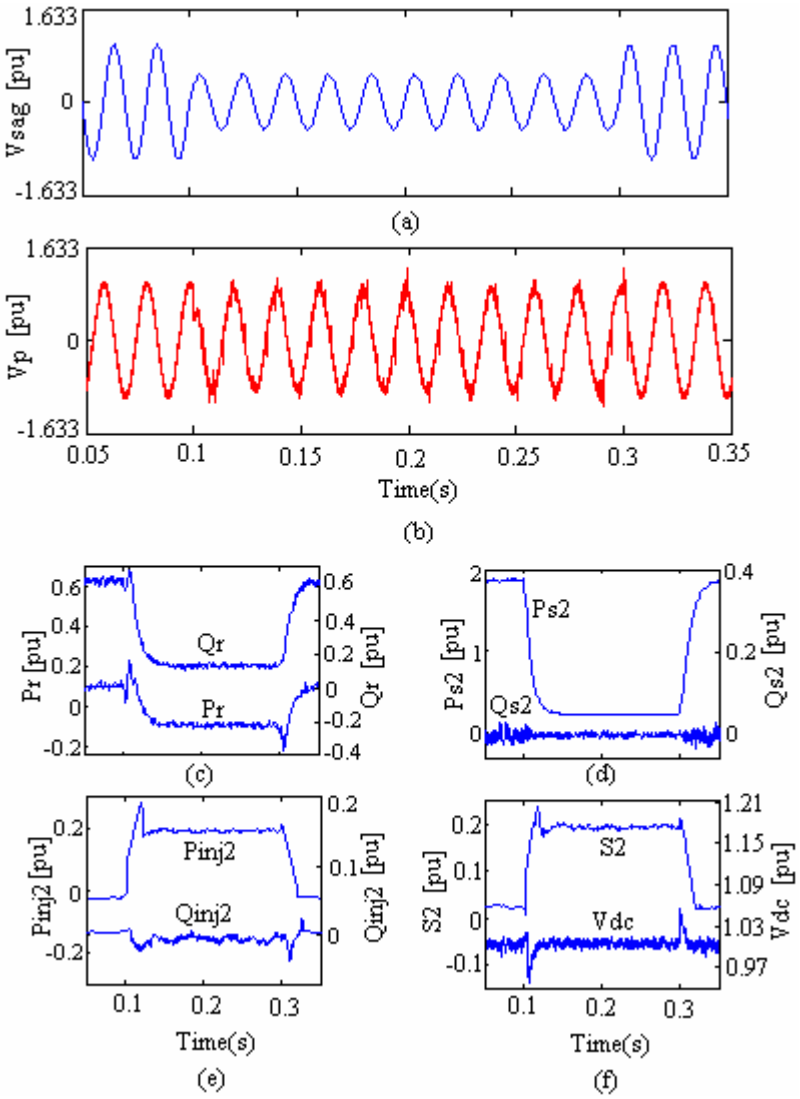

Figure 6-11 Simulation results for Scheme 2 under a 51% sag. (a) source voltage (phase a); (b) PCC voltage; (c) Active and Reactive power supplied by Inv.1; (d) Active and Reactive power supplied by the upstream system; (e) Active and Reactive power injected by the series compensator; (f) Apparent power of the SC and DC-link voltage.

6.5 Conclusions

Two voltage sag compensation schemes for the fuel cell-based Power Quality Control Center have been considered. By incorporating series compensators into the PQCC, the new schemes appear to be able to provide significant improvement in load ride-through

capability during voltage sags in comparison to the scheme shown in Chapter 5. It also allows the realization of unbundled power quality supply. The ride-through capabilities of the two PQCC-SC schemes are also analyzed and compared. The objective of the comparison is to assess the maximum ride-through that can be achieved for a given SC power capacity. The analysis shows that the preference of one scheme over the other depends on the HQ load power factor and the capacity of the SC relative to that of the HQ load. The effectiveness of the proposed schemes and the theoretical analysis have been verified by simulation studies.

Chapter 7

Conclusions and Recommendations

7.1 Conclusions

The main focus of this research is to examine the potential of using Power Quality Control Center (PQCC) for the purpose of mitigating the undesirable impacts of power quality disturbances on sensitive loads and also, to provide unbundled power quality services to customers. PQCC is a new conceptual facility designed for electric power distribution system of the future. The Center is connected between the high voltage distribution systems and the loads. Equipped with various Custom Power devices, distributed generators (DG), computers and communication lines, the PQCC is designed to meet the demand of loads for varied quality levels, through the flexible changes of network configuration.

Based on basic electric circuit principle, PWM theory and small signal linearization method, a general mathematical model of the UPS-type PQCC has been derived. This dynamic model is needed for the design of control schemes, as applied to the power electronics devices in the PQCC. It forms the basis of modeling the schemes, leading to the realization of the many proposed functions of the Center. In the latter part of Chapter 3, for example, a new power system frequency stabilization control strategy has been proposed by taking advantage of the flexibility offered by the PQCC. The example system consists of a PQCC connected to an external grid system. It is observed that in the event of system frequency deviation due to load-generation imbalance, the proposed control scheme can effectively mitigate the frequency fluctuation much more satisfactorily than the conventional control, which only relies on the actions of the generator speed-governor system.

It is also well-recognized that voltage sag is one of the most devastating power disturbances observed in power systems. Accordingly in Chapter 4, using the PQCC to

mitigate upstream voltage sag effect on sensitive loads has been examined. The analysis in the Chapter shows that voltage sag ride-through capability of sensitive loads provided by the PQCC could be improved, if the fault current in the interlink between the upstream system and the PQCC can be controlled within specified limit. This desirable outcome is achieved by regulating the active power supplied by the faulted upstream network. In the proposed scheme, the DG is controlled to supply the balance of the active power demand of the loads through regulating the DC-link voltage during the disturbance. The dynamic model of the DG suitable for analysis has also been developed. Based on the analytical results obtained, a three-stage operation scheme has been proposed. Each of the stages corresponds to one DC link voltage level. Through the control of the inverter and the DG, the proposed scheme has been shown to be effective in improving the sensitive load ride-through capability. Unlike the PQCC designs considered by other researchers, standby feeders and hybrid transfer switches are not required. The control system for realizing the proposed scheme is designed based on the PQCC dynamic model developed in Chapter 3.

Extension of the research of Chapter 4 is to use the PQCC to provide varied supply quality levels for loads. This so-called unbundled power quality supply is a desirable feature. Focusing on realizing such feature, several designs of the PQCC have been proposed in earlier works. Unfortunately in these designs, little attention has been paid on the dynamics of the DG, and yet the DG is expected to play a central role in ensuring the success of the scheme. Therefore in Chapter 5, the functional characteristic of the DG has been carefully examined before it is considered for incorporation into the PQCC. By assuming the DG in the form of a SOFC, it is found that the ability of the SOFC to accommodate instantaneous power demand change is constrained by its fuel utilization factor, DC link voltage and SOFC power limits. Based on the analysis of the SOFC characteristic, a feasible PQCC operating scheme which can cater for normal interconnected, upstream voltage sag and islanding states has been described. The aim is to provide unbundled power quality supply and also achieve maximum support for load ride-through. In the new design it is proposed that the SOFC supplies all the downstream loads under steady-state. During upstream sag condition, two possible scenarios have been considered which are in accordance to the severity of the sags: interconnected mode and islanding mode. Furthermore it is shown analytically that the determination of the current rating of the inverter in the PQCC depends on the relative sizes of the loads of

different quality levels to be supplied by the PQCC. Based on the dynamic model derived for the system and the DG, a design procedure on the PQCC control system has also been presented.

From the results obtained in Chapter 5, it is found that the ride-through capability of the fuel cell based-PQCC under upstream sag state suffers from some limitations. For sag of certain severity, the PQCC has to be disconnected from the power system and this can be undesirable. Chapter 6 therefore proposes the incorporation of a Series Compensator into the PQCC structure. This is for the purpose of improving the PQCC voltage sag ride-through capability. Investigation on the two possible PQCC-SC schemes shows that indeed, both schemes can indeed provide significant improvement on load ride-through capability. They can also achieve unbundled power quality supply. The comparison of the two schemes shows that the preference of one scheme over the other depends on the protected load power factor and the capacity of the series compensator.

7.2 Recommendations

In view of the progress described in the previous Chapters, the following directions are suggested as possible areas for further investigation.

In Chapters 4 - 6, attentions have been directed toward examining the PQCC operation under upstream system voltage-sag condition. Possible schemes have been proposed to improve the sensitive load voltage sag ride-through capability. However, for the purpose of simplification, the analysis given in the Chapters are based on the assumption that the upstream voltage sags are balanced. In practice, most faults in power systems involve only single phase or two phases [42]. The unbalance upstream voltage results in the appearance of even harmonics at the DC link voltage and odd harmonics in the input current, which could interfere with Inv.1 control and the DG operation. It is therefore necessary to re-examine the PQCC operations under such unbalanced sag conditions. It is envisaged that symmetrical components analysis can be used to design Inv.1 control scheme under the unbalanced sag conditions.

The SOFC internal dynamics under severe and prolonged disturbances may also be a fruitful area for future study. It is seen in Chapters 4 that the SOFC has been represented

simply as a constant EMF in series with a resistor under voltage sag conditions. However such model is not applicable under prolonged disturbance conditions. In Chapter 5, if the HQ load demand is outside the area of 'RSTUR' in Figure 5-3, the SOFC would be unable to satisfy the HQ load instantaneously. The internal dynamics of the SOFC, which may include the dynamics of the fuel processor and the electrochemical process, should be taken into consideration. It (typically) requires several tens of seconds for the SOFC to achieve a significant output power change. Such a slow response of SOFC will surely affect the operation of the PQCC system if the sag persists. One possible solution may be to use a buffer energy storage device in the PQCC. The storage device could be a battery or a supercapacitor, which is intended to complement for the slow dynamics of the SOFC. If the output power change cannot be satisfied by the SOFC instantaneously, the energy storage device will supply the balanced active power until the internal dynamics of SOFC has adjusted sufficiently to meet the new power demand. It is therefore expected that the size of the buffer energy device may be small in comparison with the SOFC, although it must be capable to react rapidly. The combination of the operation of a SOFC and an energy storage device to realize unbundled power quality service needs further investigation.

In the investigation described in Chapter 4, V_{dc} is assumed to be regulated in a "reasonable" range such that Inv.2 is able to handle the changes in V_{dc} and maintains the SP load terminal voltage. Similarly in Chapters 5, V_{dc} will change when the output power of SOFC changes during the islanding mode. However, it is also assumed such change is of such a magnitude that it will not affect the PQCC operation. In Chapter 6, V_{dc} is controlled to remain constant in order to ensure that the SOFC is undisturbed during the upstream sag conditions. However the ride-through capabilities provided by the PQCC-SC schemes can be further improved by varying V_{dc} in a reasonable range and therefore permitting the SOFC to supply additional amount of active power. From the above discussion, it is concluded that another possible topic for future study may concern the control of the DC link voltage. It is necessary to determine what would constitute as "reasonable" level of V_{dc} change. An excessive change in V_{dc} will result in Inv.2 runs out of its control margin and the SP load voltage may deviate outside its desirable range. Also as V_{dc} is maintained in the reasonable range under severe disturbances by Inv.1, a high performance controller for Inv.1 is needed to achieve better DC voltage dynamics. A DC

voltage control scheme with current feed forward may be a possible solution for Inv.1. Also quite possibly, it will be interesting to examine how the PQCC would operate if V_{dc} cannot maintain within such range. This could probably provide a limiting operating range of the PQCC.

In Chapter 3, an isolate power system incorporated with a micro-turbine (MT) is used as an example to show that the PQCC system is able to improve power quality. As a promising DG technology, a more detailed study on MT is suggested for future work. Similar to the examination on the use of the SOFC, operational constraints and dynamic model of MT can be included. Based on the outcome of the investigation, PQCC operation incorporated with MT can be proposed. Another possible scheme is to operate MT in parallel with SOFC in the PQCC. As the dynamic response of MT is relatively faster than that of the SOFC, MT can operate as a buffer to compensate for the slow dynamics of the SOFC. This is particularly so in situations when the PQCC system has to respond to a disturbance which has a duration longer than the normal voltage sag/swell, but shorter than the load tracking-type of changes. In which case, the coordination between the control effects of MT and SOFC has to be studied.

Finally, it is noted that the research work described in this thesis is mainly focused on using PQCC to mitigate power quality disturbances which originate in the upstream system. No attention has been directed towards disturbances due to the downstream loads which are connected to the PQCC. Under such a disturbance condition, the PQCC scheme proposed in Chapter 5 may need to be reviewed. For example, as proposed in Chapter 5, the output power of the SOFC is mainly to supply the SP load under steady-state. If the SP load is faulted and need to be disconnected from the system, the SOFC output power cannot be changed instantaneously to match the new load demand and a load-generation imbalance would occur until such time the internal dynamic of the SOFC has managed to restore to a new generation-load balance. The PQCC operation under this condition should be carefully examined. Inappropriate operational scheme would damage the SOFC.

References

[1] W. J. Lee, C. H. Lin, "Utility Deregulation and Its Impact on the Industrial Power Systems", Proc. of IEEE Industrial and Commercial Power Systems Technical Conference, May 1997, pp: 217-222

[2] J. Arrillaga, M. H. J. Bollen, N. R. Watson, "Power Quality Following Deregulation", Proceedings of the IEEE, Vol. 88, Issue 2, Feb. 2000, pp:246-261

[3] B. M. Hughes, J. S. Chan, D. O. Koval, "Distribution Customer Power Quality Experience", IEEE Trans. Industry Applications, Vol. 29, No. 6, Nov./Dec. 1993

[4] M. H. J. Bollen, "Characterization of Voltage Sags Experienced by Three-phase Adjustable-Speed Drives", IEEE Trans. Power Delivery, Vol. 12, No. 4, Oct. 1997, pp: 1666-1671

[5] M. H. J. Bollen, R. A. A. de Graaff, "Behavior of AC and DC Drives During Voltage Sags with Phase-Angle Jump and Three-Phase Unbalance," Proc. of IEEE Power Engineering Society Winter Meeting, Vol. 2, Jan. 1999, pp: 1225-1230

[6] R. A. Hanna, "Harmonics and Technical Barriers in Adjustable Speed Drives", IEEE Trans. Industry Applications, Vol. 25, Issue 5, Sept/Oct. 1989, pp: 894-900

[7] K. Nara, Y. Hayashi, "Reliable Electrical Power Supply by DGs for Unbundled Power Quality Services", Proc. of International Conference on Energy Management and Power Delivery, Vol. 1, March 1998, pp:11–16

[8] R. Lasseter, C. Hochgraf, "Unbundled Power Quality Services: Technical Issues", Proc. of International Conference on System Sciences, Vol. 5, 1997, pp: 581-588

[9] K. Nara, Hirokazu O. and Y. Mishima, "Optimal Configuration of New Power Delivery System for Customized Power Supply Services", Proc. of the 14th Power Systems Computation Conference, June 2002, Spain

[10] T. Ise, Y. Hayashi, K. Tsuji, "Definitions of Power Quality Levels and the Simplest Approach for Unbundled Power Quality Services", Proc. of International Conference on Harmonics and Quality of Power, Vol. 2, Oct. 2000, pp:385–390

[11] C. Alvarez, J. Alamar, A. Domijan Jr., Montenegro A., Song Z., "An investigation toward New Technologies and Issues in Power Quality", Proc. of International Conference on Harmonics and Quality of Power, Vol. 2, Oct. 2000, pp:444-449

[12] N. Jenkins, *Embedded Generation*, London: Institution of Electrical Engineers, c2000

[13] Ann-Marie Borbely, J. F. Kreider, *Distributed Generation: The Power Paradigm for the New Millennium*, CRC Press, 2001

[14] H. L. Willis, W. G. Scott, *Distributed Power Generation – Planning and Evaluation*, Marcel Dekker, 2000

[15] N. Jenkins, G. Strbac, "Effects of Small Embedded Generation on Power quality", IEE colloquium on Issues in Power quality, Warwick-28th November 1995

[16] A. Girgis, S. Brahma, "Effect of Distributed Generation on Protective Device Coordination in Distribution System", Proc. of Large Engineering Systems Conference on Power Engineering, July 2001, pp:115–119

[17] C. L. T. Borges, D. M. Falcão, "Impact of Distributed Generation Allocation and Sizing on Reliability, Losses and Voltage Profile", Proc. of IEEE Power Tech Conference, Vol. 2, June 2003, Bologna, Italy

[18] H. B. Puttgen, P. R. MacGregor, F. C. Lambert, "Distributed Generation: Semantic Hype or the Dawn of a New Era?", IEEE Power and Energy Magazine, Vol. 1, Issue 1, Jan.-Feb. 2003, pp: 22–29

[19] K. Nara, "Enabler of Introducing Distributed Generators and Its Effect to Power Distribution System", Proc. of IEEE/PES Transmission and Distribution Conference and Exhibition, Vol. 1, Oct. 2002, pp: 584-589

[20] C. S. Dai, Y. Baghzouz, "On the Voltage Profile of Distribution Feeders with Distributed Generation", Proc. of IEEE Power Engineering Society General Meeting, Vol. 2, July 2003

[21] N. G. Hingorani, "Introducing Custom Power", IEEE Spectrum, Vol. 32, No. 6, June 1995, pp: 41-48

[22] N. G. Hingorani, "Overview of Custom Power Applications", Proc. of International Conference and Exhibit on Power Quality '98, 1998, pp: 1-7

[23] A. Sundaram, "Custom Power – EPRI'S Response to Power Quality Issues", Southcon/94 Conference Record, 1994, pp: 398-403

[24] S. Nilsson, "Special Application Considerations for Custom Power Systems", Proc. of IEEE Power Engineering Society Winter Meeting, Vol. 2, Jan./Feb. 1999, pp: 1127–1131

[25] A. Domijan Jr., G. Heydt, Proc. of the NSF Conf. on Unbundled Power Quality Services in the Power Industry, Key West, 1996

[26] K. Nara, J. Hasegawa, "An Advanced Flexible and Reliable Distribution System", Proc. of International Conference on Energy Management and Power Delivery, Vol. 1, Nov. 1995, pp: 55-60

[27] K. Nara, J. Hasegawa, "Future Flexible Power Delivery System and Its Intelligent Functions", Proc. of International Conference on Intelligent Systems Applications to Power Systems, Jan.-Feb. 1996, pp: 261-265

[28] T. Kiichiro, N. Koichi, J. Hasegawa and T. Oyama, "Flexible, Reliable, and Intelligent Electric Energy Delivery System: Concepts and Perspective", Proc. of American Power Conference, Vol.61-I, pp: 504-511, 1999, Chicago, USA

[29] K. Nara, J. Hasegawa, "A New Flexible, Reliable and Intelligent Electrical Energy Delivery System", Electrical Engineering in Japan, Vol.121, No.1, 1997, pp:26-34

[30] T. Ise, "Functions and Configurations of Quality Control Center on FRIENDS", Proc. of Transmission and Distribution Conference and Exhibition 2002: Asia Pacific, Vol. 1, Oct. 2002, pp: 590-595,

[31] J. Hasegawa, "Studies on Quality Control Center for FRIENDS", in Proc. of International Symposium on Energy and Environment, Session on Urban Energy Systems, Jan. 2002, pp: 137-142, Osaka, Japan

[32] Y. Hayashi, M. Saisyo, T. Ise, K. Tsuji, "Configuration of Quality Control Center for FRIENDS Based on AC and DC system", Proc. of International symposium on Energy and Environment, Jan. 2002, pp: 143-148, Osaka, Japan

[33] T. Ise, M. Takami, K. Tsuji, "Flexible, Reliable, and Intelligent Electric Energy Delivery System: Configuration of Quality Control Center", Proc. of American Power Conference, Vol. 61-I, 1999, pp: 512-517

[34] M. Saisho, T. Ise, K. Tsuji, "Configuration of DC Loop Type Quality Control Center", Proc. of Power Conversion Conference, Vol. 2, April 2002, pp: 434-439, Osaka, Japan

[35] Y. Hayashi, T. Ise, K. Tsuji, "AC-type Quality Control Center for FRIENDS-System Configuration and Experimental Results", Proc. of IEEE/PES Transmission and Distribution Conference and Exhibition, Vol. 2, Oct. 2002, pp: 1191–1195

[36] T. Ise,Y. Hayashi, K. Tsuji, "Characteristics and Location of the Quality Control Center Using Three-Phase Four-Wire AC System", Proc. of International Conference on Power System Technology, Vol. 2, Dec. 2000, pp: 661–666

[37] K. Nara, Y. Mishima, J. Hasegawa, "A New Type Power Delivery System for Reliable Power Supply – FRIENDS and Its Optimal Network Design", Proc. of International Conference on Power System Technology, Vol. 2, Dec. 2000, pp: 649-654

[38] R. Hara, H. Kita, E. Tanaka, J. Hasegawa, "Emergency Operation Based on Multi Agent Technology in FRIENDS", Proc. of the 14th Power Systems Computation Conference, June 2002, Spain

[39] T. Oyama, "Demand Side Prospects of Multiple Menu Service in Power System with the Quality Control Center", Proc. of IEEE Power Engineering Winter Meeting, Vol. 1, pp: 422-426, Jan./Feb. 1999

[40] K. Tsuji, O. Saeki, J. Suetsugu, "Estimation of Daily Load Curves by Quality Level Based on a Bottom-Up Stimulation Model", Proc. of IASTED International Conf. on High Technology in the Power Industry, 1997, pp: 181-185, Orlando

[41] L. D. Zhang, M. H. J. Bollen, "Characteristic of Voltage Dips (Sags) in Power Systems", IEEE Trans. Power Delivery, Vol. 15, No. 2, April 2000

[42] M. H. J. Bollen, *Understanding Power Quality Problems: Voltage Sags and Interruptions*, New York: IEEE Press, 2000

[43] M. H. J. Bollen, "Voltage Sags: Effects, Mitigation and Prediction", Power Engineering Journal, Vol. 10, No. 3, June 1996, pp: 129-135

[44] D. O. Koval, M. B. Hughes, "Canadian National Power Quality Survey: frequency of Industrial and Commercial Voltage Sags", IEEE Trans. Industry Applications, Vol. 33, Issue 3, May-June 1997, pp: 622-627

[45] M. H. J. Bollen, G. Yalcinkaya, J. Pellis, M. R. Qader, "A Voltage Sag Study in A Large Industrial Distribution System", Conference Record of the IEEE Industry Applications Conference, Vol. 4, Oct. 1996, pp: 2372-2377

[46] Y. S. Kim and S. K. Sul, "A Novel Ride-Through System for Adjustable Speed Drives Using Common-Mode Voltage", IEEE Trans. Industry Applications, Vol. 37, issue 5, Sep./Oct. 2001, pp: 1373-1382,

[47] P. Kundur, *Power System Stability and Control*, New York, McGraw-Hill, 1994

[48] A. Sannino, M. G. Miller, M. H. J. Bollen, "Overview of Voltage Sag Mitigation", Proc. of 2000 IEEE Power Engineering Society Winter Meeting, Vol. 4, Jan. 2000, pp: 2872-2878, Singapore

[49] Y. H. Li, S. Rajakaruna, S. S. Choi, "Control of a Solid Oxide Fuel Cell Power Plant in a Grid-Connected System", In print, IEEE Trans. Energy Conversion, Paper No. TEC-00199-2004

[50] T. Wildi, *Electrical Machines, Drives, and Power Systems*, 4th edition, Prentice Hall, 2000

[51] R. C. Dugan, M. F. Mcgranaghan, *Electrical Power System Quality*, McGraw-Hill, 1996

[52] J. Arrillaga, N. R. Watson, S. Chen, *Power System Quality Assessment*, John Wiley& Sons Ltd, 2000

[53] L. Kojovic, S. Hassler, "Application of Current Limiting Fuses in Distribution Systems for Improved Power Quality and Protection", IEEE Trans. Power Delivery, Vol. 12, Issue 2, April 1997, pp: 791-800

[54] R. J. Kakalec, "Comparison of Three Phase Scott-T and Ferroresonant Transformers," Proc. of Electrical Electronics Insulation Conference and Electrical Manufacturing & Coil Winding Conference, Sept. 1995, pp: 619-623

[55] S. B. Bekiarov, A. Emadi, "Uninterruptible Power Supplies: Classification, Operation, Dynamics, and Control", Proc. of IEEE Applied Power Electronics Conference and Exposition, Vol. 1, March 2002, pp:597 – 604

[56] N. H. Woodley, L. Morgan, A. Sundaram, "Experience with an Inverter-Based Dynamic Voltage Restorer", IEEE Trans. Power Delivery, Vol. 14, No. 3, July 1999, pp: 1181-1186

[57] A. Ghosh, G. Ledwich, "Compensation of Distribution System Voltage Using DVR", IEEE Trans. Power Delivery, Vol. 17, No. 4, Oct. 2002, pp: 1030-1036

[58] N. Abi-Samra, D. Carnovale, A. Sundaram, W. Malcolm, "Role of the Distribution System Dynamic Voltage Restorer in Enhancing the Power at Sensitive Facilities," Wescon Conference Record 1996, 96CH35927, pp: 167-181, Los Angeles USA

[59] K. Chan, A. Kara, G. Kieboom, "Power Quality Improvement with Solid State Transfer Switches", Proc. of 8th International Conference on Harmonics and Quality of Power, Vol. 1, Oct. 1998, pp: 210-215

[60] C. Schauder and H. Mehta, "Vector Analysis and Control of Advanced Static VAR Compensators", IEE Proc.-Part C, Vol. 140, No. 4, July 1993, pp: 266-272

[61] G. J. Lee, M. M. Albu, G. T. Heydt, "A Power Quality Index Based on Equipment Sensitivity, Cost, and Network Vulnerability", IEEE Trans. Power Delivery, Vol. 19, Issue 3, July 2004, pp: 1504-1510

[62] ITI (CBEMA) Curve Application Note, Information Technology Industry Council (ITI), available at http://www.itic.org

[63] J. A. Cook, B. K. Powell, "Modeling of an Internal Combustion Engine for Control Analysis", IEEE Control Systems Magazine, Vol. 8, Issue 4, Aug. 1988, pp: 20-26

[64] A. Ai-Hinai, A. Feliachi, "Dynamic Model of a Microturbine Used as a Distributed Generator", Proc. of the Southeastern Symposium on System Theory, March 2002, pp: 209 – 213

[65] M. J. Moore, *Micro-turbine Generators*, Professional Engineering Publishing, Bury St Edmunds and London, UK

[66] D. M. Allen, "A Challenging Future for Improved Photovoltaic Systems", Conference Record of the Twenty Second IEEE Photovoltaic Specialists Conference, Oct. 1991, pp: 20-22

[67] J. Larminie, A. Dicks, *Fuel cell system explained*, 2nd edition, New York, John Wiley, 2002

[68] L. J. Blomen, M. N. Mugerwa, *Fuel Cell Systems*, New York: John Wiley, 1993

[69] M. W. Ellis, M. R. Von Spakovsky, D. J. Nelson, "Fuel Cell Systems: Efficient, Flexible Energy Conversion for the 21st Century," Proc. IEEE, vol. 89, No. 12, Dec. 2001, pp: 1808-1818

[70] A. Ghosh, G. Ledwich, *Power Quality Enhancement Using Custom Power Devices*, Kluwer Academic Publishers, c2002

[71] Custom Power Technology Development, techlist available at http://grouper.ieee.org/groups/1409/techdev.html

[72] L. Xu, O. Anaya-Lara, V. G. Agelidis, E. Acha, "Development of Prototype Custom Power Devices for Power Quality Enhancement", Proc. of International Conference on Harmonics and Quality of Power, Vol. 3, Oct. 2000, pp: 775–783

[73] S. Y. Park, J. K. Park, "The Modeling and Analysis of Shunt Type Custom Power Device", Proc. of IEEE Power Engineering Society Winter Meeting, Vol. 1,Jan./Feb. 2001, pp: 186–191

[74] S. W. Middlekauff, E. R. Collins Jr., "System and Customer Impact: Considerations for Series Custom Power Devices", IEEE Trans. Power Delivery, Vol. 13, No. 1, Jan. 1998

[75] T. Ueda, M. Morita, H. Arita, J. Kida, Y. Kurosawa, T. Yamagiwa, "Solid-State Current Limiter for Power Distribution System", IEEE Trans. Power Delivery, Vol. 8, No. 4, Oct. 1993, pp: 1796-1801

[76] E. Twining, M. J. Newman, P. C. Loh, D. G. Holmes, "Voltage Compensation in Weak Distribution Networks Using A D-STATCOM", Proc. of International Conference on Power Electronics and Drive Systems, Vol. 1, 2003, pp:178-183

[77] J. G. Nielsen, F. Blaabjerg, "Control Strategies for Dynamic Voltage Restorer Compensating Voltage Sags with Phase Jump", Proc. of IEEE Applied Power Electronics Conference and Exposition, Vol. 2, March 2001, pp:1267–1273

[78] IEEE Std. 1250 – 1995, "IEEE Guide for Service to Equipment Sensitive to Momentary Voltage Disturbances"

[79] S. S. Choi, B. H. Li, D. M. Vilathgamuwa, "Dynamic Voltage Restoration with Minimum Energy Injection", IEEE Trans. Power Systems, Vol. 15, No. 1, Feb. 2000, pp: 51-57

[80] H. Fujita, H. Akagi, "The Unified Power Quality Conditioner: The Integration of Series- and Shunt-Active Filters", IEEE Trans. Power Electronics, Vol. 13, No. 2, March 1998, pp: 315-322

[81] L. Gyugyi, T. R. Rietman, A. Edris, "The Unified Power Flow Controller: A New Approach to Power Transmission Control", IEEE Trans. Power Delivery, Vol. 10, No. 2, April 1995, pp: 1085-1097

[82] A. Domijan Jr., A. Montenegro, A. J. F. keri, K. E. Mattern, "Simulation Study of the World's First Distributed Premium Power Quality Park", IEEE Trans. Power Delivery, Vol. 20, No. 2, April 2005, pp: 1483-1492

[83] A. Domijan Jr, A. Montenegro, A. J. F. keri, K. E. Mattern, "Custom Power Devices: An Interaction Study", IEEE Trans. Power Systems, Vol. 20, No. 2, May 2005, pp: 1111-1118

[84] T. Wood, Franklin, "Experience with Custom Power Applications for Critical Manufacturing Facilities", Proc. of IEEE PES Transmission and Distribution Conference, Vol. 3, Sept. 2003, pp: 940 – 943

[85] R. Hara, T. Suzuki, H. Kita, J. Hasegawa, I. Iyoda, "The Effects of the Transfer Switching on the Low Voltage Side of Quality Control Center in FRINEDS", Proc. of International Conference on Power System Technology, Vol. 2, Dec. 2000, pp: 667 - 671

[86] M. Takami, T. Ise, K. Tsuji, "Studies toward a Faster, Stabler and Lower Losses Transfer Switch", Proc. of IEEE Power Engineering Society Winter Meeting, Vol. 4, Jan. 2000, pp: 2729–2734

[87] Z. P. Fang, "Application Issues of Active Power Filters", IEEE Industry Applications Magazine, Vol. 4, Issue 5, Sept./Oct. 1998, pp: 21–30

[88] N. Mohan, T. M. Undeland, W. P. Robbins, *Power Electronics: Converters, Applications, and Design*, John Wiley & Sons, c2003

[89] Y. Q. Zhan, S. S. Choi, D. M. Vilathgamuwa, "A Voltage-Sag Compensation Scheme Based on the Concept of Power Quality Control Center", IEEE Trans. on Power Delivery, Vol. 21, No. 1, Jan. 2006, 296 - 304

[90] Y. Q. Zhan, S. S. Choi, D. M. Vilathgamuwa, "Using Quality Control Center to Improve Power System Stability", Proc. of 4th International Power Electronics and Motion Control Conference, Vol. 3, Aug. 2004, pp: 1236-1241

[91] R. S. Wu, S. B. Dewan, G. R. Slemon, "Analysis of an AC-to-DC Voltage Source Converter Using PWM With Phase and Amplitude Control", IEEE Trans. Industry Applications, Vol. 27, No. 2, March/April 1991, pp: 355-364

[92] R. S. Wu, S. B. Dewan, G. R. Slemon, "A PWM AC to DC Voltage Source Converter under the Predicted Current Control with a Fixed Switching Frequency", IEEE Trans. Industry Applications, Vol. 27, No. 4, July/Aug. 1991, pp: 756-764

[93] R. Lasseter, "Dynamic Models for Micro-turbines and Fuel Cells", Proc. of IEEE Power Engineering Society Summer Meeting, Vol. 2, July 2001, pp:761-766

[94] John J. D'Azzo, Constantine H. Houpis, *Linear control system analysis and design: conventional and modern*, New York: McGraw-Hill, c1995

[95] B. H. Bae, S. K. Sul, J. H. Kwon, J. S. Byeon, "Implementation of Sensorless Vector Control for Super-High-Speed PMSM of Turbo-Compressor", IEEE Trans. Industry Applications, Vol. 39, May/June 2003, pp: 811-818

[96] A. V. Zyl, R. Spee, A. Faveluke, S. Bhowmik, "Voltage Sag Ride-Through for Adjustable Speed Drives with Active Rectifiers", IEEE Trans. Industry Applications, Vol. 34, Issue 6, Nov./Dec. 1998, pp:1270–1277

[97] J. W. Dixon, B. T. Ooi, "Indirect Current Control of a Unity Power Factor Sinusoidal Current Boost Type Three-Phase Rectifier", IEEE. Trans. Industrial Electronics, Vol. 35, No. 4, Nov. 1988, pp: 508-515

[98] M. Malinowski, M. P. Kazmierkowski, A. M. Trzynadlowski, "A Comparative Study of Control Techniques for PWM Rectifiers in AC Adjustable Speed Drives", IEEE Trans. Power Electronics, Vol. 18, No. 6, Nov. 2003, pp:1390-1396

[99] J. Paudulles, G. W. Ault, J. R. McDonald, "Integrated SOFC Plant Dynamic Model for Power Systems Simulation", Journal of Power Sources, No. 86, No 1-2, pp: 495-500, 2000

[100] Y. Q. Zhan, Y. H. Li, S. S. Choi, S. Rajakaruna, D. M. Vilathgamuwa, "The Design of a Fuel Cell-Based Power Quality Control Center to Realize Unbundled Power Quality Supply", accepted, IEEE Transactions on Power Delivery

[101] Y. H. Li, S. S. Choi and S. Rajakaruna, "An Analysis of the Control and Operation of a Solid Oxide Fuel Cell Power Plant in an Isolated System", IEEE Trans. Energy Conversion, Vol. 20, Issue 2, June 2005, pp: 381-387

[102] S. Krumdieck, S. Page and S. Round, "Solid Oxide Fuel Cell Architecture and System Design for Secure Power on an Unstable Grid", J. Power Sources, Vol.125, No.1, Jan. 2004, pp: 189-198,

[103] J. Wang, F. Z. Peng, J. Anderson, A. Joseph, R. Buffenbarger, "Low Cost Fuel Cell Converter System for Residential Power Generation", IEEE Trans. Power Electronics, Vol. 19, No. 5, Sep. 2004, pp: 1315-1322

[104] IEEE Task Force on "Load representation for dynamic performance analysis", IEEE Trans. Power Systems, Vol. 8, No. 2, May 1993, pp. 472-482

[105] O. Usta, M. A. Redfern, N. Tarkan, Z. Erdogan, "Analysis of Out of Phase Reclosing Required for the Protection of Dispersed Storage and Generation Units", Proc. of 8th Mediterranean Electrotechnical Conference, Vol. 2, May 1996, pp: 742-745

[106] Y. Q. Zhan, S. S. Choi, S. Rajakaruna and D. M. Vilathgamuwa, "Power Quality Control Center Incorporating Series Compensator", submitted, Proc. IEE, Pt C

[107] Y. Q. Zhan, Y. H. Li, S. S. Choi, S. Rajakaruna, D. M. Vilathgamuwa, "Some Recent Results on the Design of Power Quality Control Center", Accepted, 7th International Power Engineering Conference, IPEC 2005, Singapore

Appendices

Appendix A

Parameters of G_{com}(s)

In Chapter 3, the micro-turbine model G(s) in Figure 3-10 can be represented as

$$G(s)=\frac{G_2(s)}{1+G_2(s)}=\frac{as+b}{\tau Js^3+(\tau\frac{k_eV_{dc}}{r}+J)s^2+(\frac{k_eV_{dc}}{r}+a)s+b}$$

Then the expressions for $a_1 \sim a_8$, $b_1 \sim b_7$ are:

$$b_1 = D\tau JT_{RH}T_{CH}$$

$$b_2 = k_g\tau JF_{HP}T_{RH} - D[T_{RH}T_{CH}(\tau\frac{K_eV_{dc}}{r}+J)+(T_{RH}+T_{CH})\tau J]$$

$$b_3 = k_gF_{HP}T_{RH}(\tau\frac{K_eV_{dc}}{r}+J)+(k_g+F_{HP}T_{RH}k_h)\tau J+k_pk_1aT_{RH}T_{CH}$$
$$-D[T_{RH}T_{CH}(\frac{K_eV_{dc}}{r}+a)+(T_{RH}+T_{CH})(\tau\frac{K_eV_{dc}}{r}+J)+\tau J]$$

$$b_4 = k_gF_{HP}T_{RH}(\frac{K_eV_{dc}}{r}+a)+(k_g+F_{HP}T_{RH}k_h)(\tau\frac{K_eV_{dc}}{r}+J)+k_h\tau J+a[(T_{RH}+T_{CH})k_pk_1+k_ik_1T_{RH}T_{CH}]$$
$$+k_pk_1bT_{RH}T_{CH}-D[T_{RH}T_{CH}b+(T_{RH}+T_{CH})(\frac{K_eV_{dc}}{r}+a)+\tau\frac{K_eV_{dc}}{r}+J]$$

$$b_5 = k_gbF_{HP}T_{RH}+(k_g+F_{HP}T_{RH}k_h)(\frac{K_eV_{dc}}{r}+a)+k_h(\tau\frac{K_eV_{dc}}{r}+J)+b[(T_{RH}+T_{CH})k_pk_1+k_ik_1T_{RH}T_{CH}]$$
$$+a[k_pk_1+(T_{RH}+T_{CH})k_ik_1]-D[(T_{RH}+T_{CH})b+\frac{K_eV_{dc}}{r}+a]$$

$$b_6 = b(k_g+F_{HP}T_{RH}k_h)+k_h(\frac{K_eV_{dc}}{r}+a)+b[k_pk_1+(T_{RH}+T_{CH})k_ik_1]+k_ik_1a-Db$$

$$b_7 = k_hb+k_ik_1b$$

$$a_1 = 2H\tau JT_{RH}T_{CH}$$

$$a_2 = 2HT_{RH}T_{CH}(\tau\frac{K_eV_{dc}}{r}+J)+2H\tau J(T_{RH}+T_{CH})+b_1$$

$$a_3 = 2HT_{RH}T_{CH}(\frac{K_eV_{dc}}{r}+a)+2H(T_{RH}+T_{CH})(\tau\frac{K_eV_{dc}}{r}+J)+2H\tau J+b_2$$

$$a_4 = 2HbT_{RH}T_{CH}+2H(T_{RH}+T_{CH})(\frac{K_eV_{dc}}{r}+a)+2H(\tau\frac{K_eV_{dc}}{r}+J)+b_3$$

$$a_5 = 2Hb(T_{RH}+T_{CH})+2H(\frac{K_eV_{dc}}{r}+a)+b_4$$

$a_6 = 2Hb + b_5$

$a_7 = b_6$

$a_8 = b_7$

Appendix B

Typical 100 kW SOFC Power Plant Experimental Data Used for Simulation Studies

Table B-1: 100 kW SOFC power plant data [99]

Symbol	Representation	Value
P_{rate}	Rated output power	100 kW
$V_{dc,rate}$	Rated FC terminal voltage	330 V
T	Operation temperture	1273 °K
E_0	Ideal standard potential	1.18 V
N_0	Number of series cells in the stack	384
K_r	Modeling constant	0.993×10^{-3} mol/(s.atm)
u_s	Fuel utilization factor setting	0.8
K_{H2}	Hydrogen valve molar constant	0.843 mol/(s.atm)
K_{H2O}	Water valve molar constant	0.281 mol/(s.atm)
K_{O2}	Oxygen valve molar constant	2.52 mol/(s.atm)
τ_{H2}	Hydrogen flow response time	26.1 s
τ_{H2O}	Water flow response time	78.3 s
τ_{O2}	Oxygen flow response time	2.91 s
τ_f	Fuel processor response time	5 s
r	Ohmic loss	0.126 Ω
r_{H_O}	Ratio of hydrogen and oxygen	1.145
b_{act}	Tafel slope	0.11
a_{act}	Tafel constant	0.05
a_{con}	Concentration loss constant	10^{-4} V
b_{con}	Concentration loss constant	8×10^{-3}

Vita

Zhan Yanqin was born in P. R. China, in 1979. She received her B. Eng. degree from Xian Jiaotong University, China, in 2001 in Electrical Engineering. She joined the Nanyang Technological University in April 2002 and is now pursuing her Ph.D. degree. Her research areas include Power Quality and the use of Power Electronics devices for power system applications.

Research related to this dissertation has resulted in the following publications:

[1] Y. Q. Zhan, S. S. Choi and D. M. Vilathgamuwa, "A Voltage-Sag Compensation Scheme Based on the Concept of Power Quality Control Center", IEEE Trans. on Power Delivery, Vol. 21, No. 1, Jan. 2006, 296 - 304

[2] Y. Q. Zhan, Y. H. Li, S. S. Choi, S. Rajakaruna and D. M. Vilathgamuwa, "The Design of a Fuel Cell-Based Power Quality Control Center to Realize Unbundled Power Quality Supply", accepted, IEEE Transactions on Power Delivery

[3] Y. Q. Zhan, S. S. Choi, S. Rajakaruna and D. M. Vilathgamuwa, "Power Quality Control Center Incorporating Series Compensator", submitted, Proc. IEE, Pt C

[4] Y. Q. Zhan, S. S. Choi and D. M. Vilathgamuwa, "Using Quality Control Center to Improve Power System Stability", Proc. of the 4th International Power Electronics and Motion Control Conference, IPEMC 2004, Vol. 3, Aug. 2004 Page(s):1236 - 1241

[5] Y. Q. Zhan, Y. H. Li, S. S. Choi, S. Rajakaruna and D. M. Vilathgamuwa, "Some Recent Results on the Design of Power Quality Control Center", Accepted, 7th International Power Engineering Conference, IPEC 2005, Singapore